

**BIOCONJUGATED β -CYCLODEXTRIN-PERFLUOROHEXANE
NANOCONE CLUSTERS AS FUNCTIONAL AGENTS FOR
NANOPARTICLE MEDIATED HISTOTRIPSY**

A THESIS SUBMITTED TO
THE GRADUATE SCHOOL OF
ENGINEERING AND NATURAL SCIENCES
OF ISTANBUL MEDIPOL UNIVERSITY
IN PARTIAL FULFILLMENT OF THE REQUIREMENTS FOR
THE DEGREE OF
MASTER OF SCIENCE
IN
BIOMEDICAL ENGINEERING AND BIOINFORMATICS

By
Cemran Toydemir

August, 2022

BIOCONJUGATED B-CYCLODEXTRIN-PERFLUOROHEXANE NANOCONE
CLUSTERS AS FUNCTIONAL AGENTS FOR NANOPARTICLE MEDIATED
HISTOTRIPSY

By Cemran Toydemir

22 August 2022

We certify that we have read this dissertation and that in our opinion it is fully adequate,
in scope and in quality, as a dissertation for the degree of Master of Science.

Prof. Dr. Yasemin Yüksel Durmaz

Assoc. Prof. Dr. Muhammet Übeydullah Kahveci

Assist. Prof. Dr. Özge Şensoy

Approved by the Graduate School of Engineering and Natural Sciences:

Prof. Dr. Yasemin Yüksel Durmaz

Director of the Graduate School of Engineering and Natural Sciences

I hereby declare that all information in this document has been obtained and presented in accordance with the academic rules and ethical conduct. I also declare that, as required by these rules and conduct, I have fully cited and referenced all material and results that are not original to this work.

Signature :

Name, Surname: CEMRAN TOYDEMIR

ACKNOWLEDGEMENT

Foremost, I would like to express my sincere gratitude to my research supervisor Prof. Dr. Yasemin Yüksel Durmaz. It was a great chance for me to have a mentor whom I could enter whenever I needed information, and whom I could knock on the door for any subject. She always welcomed me when I lost my motivation and helped me regain my motivation again, she supported me in not only research but also daily problems. I would like to express my gratitude for the fact that she has improved me and contributed to many issues, enabled me to take part in this project, which I enjoyed working on, taught me many new things, and provided different perspectives.

Furthermore, I would like to thank my colleagues, Innovative Polymer Nano-Therapeutics Research Group all members. Especially, I thank Erhan Demirel who helps me when I need it. He is always there for support and also friendship. I also thank Merve Ercan, and Betül Kaymaz who are really good friends and colleagues. I would like to thank Waleed Mustafa for all his support and help.

A special thanks to Tansu Göver for her endless energy and happiness. She is a wonderful friend and confidant who is a partner in my every morning coffees, who can make me laugh every day I spend at school, and who shares my laughter.

My heartfelt thanks are of course my dear mother Hüsrân Toydemir and my dear father Cemalettin Toydemir. I owe all my success to them and their love. They never gave up on me and always supported me. In addition, my grandmother Mukaddes Yiğit and my aunt Ebru Yiğit have made endless efforts in my upbringing and improving myself. Being born and their daughter in a family of these wonderful people is one of the greatest luck and honor I have ever met.

Finally, I would like to thank my dear husband Mehmet Yiğit Köksal. He is an amazing partner and also an amazing friend. I feel his support and his love every second of my life from the beginning. His goodwill and compassion always make me feel safe and peaceful. It is an incredible feeling to have his love and to love him so much. The other greatest luck I have in life is to find such a perfect partner like you.

Cemran Toydemir

August, 2022

CONTENTS

	<u>Page</u>
ACKNOWLEDGEMENT	iv
CONTENTS	v
LIST OF FIGURES	vii
LIST OF TABLES	x
LIST OF SYMBOLS	xi
ABBREVIATIONS	xii
ÖZET	xiv
ABSTRACT	xv
1. INTRODUCTION	1
2. THEORETICAL PART	5
2.1. Cyclodextrins (CDs)	5
2.2. Perfluorocarbons (PFCs).....	7
2.3. Cyclodextrins and Perfluorocarbon Inclusion Complexes	8
2.4. Ultrasound (US) Based Ablation Treatment.....	10
2.5. Nanoparticles Mediated Histotripsy (NMH)	13
2.5.1. Nanodroplet mediated histotripsy	13
2.5.2. Nanocone mediated histotripsy (NMH).....	16
2.6. Bio-conjugation	19
2.6.1. Bioconjugation reactions	21
2.6.1.1. Amine and carboxylic acid group reaction: carbodiimide.....	22
2.6.1.2. Copper-catalyzed azide-alkyne cycloaddition: click chemistry	25
3. EXPERIMENTAL PART	27
3.1. Materials	27
3.2. Characterization	28
3.3. Synthesis of β CD Derivatives.....	28
3.3.1. Synthesis of tosyl cyclodextrin (Ts- β CD)	28
3.3.1.1. Synthesis of tosyl imidazole (Ts-Im).....	28
3.3.1.2. Synthesis of tosyl cyclodextrin (Ts- β CD)	29
3.3.2. Synthesis of mono-6-deoxy-6-aminopropargyl-cyclodextrin (alkyne- β CD).....	29
3.3.3. Synthesis of mono-6-azido-6-deoxy-cyclodextrin (azide- β CD).....	29
3.3.4. Synthesis of mono-6-amino-6-deoxy-cyclodextrin (amine- β CD).....	29
3.4. Synthesis of Functional Nanocone Clusters (NCC)	30
3.5. Synthesis of Bio-Conjugated Nanocone Clusters (NCC).....	30
3.5.1. Synthesis of folic acid conjugated nanocone cluster (FA-NCC).....	30
3.5.2. Synthesis of EPPT1 peptide conjugated nanocone cluster (EPPT1-NCC).....	31
3.5.3. Synthesis of PEGylated nanocone cluster (PEG-NCC).....	31
3.5.4. Synthesis of EPPT1 peptide-PEG conjugated nanocone cluster (EPPT1-PEG-NCC).....	31
3.5.5. Synthesis of FITC labeled nanocone cluster (FITC-NCC).....	32
3.6. Determination of Peptide Percentage on the Targeted NCCs.....	32
3.6.1. Determination of peptide percentage via Ellman's assay	32
3.6.2. Determination of peptide amount via Bradford assay	33
3.7. Determination of FITC Percentage on the Fluorescence Labeled NCCs	33
3.8. Determination of PFH Amount in the NCCs.....	33
3.9. Cell Culture Procedure.....	33

3.9.1.	Hemocompatibility of functional and bioconjugated NCCs.....	34
3.9.2.	The effect of functional and bioconjugated NCCs on cell viability	34
3.9.3.	Cellular uptake using confocal fluorescence microscopy.....	35
3.9.4.	Cellular uptake using flow cytometry.....	35
3.9.5.	Cellular uptake using lysis method.....	36
3.10.	Histotripsy Cavitation Threshold Study	36
4.	RESULTS AND DISCUSSION	37
4.1.	Synthesis of Monofunctional β CD Derivatives	37
4.2.	Synthesis and Characterization of Functional NCCs.....	41
4.3.	Bioconjugation of NCCs.....	44
4.4.	Biocompatibility Evaluation of Bioconjugated-NCCs	51
5.	CONCLUSIONS AND FUTURE WORK.....	62
	BIBLIOGRAPHY	64
	CURRICULUM VITAE.....	75



LIST OF FIGURES

Figure 2.1: a) The structure of cyclodextrins. ‘n’ represent number of units. b) The general cartoon picture of cyclodextrins [30].	5
Figure 2.2: High intensity focused ultrasound (HIFU) therapy system [116].	11
Figure 2.3: Set-up summary of histotripsy treatment [114].	12
Figure 2.4: An example of targeted tissue ablation using histotripsy treatment a) B-mode ultrasound imaging with histotripsy generated cavitation, b) ‘M’ shape histotripsy lesion, c) MR imaging with histotripsy generated cavitation [119].	13
Figure 2.5: a) Cartoon picture of nanodroplet, nanodroplet after affected from US, graph of nanodroplets size at different concentration, b) A picture of selective nanodroplet cavitation in agarose tissue phantom [6].	15
Figure 2.6: Efficiency of nanodroplet mediated histotripsy at different pressure with and without nanodroplet applied at the agarose tissue phantom. a-e) Efficiency of nanodroplet applied NMH on agarose tissue phantom, f) Efficiency of NMH on empty agarose tissue [18].	16
Figure 2.7: a) Nanodroplet used as US active agent for NMH, b) Nanocone used as US active agent for NMH [16].	17
Figure 2.8: a) Generation of bubble cloud with and without NCs in the agarose tissue phantom, b) Size measurement using DLS device comparison of empty β CD, methylated- β CD, and NCs prepared at 0.1 mg/mL [17].	18
Figure 2.9: Some bioconjugates that are used commonly in literature. A) streptavidin-enzyme conjugation, b) ligand-particle conjugation, c) fluorescent labeled oligo molecular beacon probe, d) fluorescently labeled streptavidin, e) ligand conjugated particle, f) biotinylated enzyme, g) antibody-enzyme conjugation, h) fluorescently labeled antibody, i) biotinylated oligo probe, k) antibody-drug conjugation, l) chelate modified dendimer- folate conjugation [132].	20
Figure 2.10: The mechanism of carbodiimide reaction between carboxylic acid and primer amine reaction using EDC-NHS catalyzed.	23
Figure 2.11: Synthesis of antibody conjugation onto nanocarriers using carbodiimide reaction [138].	24
Figure 2.12: The synthesis of FA conjugated cyclodextrin [23].	24
Figure 2.13: General equation of copper catalyzed ‘click’ chemistry.	25
Figure 2.14: A Bioconjugation application of ‘click’ reaction [146].	26
Figure 4.1: Synthesis of monofunctional azide- β CD, alkyne- β CD and amine- β CD. ...	37
Figure 4.2: a) Synthesis of Ts-Im, b) $^1\text{H-NMR}$ spectrum of Ts-Im, c) Synthesis of monofunctional Ts- β CD, and d) $^1\text{H-NMR}$ spectrum of Ts- β CD.	38
Figure 4.3: a) Synthesis of monofunctional alkyne- β CD, b) $^1\text{H-NMR}$ spectrum of alkyne- β CD, and c) FTIR analysis of β CD, alkyne- β CD and its functional and bioconjugated NCCs.	39
Figure 4.4: a) Synthesis of monofunctional azide- β CD, b) $^1\text{H-NMR}$ analysis of azide- β CD, and c) FTIR analysis of β CD, azide- β CD and its functional and bioconjugated NCCs.	40
Figure 4.5: a) Synthesis of monofunctional amine- β CD, b) $^1\text{H-NMR}$ analysis of amine- β CD, and c) FTIR analysis of β CD, amine- β CD and its functional and bioconjugated NCC.	40
Figure 4.6: Synthesis of functional NCC.	41
Figure 4.7: Change of weight of functional NCC and their bioconjugated products at the a) β CD and β CD-NCC, b) alkyne- β CD, alkyne-NCC and its bioconjugated derivative, c) azide- β CD, azide-NCC and its bioconjugated derivative, and d) amine- β CD, amine-NCC and bioconjugated derivative.	42

Figure 4.8: Elemental mapping of β CD-NCC, alkyne-NCC, azide-NCC, and amine-NCC using EDX analysis.	43
Figure 4.9: Size, size distribution and zeta potential of functional NCC and their bioconjugated products at the concentration of 0.01 mg/mL. a) alkyne-NCC and its bioconjugated derivatives, b) azide-NCC and its bioconjugated derivatives, and c) amine-NCC and its bioconjugated derivatives.	44
Figure 4.10: Bioconjugation examples using functional NCC.	45
Figure 4.11: Elemental mapping of alkyne-NCC, EPPT-NCC (1, 2.5, and 5%) and FITC-NCC (2.5 and 5%) using EDX analysis.	47
Figure 4.12: $^1\text{H-NMR}$ spectrum of 2.5% conjugated FITC-NCC (complex includes β CD (400 eq), alkyne- β CD (100 eq), FITC- β CD(2.5 eq)).	48
Figure 4.13: Elemental mapping of amine-NC and FA-NCC (2.5 and 5 %) using EDX analysis.	49
Figure 4.14: Elemental mapping of azide-NCC, PEG-NCC (2.5, 5 and 10 %) and EPPT1-PEG-NCC (2.5 %) using EDX analysis.	50
Figure 4.15: Hemolytic activities of a) functional NCC, and b) and c) bioconjugated NCC at different concentration under physiological conditions. Statistically significant differences were evaluated using the two-way ANOVA plus Tukey's posthoc comparison test. All samples were compared with untreated cells (top of each bar) and also between each other (showing using pair representation). Symbols that are assigned to each concentration denote $p \leq 0.1$ for *, $p \leq 0.01$ for \blacktriangle , $p \leq 0.001$ for \bullet , and $p \leq 0.0001$ for \blackstar	52
Figure 4.16: Cell viability study of a) functional NCC, and b) and c) bioconjugated NCC on MRC-5 cells using MTS Assay. Statistically significant differences were evaluated using the two-way ANOVA plus Tukey's posthoc comparison test. All samples were compared with untreated cells (top of each bar) and also between each other (showing using pair representation). Symbols that are assigned to each concentration denote $p \leq 0.1$ for *, $p \leq 0.01$ for \blacktriangle , $p \leq 0.001$ for \bullet , and $p \leq 0.0001$ for \blackstar	53
Figure 4.17: Cell viability study of a) functional NCC, and b) and c) bioconjugated NCC on MRC-5 cells using Resazurin Assay. Statistically significant differences were evaluated using the two-way ANOVA plus Tukey's posthoc comparison test. All samples were compared with untreated cells (top of each bar) and also between each other (showing using pair representation). Symbols that are assigned to each concentration denote $p \leq 0.1$ for *, $p \leq 0.01$ for \blacktriangle , $p \leq 0.001$ for \bullet , and $p \leq 0.0001$ for \blackstar	54
Figure 4.18: Cell viability study of a) functional NCC, and b) and c) bioconjugated NCC on MCF-10A cell line using MTS Assay. Statistically significant differences were evaluated using the two-way ANOVA plus Tukey's posthoc comparison test. All samples were compared with untreated cells (top of each bar) and also between each other (showing using pair representation). Symbols that are assigned to each concentration denote $p \leq 0.1$ for *, $p \leq 0.01$ for \blacktriangle , $p \leq 0.001$ for \bullet , and $p \leq 0.0001$ for \blackstar	55
Figure 4.19: Confocal fluorescent images showing internalization of EPPT1-NCC and FITC-NCC into a) MCF-7 human breast cancer cells, and b) MCF-10 A human health epithelial breast cells. The green fluorescent originates from FITC conjugated EPPT1-NCC and FITC-NCC NCC derivatives where Hoechst dyed nucleus shows blue fluorescence (Scale bar: 50 μm). Quantitative evaluation of fluorescence intensity for c) MCF-7, and d) MCF-10A cells were achieved by normalizing fluorescence intensity	

of internalized FITC against Hoechst fluorescence. (* $p \leq 0.1$, ** $p \leq 0.01$, *** $p \leq 0.001$, **** $p \leq 0.0001$).....	57
Figure 4.20: a) Histograms showing fluorescent intensities of EPPT1-NCC, FITC-NCC derivatives treated and non-treated cells against 10.000 events (Ex/Em:488/530 nm). Quantitative evaluation of fluorescent intensity using Lysis Method in b) MCF-7 and c) HeLa. FA was detected at 250 nm in FA-NCC treated cells. Statistically significant differences were evaluated using the two-way ANOVA plus Tukey's posthoc comparison test. All samples were compared with untreated cells and also between each other (shown with pair representation; * $p \leq 0.1$, ** $p \leq 0.01$, *** $p \leq 0.001$, **** $p \leq 0.0001$).....	59
Figure 4.21: Comparison of cavitation threshold pressure of alkyne-NCC, azide-NCC and amine-NCC mediated histotripsy.....	60
Figure 4.22: Comparison of cavitation threshold pressure of FA-NCC, EPPT1-NCC and EPPT1-PEG-NCC and FITC-NCC mediated histotripsy.	61



LIST OF TABLES

Table 2.1: Basic properties of natural cyclodextrins [33], [34], [37].	6
Table 2.2: Solubility properties of cyclodextrin derivatives [37], [44], [45].....	7
Table 2.3: Perfluorocarbons with their properties [76]–[78].	8
Table 4.1: Feature of alkyne-NCC and its bioconjugated NCCs.....	46



LIST OF SYMBOLS

α	: Alpha
β	: Beta
γ	: Gamma
μ	: Micro
$^{\circ}$: Degree
n	: Repeat unit
h	: Hour
%	: Percentage



ABBREVIATIONS

FDA	: The Food and Drug Administration
EPR	: The Enhanced Permeability and Retention
siRNA	: Small Interfering RNA
HIFU	: High-Intensity Focused Ultrasound
US	: Ultrasound
MR	: Magnetic Resonance
MRI	: Magnetic Resonance Imaging
CT	: Computed Tomography
RF	: Radiofrequency
NMH	: Nanoparticle-Mediated Histotripsy
ND	: Nanodroplet
NC	: Nanocone
NCC	: Nanocone Cluster
CD	: Cyclodextrin
αCD	: Alpha Cyclodextrin
βCD	: Beta Cyclodextrin
γCD	: Gamma Cyclodextrin
PFC	: Perfluorocarbon
PFH	: Perfluorohexane
PFP	: Perfluoropentane
Ts-Im	: 1-(p-Toluenesulfonyl) Imidazole
Ts-βCD	: Mono Tosyl Beta Cyclodextrin
MCD	: Methylated Beta Cyclodextrin
HPβCD	: 2-Hydroxypropyl-Beta-Cyclodextrin
HMβCD	: High Degree Methylated Beta Cyclodextrin
LMβCD	: Low Degree Methylated Beta Cyclodextrin
HPγCD	: 2-Hydroxypropyl-Gamma-Cyclodextrin
HMγCD	: High Degree Methylate Gamma Cyclodextrin
b.p.	: Boiling Point
r.t.	: Room Temperature
nm	: Nanometer
μm	: Micrometer
mm	: Millimeter
μg	: Microgram
mg	: Milligram
g	: Gram
μL	: Microliter
mL	: Milliliter
eq	: Equivalent
a.u.	: Atomic Unit
mmol	: Millimole
mol	: Mole
cm⁻¹	: Wavenumber
kV	: Kilovolt
kDa	: Kilodalton
mmHg	: Millimetre of Mercury
Hz	: Hertz
pH	: Potential of Hydrogen
min	: Minute

rpm	: Revolutions per Minute
ppm	: Parts per Million (mg/L)
PBS	: Phosphate Buffered Saline
¹H-NMR	: Proton Nuclear Magnetic Resonance
¹³C-NMR	: Carbon Nuclear Magnetic Resonance
GC	: Gas Chromatography
DLS	: Dynamic Light Scattering
PDI	: Polydispersity Index
FTIR	: Fourier Transform Infrared Spectroscopy
T	: Transmittance
ATR	: Attenuated Total Reflection
SEM	: Scanning Electron Microscope
EDX	: Energy Dispersive X-ray Spectroscopy
TGA	: Thermogravimetric Analysis
UV-Vis	: Ultra Violet-Visible Spectroscopy
LC-MS	: Liquid Chromatography–Mass Spectrometry
ESI	: Electrospray Ionization
RBC	: Red Blood Cell
DMEM	: Dulbecco's Modified Eagle Medium
MEM	: Minimum Essential Medium
MEBM™	: Mammary Epithelial Basal Medium
FBS	: Fetal Bovine Serum
EDTA	: Ethylenediaminetetraacetic Acid

NANOPARÇACIK ORTAMLI HISTOTRİPSİ İÇİN FONKSİYONEL AJANLAR OLARAK BİYOKONJUGE β -SİKLODEKSTRİN-PERFLOROHEKZAN NANOKAP KÜMELENMELERİ

ÖZET

Cemran Toydemir

Biyomedikal Mühendisliği ve Biyoenformatik, Yüksek Lisans

Tez Danışmanı: Prof. Dr. Yasemin Yüksel Durmaz

Ağustos, 2022

Yeni nesil nanoparçacık ortamli histotripsisi (NMH) ajanı olarak nanokap kümeleri (NCC), önceden tasarlanmış nanodamlacıkların (ND) sınırlamalarına cevap vermektedir. NCC, FDA onaylı siklodekstrinler (CD) ve uygun perflorokarbonların (PFC) karıştırılmasıyla elde edilebilen daha küçük boyutlu ve PFH miktarı saptanabilir kattılardır. NCC'ler depolanabildiklerinden ve gerektiğinde yeniden dağıtılabildiğinden saklama koşulları açısından daha kararlıdır. Yakın zamanda gerçekleştirilen deneysel ve hesaplamalı çalışmalar, NCC'nin, serbest PFC damlacıkları etrafındaki CD ve PFC konuk-konak komplekslerinin bir organizasyonu olduğunu ve bunların kümelenme davranışının, PFC'nin CD'nin iç kavitesindeki lokalizasyonuna ve CD türevlerinin suda çözünürlüğüne bağlı olduğunu göstermiştir. Beta-siklodekstrin (β CD) ve perfloroheksanın (PFH) etkileşiminden oluşan NCC'nin, test edilen çeşitli CD'ler ve PFC türevleri arasından yüksek PFC içeriğine sahip, toz olarak elde edilebilen en iyi NCC adayları olduğu kanıtlanmıştır. Bu çalışma, *in vitro* ve *in vivo* çalışmalarda kullanılacak, fonksiyonel ve yeni özelliklerin de yapıya dahil edilmesine olanak sağlayacak şekilde en iyi NCC kompozisyonunun fonksiyonlandırılmasına ve biyokonjugasyonuna odaklanmaktadır. Hedefleme, PEG'leme ve floresan etiketleme gibi en sık kullanılan biyokonjugasyon örnekleri üzerinden NCC'nin biyokonjugasyon potansiyelinin gösterilmesi amaçlanmaktadır. Bu amaçla, yapı bloğu olarak β CD, "click" reaksiyonu ve EDC/NHS çapraz bağlanması gibi etkin reaksiyonlar verebilen azit, alkin ve amin gibi gruplarla fonksiyonlandırılmıştır. Bu tek gruplu fonksiyonel β CD'ler PFH varlığında fonksiyonel NCC'ler elde etmek için yapı taşı olarak β CD ile birlikte kullanılmışlardır. Biyokonjugasyon örnekleri hedefleme ajanı olarak sıklıkla kullanılan folik asit (FA) ve daha spesifik hedefleme ajanı olarak peptit bazlı EPPT1 ile birlikte PEG'leme ve FITC ile floresans etiketleme seçilmiştir. Elde edilen biyokonjugatlar, hem yapısal olarak hem de etkinliklerini doğrulamak için *in vitro* test edilmiştir. Son olarak elde edilen bu NCC'ler kullanılarak gerçekleştirilen NMH kaviteye eşik basıncı belirleme çalışmalarında tüm biyokonjugatların kaviteye eşik basıncını başarılı bir şekilde düşürdükleri gösterilmiştir. Genel olarak bu çalışma elde edilen NCC'ler kullanılarak sadece NMH'deki kaviteye eşik basıncının düşürülmesi değil aynı zamanda NMH çalışmasını geliştirmek için ihtiyaç duyulabilecek biyokonjugasyon araçlarının yapıya dahil edilebileceği ve etkin bir şekilde çalıştıkları ortaya koymuştur.

Anahtar sözcükler: Histotripsisi, Nanoparçacık Ortamli Histotripsisi, Siklodekstrin, Perflorokarbon, Nanokap Kümelenmesi, Biyokonjugasyon.

BIOCONJUGATED β -CYCLODEXTRIN-PERFLUOROHEXANE NANOCONE CLUSTERS AS FUNCTIONAL AGENTS FOR NANOPARTICLE MEDIATED HISTOTRIPSY

ABSTRACT

Cemran Toydemir

MSc in Biomedical Engineering and Bioinformatics

Advisor: Prof. Dr. Yasemin Yüksel Durmaz

August, 2022

Nanocone clusters (NCC) as new generation agent of nanoparticle mediated histotripsy (NMH) successfully addressed all the limitations of previously designed nanodroplets (NDs). NCC can be obtained by simply mixing of FDA-approved cyclodextrins (CDs) and suitable perfluorocarbons (PFCs) resulted smaller size aggregates, detectable PFC amount and more stable for long term storage since obtained powder can be stored and redispersed when it is needed. Previous experimental and computational studies showed that NCC is an organization of inclusion complexes of CD and PFC around free PFC droplets and their aggregate behavior depend on the localization of PFC in the cavity and the water solubility of CD derivatives. It has been proved that beta-cyclodextrin (β CD) and perfluorohexane (PFH) are best candidates for NCC cluster that can be isolated as powder with high PFC content among various CDs and PFCs derivatives that are tested. This study focuses on further development of the selected best NCC composition to have advanced tools for in-vitro and in-vivo study. It is aimed to show the bioconjugation potential of NCC through the example of most commonly used functionalization such as targeting, PEGylation and fluorescent labeling. For this purpose, β CD as building block was monofunctionalized with the groups like azide, alkyne and amine that are capable for effective coupling reactions such as “click” reaction and EDC/NHS coupling. These monofunctional β CDs were used as building blocks of NCC in the presence of PFH to obtain functional NCCs as precursors of bioconjugation. EPPT1 as peptide based more specific and folic acid (FA) as most commonly used targeting agent along with PEGylation have been successfully showed as bioconjugation examples. Lastly, fluorescently labeled NCC was obtained via FITC and alkyne functional NCC reaction through propargyl amine and isothiocyanate group reaction. The obtained bioconjugates were tested in vitro to validate the conjugation and finally, their ability to lower cavitation threshold pressure on NMH were shown. All obtained bioconjugates not only successfully lowered the cavitation threshold pressure but also they were perfectly acting on desired bioconjugation tools to enhance the NMH study.

Keywords: Histotripsy, Nanoparticle Mediated Histotripsy, Cyclodextrin, Perfluorocarbon, Nanocone Cluster, Bioconjugation.

CHAPTER 1

1. INTRODUCTION

Histotripsy is a non-invasive and non-thermal technique that performs mechanical tissue ablation by creating an acoustic cavitation mechanism with high-pressure, short-term, and focused ultrasound (US) pulses [1]–[3]. In this technique, US signals interact with small-sized gas bubbles which are dissolved in the tissue to form bubble clouds [4], [5]. These gas bubbles are transformed into highly energetic microbubbles that can expand to a size greater than 50 μm with the help of high negative pressure of US signals [2], [6], [7]. This process is called cavitation and the energy released as a result of this cavitation caused the tissue to get fractionated and completely liquefied that can finally be eliminated by the body without causing any metastasis [1], [3], [8]–[10]. Therefore, there is no solid waste generation and heat output in this technique. Although histotripsy has promising potential for many clinical applications, including benign prostatic hyperplasia, deep vein thrombosis, congenital heart disease, and cancer ablation, the efficiency of this technique is limited in some cases [8], [10]–[13]. One of these limitations is that it requires high-pressure values of 25-30 MPa to produce the desired cavitation in the tissue. Thus, high pressure value may cause cavitation of any tissue outside of the focused area if it is not properly applied. For this reason, histotripsy should be supported by a secondary imaging system to minimize the damage of the healthy neighboring cell and to completely scan the targeted area. Additionally, the effectiveness of this technique is limited to the ability to identify and image a single target tumor before the treatment. Therefore, it is not appropriate for the treatment of micrometastases or multiple tumor nodules.

For the purpose of addressing these limitations of selectivity, targetability, and high cavitation pressure, nanoparticle-mediated histotripsy (NMH) has been developed as a novel ablation method which combines histotripsy with acoustically active nanoparticles [14]–[21]. The feasibility of this method in reducing high-pressure cavitation energy has

been initially demonstrated by using perfluorocarbon (PFC) encapsulated nanodroplets (ND) as a histotripsy agent and it has been shown that the use of NDs as the cavitation nuclei substantially reduced the cavitation threshold pressure [15]–[18]. Moreover, it became possible for cavitation to occur selectively only in regions where NDs are localized [18]. Although NDs address the selectivity and high cavitation pressure limitations of histotripsy, there are some limitations in their usage as histotripsy agent. For instance, ND synthesis consists of several steps that require expertise in polymer chemistry and does not allow for determining the encapsulated PFC amount in the core. Moreover, their long-term stability is very low which requires cold storage. Due to these shortcomings of NDs, nanocone clusters (NCC) have been developed in our laboratory as a new generation agent for NMH [14], [19]–[21]. The building blocks of NCC is the inclusion complex of cyclodextrin and PFC [20]. As well known in the literature, cyclodextrins (CDs) have a conical structure with a hydrophobic inner cavity and hydrophilic outer surfaces and have a tendency to form inclusion complexes with hydrophobic compounds to increase the solubility, bioactivity, and stability of many hydrophobic molecules. It is also frequently reported that CDs have a tendency to form aggregates in irregular size and arrangements by themselves or through their inclusion complexes [22]. NCC is simply an aggregate of CD and PFC inclusion complexes around PFC nanodroplets based on the experimental and computational studies on NCC formation that was recently reported by our group [20]. The study proved that all CD derivatives except alpha-cyclodextrin (α CD) and high degree methylated gamma-cyclodextrin (HM γ CD) can form inclusion complexes with PFC derivatives and these complexes can organize (cluster) around a hydrophobic PFC core. The size of the hydrophobic cavity of cyclodextrin derivatives and the localization of PFC in this cavity dictates the stability of complex and further cluster formation. If formed inclusion complex provides a chance for guest PFC to interact with free PFC, a more compact and stable NCC can form. It was also shown that water solubility of CD derivatives and how it interacts with PFC determines whether formed NCC can be obtained as precipitate for further use. For instance, hydroxy propylated β -cyclodextrin (HP β CD) derivative can make inclusion complex with PFC derivatives however PFC in the cavity does not interact with free PFC due to the elongated cavity result more loose interaction between core and surrounded inclusion complexes [20]. Moreover, HP β CD has best water solubility which lowers the precipitation potential of any formed clustering. Given the fact that PFC derivatives used for this application is volatile, it is almost not possible to

obtained NCC including PFC as ultrasound active part without direct precipitation. Although the mentioned studies address that beta-cyclodextrin (β CD), low degree methylated beta-cyclodextrin (LM β CD) and gamma-cyclodextrin (γ CD) can form NCC as precipitate for further use, only β CD and LM β CD NCC showed good potential for desired application and β CD was selected for further use because it is most commonly used CD derivatives, commercially available, FDA approved and does not require any further modification [20]. It was also reported that both perfluoropentane (PFP, b.p. 29 °C) and perfluoreohexane (PFH, b.p. 56 °C) as PFC can be used as the acoustically active liquid that are transferred from liquid to gas through acoustic droplet vaporization [19]. However, histotripsy cavitation threshold pressure study showed that PFH containing NCC produced more compact bubble cloud without scattering indicating the better reagent for nanoparticles designed for NMH [21].

Even though the ability of lowering cavitation threshold using NCC as nanoparticles for NMH has been effectively shown using tissue mimicking phantom [6], [12], *in-vivo* NMH study is needed to show the efficiency of NCC mediated NMH in the body and it is crucial for NCC to have some bioconjugation such as targeting agent for cell specific treatment or fluorescent labeling to follow up cellular uptake and biodistribution of the particles. The ability of practically decorating the surface of nanoparticles that is planned to circulate in the blood system before site specific tumor accumulation is very important and desired tool for developed NCC. This study aims to show the potential way of having functional NCC that allows required bioconjugation through commonly used and effective coupling reactions. On this regard NCC has an advantage of having β CD as building block since β CD contains seven glucopyranose units including primary hydroxyl group at the primer edge that allows chemical modification on the surface [22]. This is another reason that makes β CD as better candidate for desired application. There are several examples in the literature that use the hydroxyl group of β CD to conjugate different biological moieties including peptides, antibody fragments, fluorophore, drug etc., [23]–[26]. The desired chemical modifications can be either done for all the hydroxyl at the primary surface or it can be done on a single hydroxyl group which provides more side specific functionalization [23]–[25], [27], [28]. For example, Hu and coworkers conjugated folic acid to single amine functional, drug loaded β CD through EDC/NHS coupling to use it as targeted drug delivery system [23]. Lartia et al. alkyne functional peptide to single azide functional β CD via 'click' chemistry as another example [24].

In this study, it was aimed to show the bioconjugation potential of NCC through the example of most commonly used functionalization such as targeting, PEGylation and fluorescent labeling. For this purpose, monofunctionality like azide, alkyne or amine was obtained at the surface of β CD as first step to have functional precursor for future conjugation using effective coupling reactions. These monofunctional β CDs were used as building blocks of NCC in the presence of PFH to obtain functional NCCs as precursors. While folic acid (FA) as most commonly used targeting agent was conjugated to amine-NCC using EDC/NHS coupling reaction, EPPT1 as peptide based more specific targeting agent were conjugated through the azide-alkyne 'click' reaction between azide functional EPPT1 peptide and alkyne-NCC. Similar method was used for PEGylation which is one of the common conjugations for nanoparticles to increase biocompatibility and blood circulation time. In this case, alkyne-PEG or alkyne-PEG-EPPT1 is conjugated to azide-NCC to have either PEGylated NCC or targeted PEGylated NCC. Lastly, fluorescently labeled NCC was obtained via FITC and alkyne-NCC reaction through propargyl amine and isothiocyanate group reaction [29]. Even though these bioconjugations were selected based on the NMH studies that they have been on progress; they are commonly used and easily adaptable any required system. The role of obtained bioconjugates were tested *in vitro* to validate the conjugation and finally, their ability to lower cavitation threshold pressure on NMH were shown.

CHAPTER 2

2. THEORETICAL PART

2.1. Cyclodextrins (CDs)

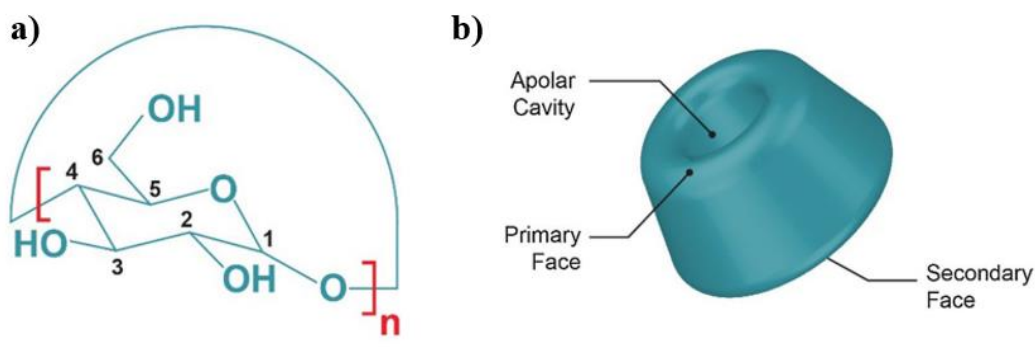





Figure 2.1: a) The structure of cyclodextrins. 'n' represent number of units. b) The general cartoon picture of cyclodextrins [30].

FDA-approved cyclodextrins are biocompatible, nano-sized molecules composed of glucopyranose units and are known as oligosaccharides, which consist of different numbers of cyclic sugars [31], [32]. They take different names according to their carbon numbers and accordingly their sizes vary (**Table 2.1**). They are found in nature and are formed by the enzymatic degradation of starch. Cyclodextrins, which are used in many different areas, have hollow conical shapes with hydrophilic outer surfaces and hydrophobic inner surfaces [33]. The main factor in this difference of hydrophobicity is the configuration of the hydroxyl groups [34]. This difference between the surfaces makes it possible to use cyclodextrins especially as carrier agents, and it is one of the first molecules that come to mind in increasing the solubility of hydrophobic materials, improving their bioactivity and stability by forming a guest-host complex [33], [35], [36]. There is no covalent bond for this complex, rapid equilibrium occurs between the CD and the hydrophobic molecule because of the hydrophobicity. The potential to form stable

inclusion complexes gives an opportunity to use CDs in pharmaceutical applications [37]. Studies have shown that the size of the PFC chains is effective in forming inclusion complexes with β CD and PFC, especially due to its compatibility with the internal space of the cyclodextrin [38].

Table 2.1: Basic properties of natural cyclodextrins [33], [34], [37].

	α -cyclodextrin	β -cyclodextrin	γ -cyclodextrin
n*	6	7	8
Chemical Formula	$C_{36}H_{60}O_{30}$	$C_{42}H_{70}O_{35}$	$C_{48}H_{80}O_{40}$
Structure			
Inner Cavity Diameter (nm)	0.53 nm	0.65 nm	0.83 nm
Outer Cavity Diameter (nm)	1.46 nm	1.54 nm	1.75 nm
Solubility (mg/mL)	130	18.5	249

*n: repeat unit of glucopyranose

Cyclodextrins are basically found in 3 different ways. These are alpha-cyclodextrins, beta-cyclodextrins, and gamma-cyclodextrins. As indicated in **Table 2.1**, varying carbon numbers make a difference between their solubility, as well as the size change mentioned above [34]. Having lowest solubility is β CD, with a solubility of 18.5 mg/mL [37]. Although this poor solubility negatively affects the complexation efficiency, the complexes it forms more stable structures. For an efficient study, conjugations were tried to increase the solubility of the complex made using β CD, since both are important properties. As can be seen in **Table 2.2**, the addition of functional groups had positive effects on solubility.

It was initially thought that there should be a secondary material for aggregates formed by CDs. Further studies revealed that CDs were able to form aggregates spontaneously, without the need for a secondary material. It is known that CDs can remain in aggregate form due to the hydrogen bonding [39], [40]. In addition, since the inner parts of CDs have hydrophobic properties, they can take hydrophobic materials into the core of the

aggregates they form. When the aggregates formed only by CDs and made by putting hydrophobic material inside the CDs were examined, it was determined that tendency to form aggregates was higher when hydrophobic material was added [41], [42]. Because of the solubility decreasing after the aggregation, functional groups or other solubility enhancing effects are used for to increasing solubility [41], [43].

Table 2.2: Solubility properties of cyclodextrin derivatives [37], [44], [45].

Cyclodextrin Derivatives	Abbreviation	Precursor	*n	Solubility (mg/mL)
High Degree Methylated Beta Cyclodextrin	HM β CD	β CD	7	> 600
HydroxypropylBeta Cyclodextrin	HP β CD	β CD	7	> 600
High DegreeMethylated Gamma Cyclodextrin	HM γ CD	γ CD	8	230
HydroxypropylGamma Cyclodextrin	HP γ CD	γ CD	8	>500

*n: repeat unit of glucopyranose

There are many examples of modification of cyclodextrins in the literature. Some of them modify all existing hydroxyl functions, while others target one or more groups, either selectively or non-selectively [27], [46]–[48]. These modifications can be used directly or for the purpose of polymerization or bonding to a polymer [28], [43], [46], [49], [50]. As mentioned above, cyclodextrins, which are widely used to carry hydrophobic drugs, serve as carrier agents of many drugs, especially cancer, by attaching a targeting agent for this purpose or by taking advantage of the enhanced permeability and retention (EPR) effect [23], [51]–[56]. Mohammed et al developed an active transportable drug delivery system by targeting siRNA-containing cyclodextrins infused with doxorubicin in this direction [56]. In another example, the complex formed obtained between doxorubicin and albumin conjugated trimer- β CD was used in targeted drug for cancer cells [54].

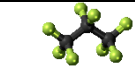
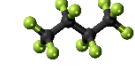
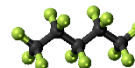
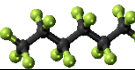
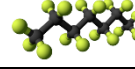
2.2. Perfluorocarbons (PFCs)

As known for their hydrophobicity, chemically inert structure, and rigid molecular skeleton, perfluorocarbons (PFCs) are synthetic molecules consist of carbon and fluorine atoms with different numbers [57]–[60]. Thanks to these feature, PFCs can used in not

only industrial but also biomedical applications like oxygen carrying agent, diagnostic ultrasound imaging, and pulmonary drug and gene delivery [61]–[64]. Studies about these area show us to PFCs ability of binding and carrying with oxygen 50 times more than hemoglobin [65], [66]. Because of strong hydrophobicity, a carrier is needed to increase the water solubility especially in medical application [67]. Loading into micelles and forming inclusion complexes are the most common methods for increasing water solubility for PFCs [68]–[74].

PFCs that are made of carbon and fluorine, are chemically inert molecules. The low boiling point property of PFCs makes them ideal US imaging agents. When US pulses are present this property enables them to convert them from liquid to gas phase. Their boiling point increases with increasing of number of carbons. For example boiling point of decafluorobutane that is consist 4 carbon atoms, is -2 °C, but the boiling point of perfluoropentane that consists 5 carbon atoms, is 29 °C. Similarly, number of carbon dictates the dimension of molecule and how perfectly they will fit into hydrophobic cavity of cyclodextrins [75].

Table 2.3: Perfluorocarbons with their properties [76]–[78].

Chemical Formula	Name	Structure	Mw (g/mol)	Boiling Point (°C)
C ₃ F ₈	Octafluoropropane		118	-36.7
C ₄ F ₁₀	Perfluorobutan		238	-1.7
C ₅ F ₁₂	Perfluoropentan		288	29
C ₆ F ₁₄	Perfluorohexan		338	56
C ₇ F ₁₆	Perfluoroheptane		388	84

2.3. Cyclodextrins and Perfluorocarbon Inclusion Complexes

As it was mentioned in previous section, PFC has several biomedical application such us US imaging and US carryings agent due to the their chemically inert nature. These specific PFCs don't metabolize in the body and can be removed by simple inhalation after they are administered into body. However, these features cannot be attributed to all PFC derivatives which they might include different functional groups and different fluorinated

chain length. Besides biomedical applications, PFCs are known as persistent organic pollutants [79]–[81]. They are formed via by-products of fluoropolymer and fluorotelomer synthesis. For this reason, it has been detected in drinking water, in the body of animals and also humans, and in many consumer products [81]–[84]. It is known that such PFCs, which have serious toxic effects on living things even exposed to very low amounts, cause cancer, thyroid, infertility, and infantilism [84]–[87]. Many methods have been tried for PFC removal including the use of activated carbon, adsorption, nanofiltration, advanced oxidation, and ultrasonic degradation [88]–[90]. Due to their stable structure, it was thought that adsorption rather than chemical degradation could be a more effective way to remove this pollution. For this purpose, the idea of removal by trapping with a host material is generally preferred. Therefore, the interaction between cyclodextrins and PFCs can be used as a trapping method. Studies with CDs have demonstrated the ability to remove many pollutants such as phenols, dyes, pharmaceuticals, and heavy metals in aqueous media [91]–[95]. In a study by Weiss-Errico et al., the interaction of CDs with polluting materials in different water qualities was investigated. These water results revealed that the structures designed using CDs could be promising agents for decontamination removal [96]. These studies were the initial examples of inclusion complex formation between CD and PFCs.

More relevant and inspiring examples for the use of PFCs and CDs is imaging. Molecular imaging systems such as ultrasound (US), computed tomography (CT), and magnetic resonance imaging (MRI) are known as noninvasive imaging systems. In these systems, contrast agents are used to provide a diagnosis[97]. Even though there are many other usage areas for nanoparticles and microparticles, they can also be utilized as diagnostic materials [98], [99]. It is known that PFC-based agents can be clinically used in multiple imaging modalities. Since they are known to be both lipophilic and hydrophobic, they are insoluble in aqueous systems. In other words, they are immiscible with biological fluids in cellular and biological environments. For this reason, modification is required for the use of these chemicals for biological applications. Host-guest complexes formed by CDs and PFCs have been considered as viable and promising systems. As an example, Yao et al. developed an agent to be used to increase ultrasound imaging contrast. In this study, FC-77 was chosen as a PFC model that can be employed in clinical studies. In order to increase the stability and bioavailability of FC-77, the inclusion complex was prepared

using β CD and created an agent that can be put to use as a contrast agent that increases the contrast in ultrasound imaging [100].

As the last example, the CD and PFC inclusion complex was used as histotripsy agent to reduce the cavitation threshold pressure of nanoparticle mediated histotripsy. A brief explanation will be given in the next chapters. The new generated US active agents were named nanocone which was formed by mixing CDs and PFCs in certain proportions in the aqueous media. The histotripsy efficiency and biological compatibility of this new agent produced were examined [21].

2.4. Ultrasound (US) Based Ablation Treatment

Due to the new diseases that occur in response to the increasing human population, new treatment methods need to be developed. Even though it is known that the most common therapy method is surgery, new medical technologies are creating for treatment because of having risks and limitations of surgery like tolerating elderly, comorbid patients, long recovery time, complications etc., [101]–[104]. One of these new methods is minimal invasive (laparoscopy, endoscopy etc.) that is preferred to standard open-surgeries for many cases. Especially ablation that is to disintegrator the target tissue, is one of the most common minimal invasive method the way of using radiofrequency, microwaves, laser energy, freezing [105]–[107]. Because of being an advantage for the patient that had unsuccessful chemotherapy, radiotherapy or surgical, tumor ablation is generally used via minimally invasive ablation technique in the tumor tissue of liver, kidney, bone and lung [108]. Proton beam, X-ray or gamma radiation and focused ultrasound are the way of non-invasive ablation method that have been used clinical [109]–[111].

One of the non-invasive medical application is ‘High Intensity Focused Ultrasound’ (HIFU). HIFU, which is clinical thermal ablation technique, is focused to damage of targeted tissue using ultrasound beam (**Figure 2.2**) [112]. HIFU, is used on benign and malignant tumors in kidney, liver and prostate cancer, is came forward as being non-invasive from other thermal ablation techniques like radiofrequency (RF) or laser ablation [112]–[115]. Even though offering so many benefits, HIFU is also limited as requires real time imaging like magnetic resonance imaging thermometry (MRI) and quantitative B-mode imaging for feedback of treatment during the long treatment times [106], [112]. Also in this technique, temperature is carried above 55 °C and retain for a second before the decreasing the temperature to body temperature. This situation can cause

unpredictable thermal injury margin and even can lead to thermal injury in near the target tissue [1]. Because of these limitations, histotripsy, that is non-invasive and non-thermal treatment method, were developed.

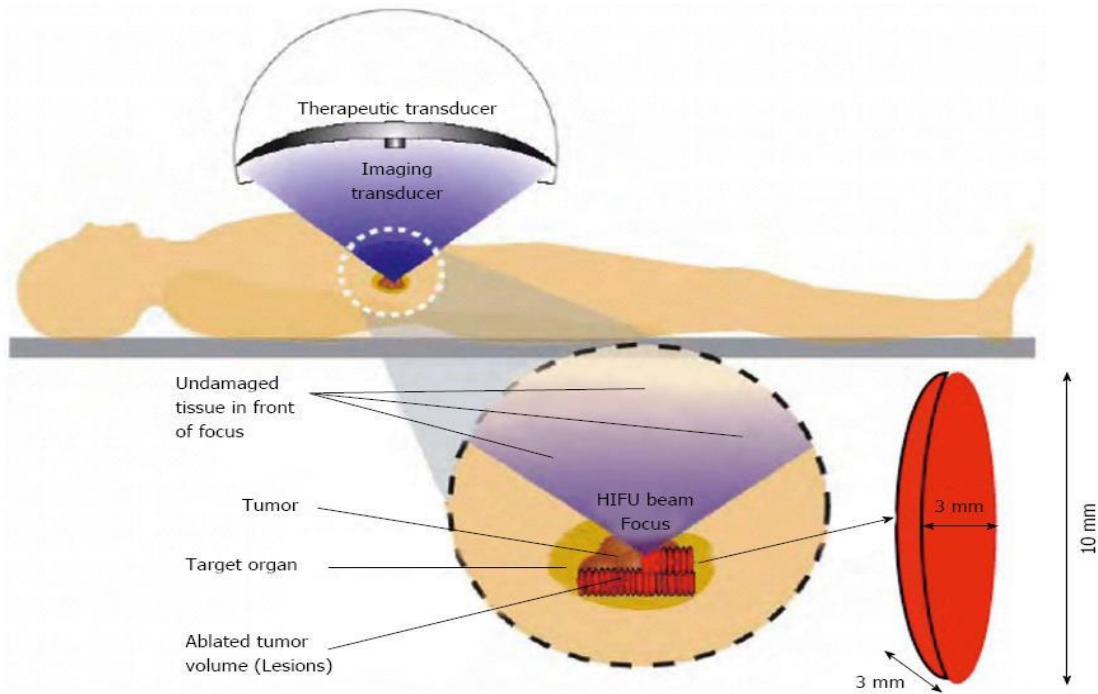


Figure 2.2: High intensity focused ultrasound (HIFU) therapy system [116].

Histotripsy is a mechanical ultrasound ablation method using with high acoustic pressure and short pulses at microseconds. After these high pressure, and short term pulses, microbubbles cluster (bubble cloud) are generated and microbubbles collapse with high energy and fragment adjacent cell into subcellular debris [3], [117]–[121].

As seen by **Figure 2.2**, ultrasound transducer is focused in the target tissue using with concave shaped small ultrasound transducers called ‘histotripsy transducers’. These transducers contain also an ultrasound imaging probe that is a necessary equipment for targeting and also guidance. Since imaging and therapy system were created using these equipments, targeting tissue, that is guidance with US imaging, mediated with high pressure on the target tissue because of the focusing via shape of transducers. For a successfully treatment, US transducers should be manually located to the target area by clinician. During the treatment, US pulses interact with already existing dissolved gas bubbles in the target tissue. These gas bubbles usually smaller than 10 nm can be expended to a bubble cluster more than 50 μm and form the highly energetic microbubbles. Eventually they collapse (cavitation) and release energy to neighboring

cells that caused mechanical fragmentation in the tissue. Because of the high-amplitude ablations happen so short time but repeatedly, bubble clouds expand and contract. This mechanical push causes the disintegration of tissue to a subcellular level [1], [2], [122], [123].

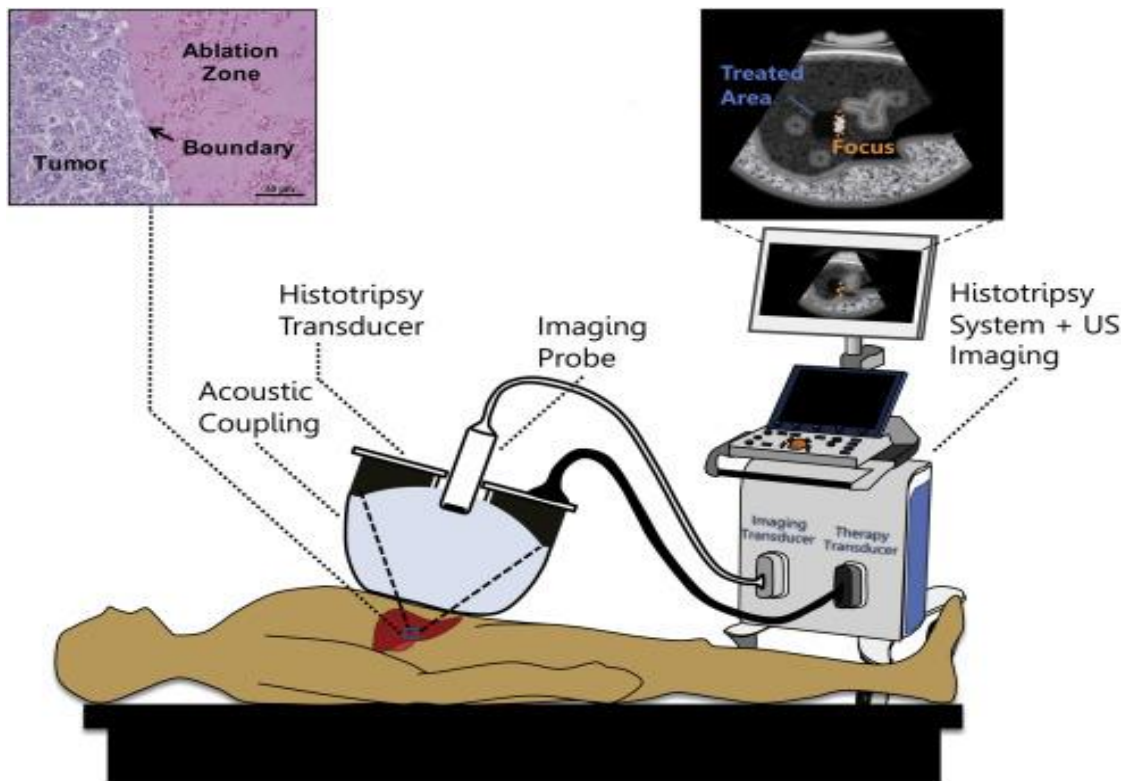


Figure 2.3: Set-up summary of histotripsy treatment [114].

To ablate a soft tissue using histotripsy, a cavitation threshold pressure around 25-30 MPa is needed. The high pressure causes the explosion of bubble clouds in the focused region. In **Figure 2.3** is shown an example of the target tissue ablation by histotripsy. Since there are minimally harmful against the neighboring healthy cell, it is thought histotripsy is noninvasive treatment method. The most popular areas used histotripsy are obstruction treatment, fetal septal defects treatment, kidney stones treatment, hepatocellular carcinoma treatment etc., [12], [124]–[126]. This method is not only treatment of soft tissue, but also opens up new treatment method for urinary calculi and some type of cancer treatment [127]. In 2010, in-vivo activity of histotripsy was shown on VX-2 tumor tissue that is known a malignant cancer cell line of rabbit kidney, and the result of this study showed to histotripsy is a potential cancer treatment method [8].

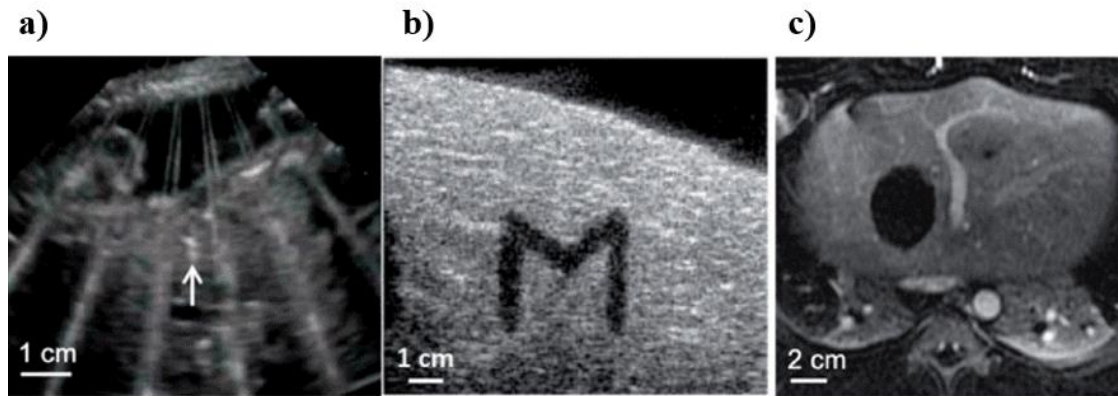


Figure 2.4: An example of targeted tissue ablation using histotripsy treatment **a)** B-mode ultrasound imaging with histotripsy generated cavitation, **b)** ‘M’ shape histotripsy lesion, **c)** MR imaging with histotripsy generated cavitation [119].

As it can be understood from the information mentioned so far, although histotripsy provides many new possibilities as a treatment method, there are still issues that need to be developed. Firstly, the difficulty of application on irregular shape and arrangement of cancer tissue. This may prevent focus and successful ablation of these type of tumors. In addition, taking into account the fact that this is achieved by the technician, the risk of misapplication of the treatment and ablation of the healthy cells, which are around the tumor tissue, increases due to human errors. In addition to these problems, ultrasound imaging used in histotripsy is not useful for each tumor. It is almost impossible to detect metastatic cancer cells with ultrasound, because the size of these cells is very small. For these reasons, it was aimed to develop a more effective treatment method with less side effects and nanoparticle mediated histotripsy (NMH) was discovered which uses the nanoparticles as cavitation nuclei to lower cavitation threshold pressure to have more selective ablation at the location that nanoparticles were accumulated [21].

2.5. Nanoparticles Mediated Histotripsy (NMH)

2.5.1. Nanodroplet mediated histotripsy

Nanoparticle mediated histotripsy (NMH) is focused to generate a histotripsy treatment method with lower pressure cavitation, targetability and selectivity. NMH uses the ultrasound active nanoparticles as cavitation nuclei instead of already existing gas pocket in the body. These nanoparticles contain the ultrasound active agent and they can make phase transition and form gas bubble to initiate cavitation under the US signals. Moreover, these nanoparticles have a tendency to selectively accumulate on tumor tissue

through EPR effect due to the size. Since they can accumulate and their concentration can locally increase, they can be active at only the location even if it is scanned a wider area by ultrasound which still create safer environment for neighboring healthy cells. In the early stage of the NMH research, nanodroplets (NDs) were developed as first nanoparticle for NMH. NDs are polymeric micelle containing ultrasound active agent in the core. For ultrasound active agent, perfluorocarbons are chosen because of the one of the best option for filled the NDs (see Perfluorocarbons section) [18]. As first agent of NMH, tri-block-amphiphilic co-polymer was synthesized. Since this co-polymer exhibits self-assembly properties because of having both hydrophilic and hydrophobic parts, hydrophobic PFC derivatives were encapsulated in the hydrophobic core of micelle in the aquatic environment. Their size was determined to be approximately 200 nm (**Figure 2.5 a**) that is sufficient for it to reach the tissues by entering the gap known as EPR effect seen in the tumor tissues. NDs made in the form of micelles with PFCs, which are known to have a low boiling temperature, passed from the liquid phase to the gas phase with US pulses and behaved like nanobubbles (**Figure 2.5 a**). Effective results were seen at much lower pressures, as it was intended to evaporate PFCs. In other words, even the cells around the tumor tissue i.e., neighbor cells of the targeted cells, will not be affected because of the low pressure of US pulses (**Figure 2.6**) [16]–[18], [128]. Previous studies have shown that PFC nanodroplets act as sustainable cavitation nuclei in the presence of multiple pulses. Additionally, they obtained well-defined and consistent fractionation even below the intrinsic threshold of the pressure levels of histotripsy in the tissue phantoms [15], [18].

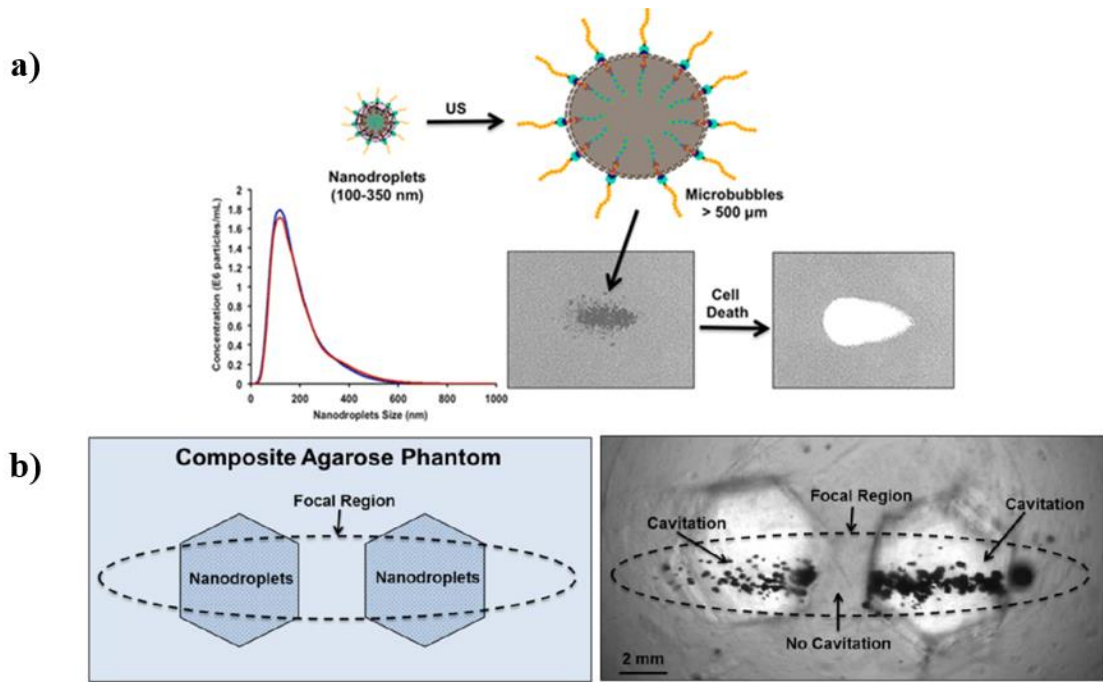


Figure 2.5: a) Cartoon picture of nanodroplet, nanodroplet after affected from US, graph of nanodroplets size at different concentration, b) A picture of selective nanodroplet cavitation in agarose tissue phantom [6].

Although NDs addressed the limitation of histotripsy and effectively lowered the cavitation threshold pressure, NDs had limitations as well. Some of these limitations are the undetectability of PFCs and their varying amount in each NDs. For creating an effective treatment method, these two factors are so important because losing PFCs or loading low concentration PFCs are directly related to the efficiency of treatment. In addition, maintaining the stability of NDs is another limitation because they should be stored in a cold environment. Another constraint is that for co-polymer synthesis, a competent person should synthesize the polymer with complex and multistep experiments. For this reason, there is a need for a practical, stable, and biocompatible agent with more comfortable storage conditions, in which the amount of PFC can be determined [21].

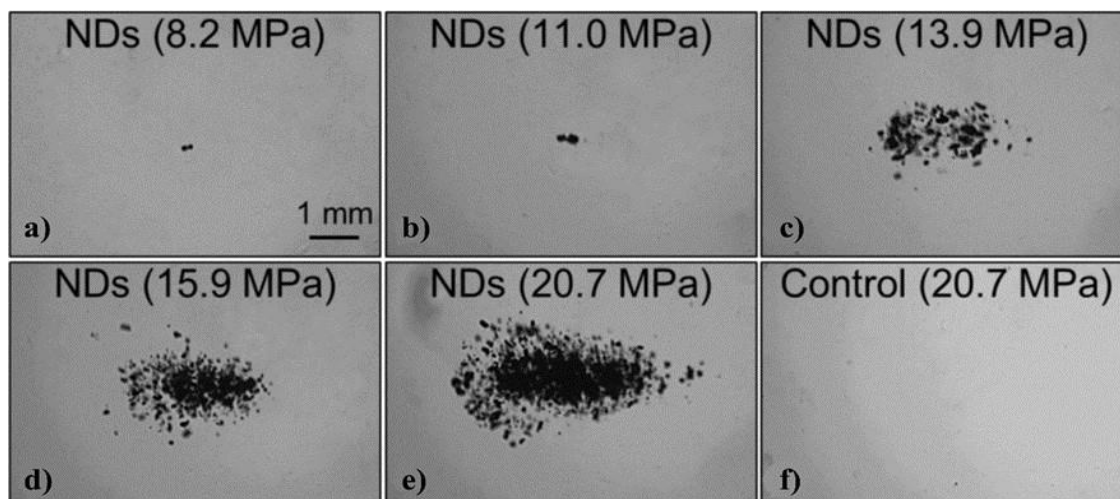


Figure 2.6: Efficiency of nanodroplet mediated histotripsy at different pressure with and without nanodroplet applied at the agarose tissue phantom. **a-e)** Efficiency of nanodroplet applied NMH on agarose tissue phantom, **f)** Efficiency of NMH on empty agarose tissue [18].

2.5.2. Nanocone mediated histotripsy (NMH)

It is aimed to develop a new agent due to the above mentioned limitations of NDs. For this reason, PFCs, which are known to be ultrasound active and mentioned in the previous sections, are intended to form inclusions complexes with cyclodextrins. This new structure was named 'nanocone' (NC) (**Figure 2.7 b**), based on the conical shape of the cyclodextrins [75]. Cyclodextrins were chosen for the 'host-guest' interaction with the US agent, both because the inner surface is hydrophobic and the interior volume is suitable for the localization of PFCs. The fact that it is FDA-approved and functions with many different reactions in the literature has also shed light on further studies and the possibilities of its development have been considered [14], [19], [21]. More detailed information about both PFC and CD can be found under their own headings.

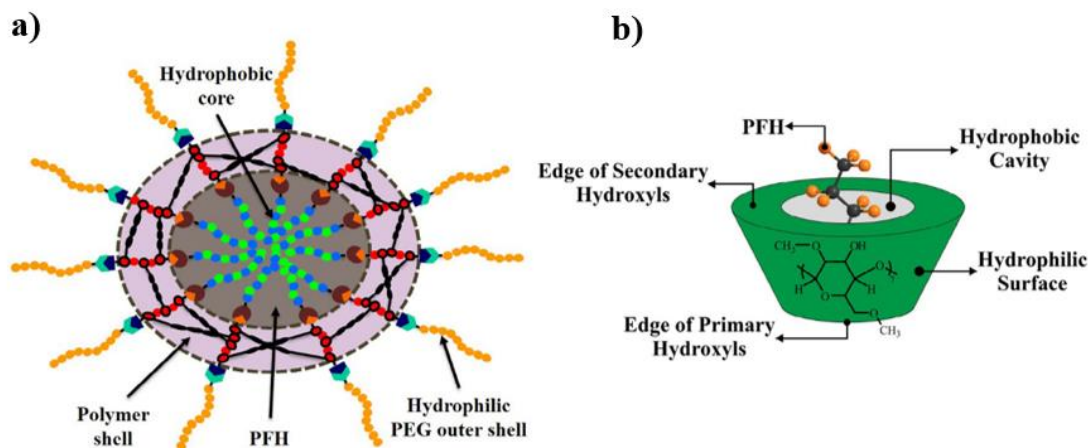


Figure 2.7: a) Nanodroplet used as US active agent for NMH, b) Nanocone used as US active agent for NMH [16].

In case of nanocone, PFCs are intended to penetrate the hydrophobic core of cyclodextrins by exploiting the hydrophobicity difference. For this reason, it must be prepared in water in order to create a hydrophilic environment. PFC is stabilized in the cavity of cyclodextrins due to the host-guest interaction and it is also ensured that they are obtained in solid form from the water mixed at a certain rate with the help of filtration. Storage conditions and stability of NCs has been naturally simplified compared to NDs because it is obtained in solid form. The amount of PFC in NCs can be determined by gas chromatography (GC) in anisole and trifluoroacetic acid (TFA) medium. Great advances have been made in terms of ease of synthesis and purification and also protection of the US agent. In addition, histotripsy studies were performed and it was still found to be an effective agent for NMH (**Figure 2.8 a**). In addition, PFC containing NCs were resulted smaller size than NDs that are suitable for tumor accumulation (**Figure 2.8 b**). Precursor cell studies of NCs have been carried out with CDs, which are currently FDA-approved and have many studies in the literature. At this study, hemolytic activity on fresh red blood cells and cell viability on HEK-293T healthy kidney cells were performed with NCs as new histotripsy agent. The obtained results are very promising as well as the pioneer of many new studies [14].

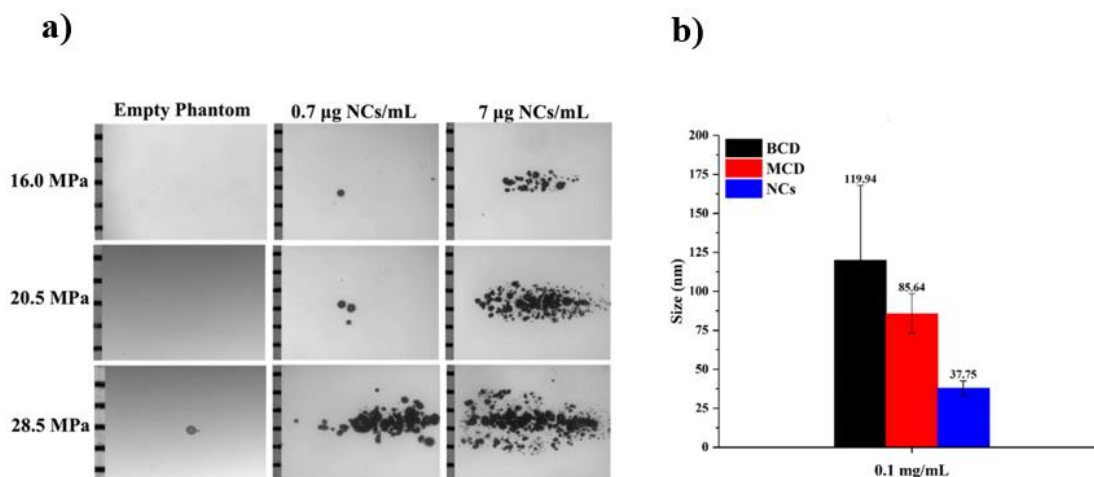


Figure 2.8: a) Generation of bubble cloud with and without NCs in the agarose tissue phantom, b) Size measurement using DLS device comparison of empty β CD, methylated- β CD, and NCs prepared at 0.1 mg/mL [17].

Recently, more effort has been shown to determine the most effective cyclodextrin and PFC combination. Following this purpose, the complex of cyclodextrins (β CD, LM β CD, HM β CD, HP β CD, α CD, γ CD, HP γ CD, HM γ CD), and PFCs (PFP, PFH) were computationally and experimentally tested with different ratio. It has been shown that almost all CD derivatives form inclusion complexes with PFC except α CD and HM γ CD because the interior space of α CD is not enough for inclusion complex formation and very wide cavity can not hold the PFC in case of HM γ CD. Complexes formed with cyclodextrin derivatives with high solubility could not be precipitated which precipitation is an effective way to obtain these ultrasound active agents as powder for further use. As a result of the studies, it was revealed that the complex made with β CD and PFH was the most ideal combination in terms of both stability and precipitation. Another important point that emerged in this study is the examination of the behavior of CDs and PFCs. While it was previously thought that one PFC was inserted into each CD molecule, computational data suggested another hypothesis. Accordingly, it showed that there are free PFCs located in the core surrounded by CDs and inclusion complexes of CD and PFCs. This structure was named the nanocone cluster (NCC), the clustering made out of inclusion complexes of cyclodextrin and PFC (nanocones) that is organized around free PFC core [20].

2.6. Bio-conjugation

Unraveling the diversity of living things and the complexity of their metabolism was one of the first research subjects that attracted the attention of scientists, and even today, studies on this subject continue with many unknown subjects. Discovering the importance of genes and proteins in living things was a very important step in these researches and revealed many new different research topics [129]–[131]. For this reason, research has been deepened and fast and reliable methods have been sought; bioconjugates have been discovered as a solution [132].

Bioconjugation is a type of conjugation in which at least one of the combining elements is a biomolecule, at least two molecules combine with a covalent bond to form a conjugate. The activity of the elements of bioconjugation is preserved as a result of conjugation, and the product formed as a result of the combination can create an effect that the components cannot do separately. In other words, the elements of bioconjugation have different functions. When these elements are combined, they can both fulfill these purposes and also can be used for a new purpose as a result of their combination. Functional groups are fundamental in the combination of these elements. These functional groups can be formed by modifications or present in their natural structure. These groups are linked with each other by compatible and complementary groups that are situated on the surface of the bioconjugation elements. The final biomolecule is synthesized with this binding. Intracellular mechanisms, diagnosis of diseases, and discovery and development of drugs; requires perfectly synthesized biomolecules, and need to be biocompatible, innovative, easy to penetrate, and traceable within the body [132], [133].

Bioconjugation is vital both for the understanding and recognition of proteins and living metabolism, and because it is one of the foundations of steps towards solving various problems [132]. During to bioconjugated materials, cellular events can be monitored, modifying proteins in this area is a very useful way. For example, when a fluorescently active structure binds to a protein, the position of the protein can be determined [134]. In another application, we can provide selective delivery of the drug to the cell by attaching a suitable protein to a material that we want to be delivered to a particular cell, for example, a cancer drug, to the targeted cell [135]–[137].

Generally, bioconjugates are formed by the covalent bonding of molecules from a biological and non-biological source. There are many different methods for

bioconjugation that can be formed with one biological source and one synthetic source, or with two biological sources [132]. A wide variety of bioconjugates can be synthesized, depending on the purpose and mechanism of usage. The elements of bioconjugation are chosen as polymer-drug, polymer-polypeptide, polymer-protein, polymer-nanoparticle, protein-protein, antibody-drug(ADC), lipid-drug, liposome-nanoparticle, nanoparticle-antibody, fluorescence imaging agent-drug, etc., [54], [132], [133], [138]. Polymers can be either synthetic or natural polymers [133].

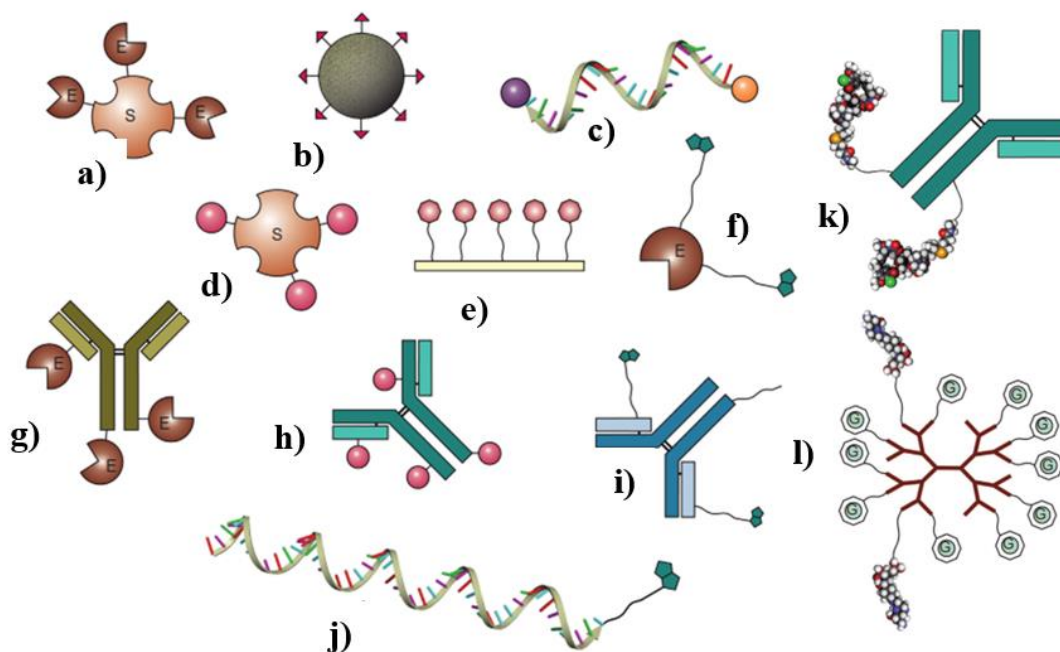


Figure 2.9: Some bioconjugates that are used commonly in literature. **A)** streptavidin-enzyme conjugation, **b)** ligand-particle conjugation, **c)** fluorescent labeled oligo molecular beacon probe, **d)** fluorescently labeled streptavidin, **e)** ligand conjugated particle, **f)** biotinylated enzyme, **g)** antibody-enzyme conjugation, **h)** fluorescently labeled antibody, **i)** biotinylated oligo probe, **k)** antibody-drug conjugation, **l)** chelate modified dendimer- folate conjugation [132].

There are many reasons why bioconjugation is needed. These may be to increase the solubility of the molecule in water, to follow the molecule, to ensure that the molecule is transported to the cell, to ensure that the molecule is attached to the cell, and even to protect it from enzymatic effects [23], [56], [134], [137], [139]. For these reasons, bioconjugates of natural and synthetic molecules have many applications in health research and bioengineering. Proteins are one of the most used structures, especially in the treatment of diseases that require selective transport [26], [132]. Protein bioconjugation can be done by many methods. There are many examples of modifications of cysteine and lysine in the literature. Thiol groups in cysteine can react with disulfides

to 'disulfide exchange', with α,β -unsaturated carbonyl compounds to 'Michael addition', with alkyl halides to 'alkylate' [140]. Lysine, on the other hand, can react with activated esters, sulfonyl chlorides, isocyanates and isothiocyanates. As a result, amides, sulfonamides, ureas and thioureas can be formed, respectively [141].

2.6.1. Bioconjugation reactions

Bioconjugation studies, which have many examples and are still under development, are in an endless process of creation. There are many bioconjugates that can be used for different purposes and are still being created. The most important thing during bioconjugate selection is the purpose of the study and the most precise and short-cut solution that can be achieved with this study. For this reason, the bioconjugation elements must also vary [132]. When examined comparatively, different transport and release systems are needed for cancer and hormone therapy. Firstly, cancer treatment is considered. One of the most common cancer drugs in the literature, doxorubicin, which is known to be extremely toxic, is targeted to be transported to the cancerous cell directly. A system that will not release doxorubicin until the drug enters the cancerous tissue and transport it to the targeted tissue very quickly is required for this transport system [54]–[56], [135]. On the other hand, the drugs used in hormone therapy should be released slowly and it should be left at an equal level until the next drug vaccination. If the system used in doxorubicin is used in hormone therapy, the patient will be exposed to the hormone drug on a high surface in a short time, and then the drug will be rapidly excreted from the body [142]–[144]. For this reason, it is very important to form bioconjugates following the purpose. In this context, appropriate elements should be selected according to the intended goal and the application field. Another important point is to combine these selected elements without toxic effects on the body. Therefore, many different bioconjugation reactions can be used [132].

Even though the variable parameters in bioconjugation reactions bring possible risks with itself, in general there are points to be considered in a bioconjugation reaction. The first point is that while the bioconjugates react with each other, they should not affect the intrinsic activity of the biomolecules. Otherwise, even if the aimed reaction is done, the treatment will not be effective because the biomolecule will lose its functionality. The second important point is the determination of conjugated biomolecule amount onto the drug after obtaining the bioconjugation reaction. In this way, a useful treatment method

can be developed by preventing possible non-binding of bioconjugation elements, increased toxic properties, and failures in the delivery/targeting system. Another important feature is that the bioconjugates and the bonds formed as a result of bioconjugation should be stable in physiological conditions. It is obvious that an effective treatment drug, that cannot maintain its stability after being treated in the body, cannot come through. In some cases, it can even lead to life-threatening situations. As an example, a toxic cancer drug loses its stability in the non-targeted tissue and becomes active, creating a destructive effect on healthy tissues. Bioconjugation reactions should be controllable in aqueous media and the reaction must be rapid and stoichiometrically efficient [132]. Biomolecules should be easily incorporated onto the structure during synthesis [133]. Various elements that can cause degradation of the biomolecules involved in the structure (such as oxidizers, reducers, etc.), should not be present. Finally, bioconjugates should not form non-targeted bonds with any structure in the biological system. Binding of drug delivery agents to a tissue, other than the targeted tissue, may lead to unsuccessful therapy, and in some cases may affect cell activity [132].

Highly preferred functional targets for creating bioconjugates are; amino acids, peptides, proteins, sugars, polysaccharides, glycoconjugates, nucleic acids and oligonucleotides. The most used reactions during bioconjugation are amine reactions (carbodiimides, anhydrides, NHS esters, tosylate esters, etc.), thiol reactions (vinyl sulfone derivatives, thiol-disulfide exchange reagent, aziridines, haloacetyl and alkyl halide derivatives, etc.), carboxylate reactions (N'-N'-carbonyl diimidazole, diazoalkanes and diazoacetyl compounds, carbodiimides), hydroxyl reactions (epoxides and oxiranes, alkyl halogens, isocyanates, etc.), aldehyde and ketone reactions (hydrazine and hydrazone derivatives, reductive amination, mannich reaction), etc.), photochemical reactions (benzophenones, diazirine derivatives, etc.), cycloaddition reactions (diels-alder reactions, click chemistry, etc.) [52], [53], [132], [134], [141], [145]. The topics of the wide variety of bioconjugation reactions that are important to this article are described below.

2.6.1.1. Amine and carboxylic acid group reaction: carbodiimide

Amine and carboxylic acid reactions, which are bioconjugation reactions between the amine and carboxyl group, were chosen as most commonly used example. EDC and NHS are used as catalysts in the reaction between the primary amine and the active carboxyl group (**Figure 2.10**). Amine-acid reactions are essential for bioconjugation, as it contains

especially amine groups which is generally main reactive group for bioconjugation reactions.

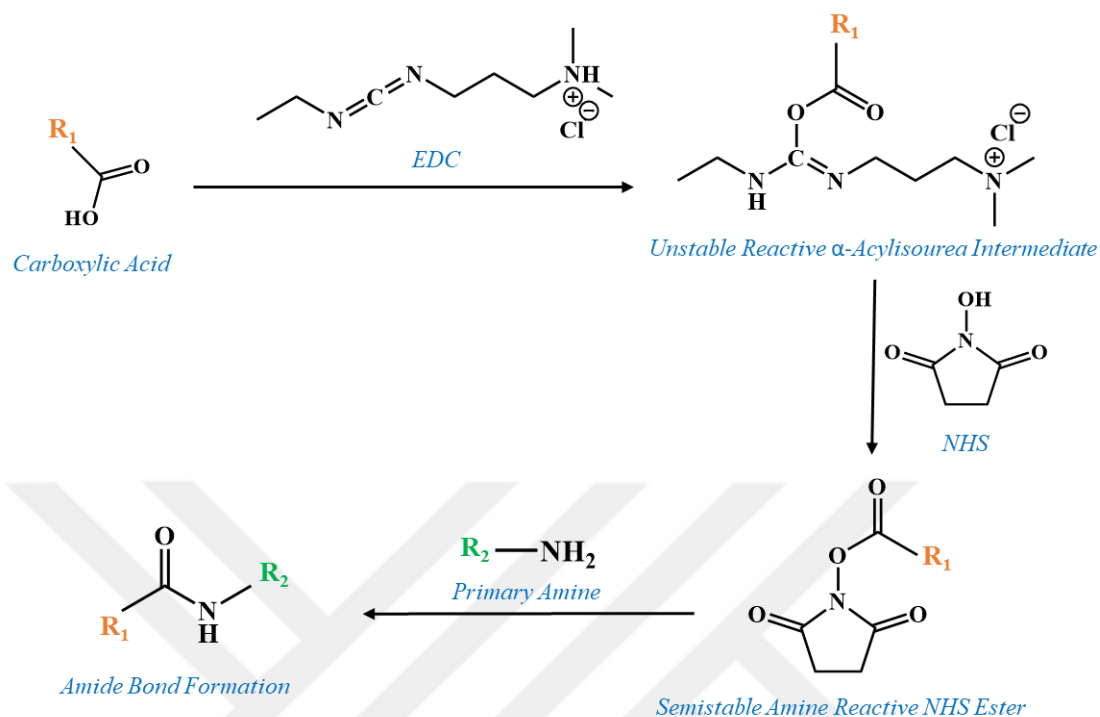


Figure 2.10: The mechanism of carbodiimide reaction between carboxylic acid and primer amine reaction using EDC-NHS catalyzed.

Antibodies are suitable agents for the drug delivery system as they have a specific and strong binding affinity. An antibody offers many flexible options for the bioconjugation reaction. Wang et al. studied the possible bioconjugation reactions that can occur between antibodies and nanocarriers (**Figure 2.11**). One example of this conjugation is the reaction between antibodies and nanocarriers. For this purpose, the acid terminated antibody is first activated with EDC. This intermediate product is formed put into reaction with the NHS and then active NHS-IgG antibodies are obtained. NHS-IgG antibodies react with the primary amine-terminated nanocarrier; Cs-NH₂. As a result of this study, the conjugation between the antibody and nanocarrier were successfully achieved by this amide bond synthesis [138].

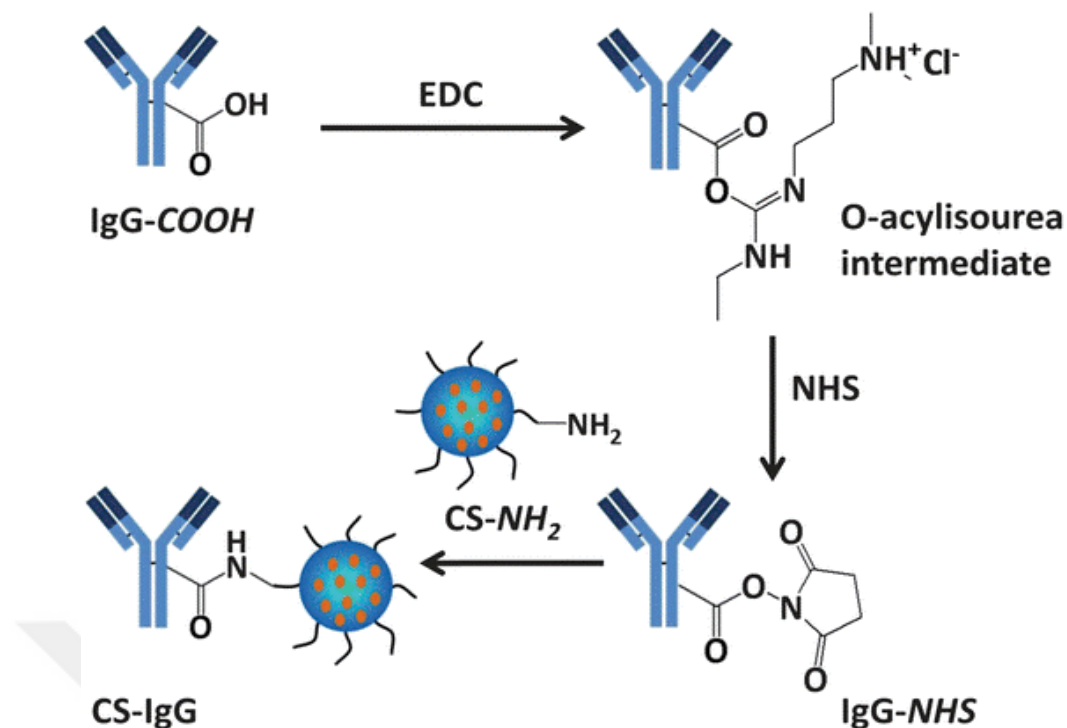


Figure 2.11: Synthesis of antibody conjugation onto nanocarriers using carbodiimide reaction [138].

Another example, it can be given to conjugation between folic acid (FA) with CDs, which are used for drug delivery system and this thesis too. As a first step, the carboxyl group in FA was activated with NHS and EDC catalyze system and an intermediate form was obtained. This intermediate form was mixed with commercial cyclodextrin with one hydroxyl group changed to amine, and conjugation was accomplished in high yield in a short time. The potential cancer drug, docetaxel, was cavitated into the interior of the CD and then entry into FA-active cells was studied. The result of the study was promising both in terms of conjugation and its effect on cells [23].

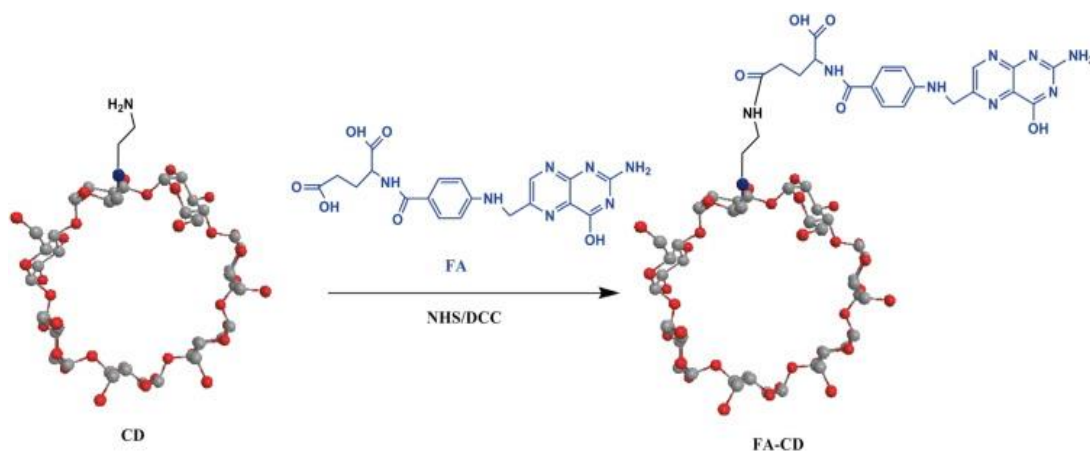


Figure 2.12: The synthesis of FA conjugated cyclodextrin [23].

As Hermanson clearly states in his book 'Bioconjugation Technique', the two-stage EDC/NHS catalyzed conjugation reaction happens with high yield. Although there are problems such as rapid collapse-precipitation during the binding of proteins, the fact that it is realized with high efficiency and the problems encountered are solvable have made this mechanism very useful [132].

2.6.1.2. Copper-catalyzed azide-alkyne cycloaddition: click chemistry

Click chemistry is a type of conjugation that is widely used especially in organic chemistry and polymer chemistry and is known for its speed and high efficiency (**Figure 2.13**). It is divided into two as Copper Free and Copper Catalyzed. Copper-catalyzed versions can be realized in organic solvents, or the solvent can be used as water. It is necessary to use suitable catalysts according to the solvent structure. Cu(I)-containing catalysis is usually carried out in organic solvent using the degases mechanism called 'Freeze-Pump-Thaw'. The reactions that take place in the aquatic environment, on the other hand, generally prefer the inert gas bubble as degases in Cu(II) catalysis [146].

Click chemistry is used a lot in the field of polymer and organic synthesis, as well as in bioconjugation. An azide-terminated protein can be attached to an alkyne-terminated target and vice versa. Organic chemistry synthesis basis is used during the construction of this reaction, which takes in high yield. There are numerous examples in the literature; there are many types among these, such as protein-target conjugation, PEGylation, imaging agent conjugation, enzyme-enzyme conjugation [52], [145]–[150].

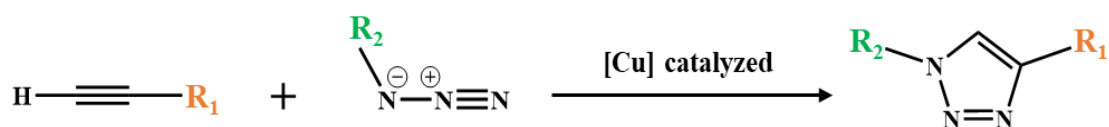


Figure 2.13: General equation of copper catalyzed 'click' chemistry.

In the study of Zhang et al., potential inhibitor pairs were combined with copper-catalyzed azide-alkyne 'click' for conjugation of enzymes (**Figure 1.14**). When the appropriate pairs of synthesized enzymes conjugated, they combined with the enzyme through two different pathways and inhibited the enzyme. As in many similar studies, copper-catalyzed azide-alkyne 'click' conjugation is carried out with high efficiency and reliability [146].

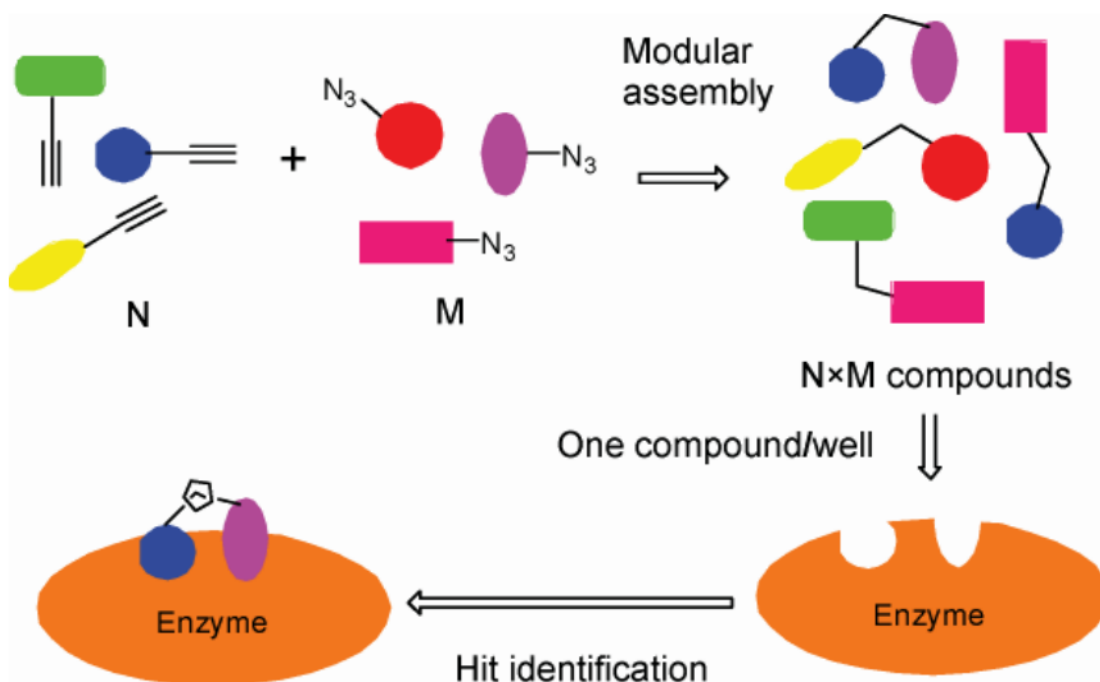


Figure 2.14: A Bioconjugation application of 'click' reaction [146].

PEGylation is the most widely used bioconjugation method. By this means, the water solubility of many drugs is increased, their excretion from the body is facilitated and their toxic effects are reduced. 'Click' conjugation is one of the most used methods in PEGylation. For this reaction, an azide or alkyne-linked PEG polymer is synthesized and then attached to the target. One of the studies on this subject is Antoniuk et al. Accordingly, as a first step, a cyclodextrin with a mono azide at the end was synthesized. Then, PEG with an alkyne group at the end was conjugated. As a result of this reaction, the analyzes were completed and it was shown with analysis that pure PEG-CD was obtained. Increasing the water solubility of CD, which tends to form aggregates, is a very important parameter. Studies carried out in this direction have resulted in success [151].

CHAPTER 3

3. EXPERIMENTAL PART

3.1. Materials

Materials used were imidazole (Sigma-Aldrich, 99%), p-toluene sulfonyl chloride (Sigma-Aldrich, 98%), sodium hydrogen carbonate (NaHCO_3 , Alfa Aesar, 99%), sodium sulfate anhydrous (Fisher Bioreagents, 99%), sodium hydroxide (NaOH, Merck, 98%), beta cyclodextrin (βCD , Sigma-Aldrich, 97%), ammonium chloride (Sigma-Aldrich, 99%), sodium azide (NaN_3 , Sigma-Aldrich, 99%), 1,1,2,2-tetrachloro ethane (Sigma-Aldrich, 98%), propargylamine (Sigma-Aldrich, 98%), copper (I) bromide (CuBr , Sigma-Aldrich, 98%), *N,N,N',N'',N'''*-pentamethyldiethylenetriamine (PMDETA, Sigma-Aldrich, 99%) triphenylphosphine (Ph_3P , Sigma-Aldrich, 99%), N_3 -EPPT1-FAM (NH_2 -5-FAM-AHX-YCAREPPTRTFAYWGK-azido-homoalanine, 95.18% Primm SRL, Italy), EPPT1 (YCAREPPTRTFAYWG, C terminus capped, N terminus free >95%, Metabion International AG, Germany), alkyne-PEG-NHS (3000 g/mol, Rapp Polymere), methoxy capped-PEG (2000 g/mol, Sigma Aldrich), copper(II) sulfate pentahydrate (Sigma-Aldrich, 98%), sodium L-ascorbate (Sigma-Aldrich, 99%), folic acid (Sigma-Aldrich, >97%), N-(3-dimethylaminopropyl)-N'-ethylcarbodiimide hydrochloride (EDC, Sigma-Aldrich), N-hydroxysuccinimide (NHS, TCI, 98%), fluorescein isothiocyanate (FITC, Sigma-Aldrich, >90%), Pierce™ Coomassie (Bradford) Protein Assay Kit (23200, Thermo Fisher Scientific), Hoechst 33342 (H3570, Invitrogen™), perfluorohexane (PFH, Sigma-Aldrich, 99%), aluminum oxide (neutral, Sigma-Aldrich), dimethyl sulfoxide anhydrous (DMF, Sigma-Aldrich, 99.8%), acetone (Sigma-Aldrich, 99.5%), diethyl ether anhydrous (Sigma-Aldrich, 99%), acetonitrile (Rankem, 99%), tetrahydrofuran, anhydrous (THF, Sigma-Aldrich 99%), triethylamine (TEA, J.T.Baker, >99.5%), diethyl ether anhydrous (J.T.Baker, 99%), dichloromethane anhydrous (DCM, Sigma-Aldrich, 99%), hexane (Sigma-Aldrich, >95%) were used as received.

3.2. Characterization

^1H (500 MHz) and ^{13}C (125 MHz) spectra were recorded using an Agilent VNMRs 500 instrument in CDCl_3 , d-DMSO, and D_2O with $\text{Si}(\text{CH}_3)_4$ as internal standard. The particle size and zeta potential of NCC derivatives were determined in distilled water by dynamic light scattering (DLS) using Malvern Zetasizer Nano ZSP. PFH amount inside of NCC were detected using gas chromatography (GC) Agilent Technologies 7820A GC system using previously published method [20]. Fourier transform infrared (FTIR) spectra were recorded on an Agilent Technologies Cary 630 FTIR instrument using attenuated total reflectance (ATR) mode, over the range $4000\text{--}400\text{ cm}^{-1}$. For SEM imaging, samples were prepared by mounting them on double adhesive carbon-coated tape on aluminum stubs. Samples were coated with Gold/Palladium for 10s and then introduced to Gemini 500 SEM with EDX detector. SEM images were taken at 50,000 X at 5 kV whereas Carbon (C), Oxygen (O) and Fluorine (F) elemental percentages were measured at 1000 X at 20 kV with C and F traces shown as vital elements in EDX analysis. Thermogravimetric analyses (TGA) were done by using TGA 8000, Perkin Elmer instrument, under N_2 atmosphere with $10\text{ }^\circ\text{C}$ per minute heat rate, between $30\text{--}800\text{ }^\circ\text{C}$. UV-Vis absorption measurements were recorded using Shimadzu UV-1800 spectrophotometer in CH_2Cl_2 wherein particles were excited at 345 nm and emission recorded. SpectraMax® i3, Molecular Devices LLC plate scanners were used for spectroscopic analysis of 96 well plates. The mass spectra were recorded using a Shimadzu LC-MS 2040 C mass spectrometry system equipped with an Electrospray Ionization (ESI) source operating in positive mode (Kyoto, Japan).

3.3. Synthesis of β CD Derivatives

3.3.1. Synthesis of tosyl cyclodextrin (Ts- β CD)

3.3.1.1. Synthesis of tosyl imidazole (Ts-Im)

Imidazole (12 g, 0.17 mol), p-toluene sulfonyl chloride (35.3 g, 0.18 mol) and 100 mL DCM were mixed in an erlenmeyer with a magnetic stirrer. TEA (2.69 ml, 0.02 mol) is added the mixture after the addition of the 200 mL aqueous NaHCO_3 (18.5 g, 0.22 mol) solution. The reaction mixture was stirred for 24 h at room temperature before the separated with separation funnel and dried with sodium sulfate anhydrous. The DCM was removed with evaporator from the resulting solution and hexane was added for the

crystallization in fridge. The final product, dried under reduced pressure, was obtained as yellow-white solid.

3.3.1.2. Synthesis of tosyl cyclodextrin (Ts- β CD)

β CD (10 g, 9 mmol) and 250 mL deionized water were mixed at 60 °C in a round-bottomed flask with a magnetic stirrer until turned to clear solution. After the cooling down, tosyl imidazole (7.83 g, 0.035 mol) was added and unclear solution was mixed for 2 hours at room temperature. The mixture of 4.58 g NaOH and 25 mL deionized water was added to the reaction solution using with dropping funnel. After the adding ammonium chloride (11.78 g, 0.22 mol), reaction solution was mixed overnight at room temperature. The resulting solution was filtered and washed with cold water and cold acetone. The final product, dried under reduced pressure, was obtained as white solid.

3.3.2. Synthesis of mono-6-deoxy-6-aminopropargyl-cyclodextrin (alkyne- β CD)

Ts- β CD (200 mg, 0.155 mmol) was solved with DMF under inert atmosphere in a round bottom flask with magnetic stirrer at room temperature. Propargyl amine (377.6 μ L, 5.89 mmol) was added and mixed with condenser at 60 °C for 24 h. The resulting solution was precipitated with acetonitrile at several times. The final product, dried under reduced pressure, was obtained as white solid.

3.3.3. Synthesis of mono-6-azido-6-deoxy-cyclodextrin (azide- β CD)

Ts- β CD (4.48 g, 3.47 mmol), NaN₃ (4.52 g, 69.4 mmol) and 300 mL deionized water were mixed in a round bottom flask with magnetic stirrer and condenser at 100 °C for 24 h. After the filtration of solution at room temperature, the filtered solution was concentrated to 30 ml. 1,1,2,2-tetrachloroethane (5.46 g, 51.61 mmol) was added the solution with dropping funnel and mixed the solution for 1 hour. The resulting solution was centrifuge at 4 °C, 3500 rpm for 25 minutes and take the white phase. The final product, dried under reduced pressure, was obtained as white solid.

3.3.4. Synthesis of mono-6-amino-6-deoxy-cyclodextrin (amine- β CD)

N₃- β CD (1g, 0.862 mmol), PPh₃ (0.25g, 0.948 mmol) and 25 mL DMF were mixed at 3 h under inert atmosphere at room temperature in a round bottom flask with magnetic stirrer. 1 mL deionized water was added the system and mixed the reaction solution at 90 °C at 3 h with condenser. After the removing water using with N₂ gases, acetone was

added the system and cooled down in the fridge for 15 min. For the separation of phases, resulting product was centrifuged. The final product, dried with freeze drying machine, was obtained as white solid.

3.4. Synthesis of Functional Nanocone Clusters (NCC)

Alkyne-NCC, azide-NCC, and amine-NCC were synthesized as functional NCC. 20 mg (20% w/w) monofunctional- β CD (azide- β CD or alkyne- β CD or amine- β CD), 80 mg (80% w/w) β CD were solved in double-distilled water (5 mL for β CD, 5.5 mL for alkyne- β CD, 6 mL for azide- β CD, and 5.5 mL for amine- β CD) at 60 °C stirring at 1,000 rpm to ensure the solubility of monofunctional- β CD derivatives. After obtaining a clear solution, it was allowed to reach room temperature in order to prevent the evaporation of PFH once it is added. After PFH (86.3 μ L for alkyne-NCC, 87.3 μ L for azide-NCC, and 89.3 μ L for amine-NCC) was added to the solution and stirred overnight in an ice bath, the solution was taken and centrifuged at 4 °C. The supernatant was decanted, and the resulting solid was dried under vacuum. Non-functional NCC using native β CD was prepared as a control based on previously published protocols [19], [21], and characterized with FTIR, DLS, MS, TGA, SEM, and EDAX. Yield of alkyne-NCC: 60%, the yield of azide-NCC: 66%, yield of amine-NCC: 64%.

3.5. Synthesis of Bio-Conjugated Nanocone Clusters (NCC)

3.5.1. Synthesis of folic acid conjugated nanocone cluster (FA-NCC)

For the preparation of 2.5% folic acid-conjugated NCC, it was assumed that all amine- β CDs are in NCC as 20% (w/w) and 2.5 mol percent of the amine groups were targeted for conjugation. The procedure shared previously by Hu et al. was modified [23]. Folic acid (FA) (2.5 eq., 0.0734 mg) was dispersed in 600 μ L double-distilled water. Then, EDC (3 eq., 0.04 mg) and NHS (6 eq., 0.046 mg) were added to the solution and it was stirred at 1000 rpm for 2 h in the dark at room temperature to activate the carboxyl groups of FA. The synthesized amine-NCC (100 eq. corresponds to amine mole of 20% (w/w) amine- β CD in NCC, 40 mg) was added to the system and the resulting reaction mixture was allowed to proceed for 4 h. Then, the solution was centrifuged at 9,600 rpm for 1 min to collect FA-NCC as precipitated and wash out the other reagents. The precipitate was washed several times with small amount of double-distilled water and centrifuged. FA

conjugated NCC was collected as yellow precipitate and dried under vacuum and characterized by UV-Vis spectroscopy and FTIR (Yield: 50%).

3.5.2. Synthesis of EPPT1 peptide conjugated nanocone cluster (EPPT1-NCC)

FAM-labeled, azide end functional EPPT1 peptide is conjugated into alkyne-NCC via 'click' reaction. Different mol percent (1, 2.5, 5 and 10) EPPT1 peptide were aimed to conjugate on alkyne-NCC by considering the total mole of alkyne- β CD thought to be in NCC. To target 1% EPPT1 on NCC; alkyne-NCC (100 eq., corresponds to alkyne mole of 20% (w/w) alkyne- β CD in NCC, 50 mg) was dispersed in double-distilled water (500 μ L) at room temperature and azide-EPPT1 peptide (1 eq., 0.168 mg), CuSO₄ (1.5 eq., 0.025 mg) and sodium ascorbate (1.5 eq., 0.02 mg) were added on this dispersed solution and degassed by nitrogen bubbling. The solution was stirred for 4 h at room temperature in the dark. After completion of the 'click' reaction, the reaction mixture was centrifuged at 9,600 rpm for 2 min to precipitate the product and CuSO₄ /sodium ascorbate system was removed from the solution by washing several times with small amount of double-distilled water. EPPT1-conjugated NCC was obtained as yellowish solid powder and was dried under vacuum (Yield: 60%).

3.5.3. Synthesis of PEGylated nanocone cluster (PEG-NCC)

Alkyne-PEG₂₀₀₀ was synthesized via esterification reaction of methoxy capped-PEG and 4-pentynoic acid based on previously published protocols [17]. 2.5 mol percent of azide was aimed to be conjugated with PEG in azide-NCC. Alkyne-PEG₂₀₀₀ (2.5 eq., 0.41 mg), azide-NCC (100 eq. corresponds to azide mole of 20% (w/w) azide- β CD in NCC, 61 mg), CuSO₄ (2.5 eq., 0.051 mg), and sodium ascorbate (2.5 eq., 0.04 mg) were dissolved in 500 μ L double-distilled water at room temperature and degassed by nitrogen bubbling. After 4 h of stirring at room temperature, the solution was centrifuged at 12,600 rpm at 5 min at 4 °C. The precipitate was washed several times with 100 μ L double-distilled water and centrifuge. The precipitate was dried under vacuum overnight and characterized (Yield: 37%).

3.5.4. Synthesis of EPPT1 peptide-PEG conjugated nanocone cluster (EPPT1-PEG-NCC)

Alkyne-PEG-NHS (1.1 eq, 16.35 mg), NH₂-EPPT1 peptide (1 eq, 9 mg), EDC (1 eq, 0.95 mg), and NHS (0.5 eq, 0.29 mg) were dissolved in pH 8.2 PBS solution and stirred for 24

hours at 37 °C. After 24 hours, reaction mixture was transferred into a dialysis bag with 1 kDa cut-off value and dialyzed against first PBS solution to remove unreacted EDC and NHS from the system then dialyzed against water to remove salts from PBS solution. The resulting solution was lyophilized and characterized by ¹H-NMR spectroscopy (Yield: 92.4%).

Azide-NCC (100 eq. corresponds to azide mole of 20% (w/w) azide-βCD in NCC, 50 mg) was dispersed in double-distilled water (500 μL) at room temperature. Alkyne-PEG-EPPT1 (2.5 eq., 0.78 mg), CuSO₄ (2.5 eq., 0.04 mg) and sodium ascorbate (2.5 eq., 0.033 mg) were added on this dispersed solution respectively, and degassed by nitrogen bubbling. The solution was stirred for 4 h at room temperature. After completion of the reaction the solution was centrifuged at 9,600 rpm for 2 min to precipitate the EPPT1-PEG-NCC and the catalytic system was removed by multiple wash and centrifugation steps. EPPT1-PEG-NCC was obtained as white solid powders and was dried under vacuum (Yield: 25%).

3.5.5. Synthesis of FITC labeled nanocone cluster (FITC-NCC)

Alkyne-NCC (100 eq. corresponds to alkyne mole of 20% (w/w) alkyne-βCD in NCC, 60 mg.) was dispersed in 1 mL double-distilled water, and FITC (2.5 eq., 0.087 mg) was added to the NCC suspension. After 4 h stirring, centrifugation at 9,600 rpm was done, and the precipitate was washed with 200 μL double-distilled water several times to remove non-reacted FITC and catalyst system. The resulting precipitate was dried under vacuum and protected from light exposure (Yield: 60%).

3.6. Determination of Peptide Percentage on the Targeted NCCs

3.6.1. Determination of peptide percentage via Ellman's assay

The percent of conjugated EPPT1 was calculated using Ellman's reagent that uses the thiol group in the peptide to quantify the peptide amount in the system. 50 μL, 50 μM DTNB solution, 100 μL 1 M Tris solution, and 840 μL double distillation water were mixed with EPPT1 peptide as different EPPT1 peptide concentration (0-10 μL/mL). After 5 minutes incubation in room temperature, 200 μL mixture was seeded 96 well plate as triplicate, and measured the absorbance at 412 nm to create calibration curve at different EPPT1 peptide concentration. As the same method, EPPT1-NCCs were prepared as 5

$\mu\text{g/mL}$ solution, and UV-Vis absorption of each well was measured and collected data were used for determination peptide amount onto the NCCs.

3.6.2. Determination of peptide amount via Bradford assay

Other detection method of peptide was Bradford Assay. 660 μL Bradford Reagent was mixed with different amount of EPPT1 peptide solutions (0-10 $\mu\text{L/mL}$) that were already solved with PBS solution to create the calibration curve at different free EPPT1 peptide concentration. After 10 minutes incubation in room temperature, 200 μL of the mixture was seeded 96 well plate as triplicate, and measured the absorbance at 595 nm. Bradford reagent was added to EPPT1-NCCs prepared as 13.2 $\mu\text{g/mL}$ solution, and UV-Vis absorption of the solution was measured and collected data were used for determination of peptide amount on the NCCs.

3.7. Determination of FITC Percentage on the Fluorescence Labeled NCCs

1 mg FITC was solved 10 mL PBS as stock solution and different concentrations (0-15 μM) FITC solution were obtained by dilution. Each concentration seeded as 200 μL into the 96 well plate as triplicate and measured the absorbance at 490 nm to build a calibration curve for free FITC. To determine the FITC or FAM concentration in labeled FITC-NCCs and EPPT1-NCCs, their 0.5 $\mu\text{g/mL}$ solution in PBS were prepared and UV-Vis absorptions were measured. The collected data were used for determination of FITC amount in the related NCCs.

3.8. Determination of PFH Amount in the NCCs

The amount of PFH was detected using GC based on previously published method [20]. Initially, a calibration curve using different amount of PFHs in 400 μL TFA and 4 μL anisole were build. Known concentration of NCC solution were prepared in same solvent system and injected into system. Detected PFC signal was compared with anisole signal as internal standard to quantify the amount of PFC in each mg of NCC.

3.9. Cell Culture Procedure

Healthy human fibroblast lung cell line (MRC-5), human epithelial cervical carcinoma cell line (HeLa) and human epithelial breast cancer cell line (MCF-7) were maintained in

DMEM medium which supplemented with 10% fetal bovine serum (FBS), 1% MEM non-essential amino acids, 1% Penicillin/Streptomycin and incubated 37 °C with 5% CO₂. Human epithelial breast cell line (MCF-10A) was cultured by using mammary epithelial cell growth basal medium (MEBM™) and Single Quots™ kit at physiological conditions. All cell lines were cultured in T75 flasks, once 70-80% confluency is reached cells were washed with PBS and passaged by Trypsin/EDTA solution. Cells were counted by using trypan blue staining with a hemocytometer and seeded into required dish in accordance with the assay protocols.

3.9.1. Hemocompatibility of functional and bioconjugated NCCs

Hemolytic activities of the NCC were tested on red blood cells (RBC). 5 mL whole blood that is donated by a volunteer was centrifuged for 5 min at 3500 rpm, serum was removed, and equal volume of an isotonic saline solution (0.15 M) was added. Solution was centrifuged under these conditions and the process was repeated 3 times. RBC were diluted 10 folds using to PBS at pH 7.4, and 10⁸ cells were obtained in 200 μL solution.

Stock solutions of NCCs were prepared in PBS and mixed with 200 μL of RBC at 0.01, 0.1 and 0.5 mg/mL concentrations in a total volume of 1 mL in micro tubes as triplicates. After incubation at 37 °C for 1 hour, tubes were centrifuged at 13,000 rpm and 200 μL of supernatants were transferred to a 96-well plate followed by absorbance reading of each well at 541 nm. While 1% Triton X-100 solution treated cells used as positive control, untreated RBCs were used as negative control. Percent hemolysis induced by NCCs were calculated by equation below (3.1).

$$\text{Hemolysis \%} = \frac{\text{Test Well} - \text{Negative Control}}{\text{Positive Control} - \text{Negative Control}} \times 100 \quad (3.1)$$

3.9.2. The effect of functional and bioconjugated NCCs on cell viability

MTS ([3-(4,5-dimethylthiazol-2-yl)-5-(3-carboxymethoxyphenyl)-2-(4-sulfophenyl)-2H-tetrazolium]) assay was used to determine the cell viability of lung fibroblast (MRC-5) and breast epithelial (MCF-10A) cells against NCCs. 10,000 cells were seeded in the 96-well plate and incubated for 24 h at 37 °C with 5% CO₂. NCCs stock solutions were prepared in PBS and diluted with FBS free growth medium at 0.01 mg/mL, 0.1 mg/mL, 0.2 mg/mL, and 0.5 mg/mL concentrations in triplicates and incubated on the seeded cells for 24 h under physiological conditions. After incubation time NCCs containing medium

was removed, cells were washed with PBS then 10 μ L MTS reagent was applied on the cells in 100 μ L culture medium, incubated for 2 hours. Untreated cells incubated with MTS reagent was used as positive control where reagent free untreated cells used as negative control. For obtaining viability data, UV absorption of each well was recorded at 490 nm and collected data were used for calculation of cell viability by the equation that given below (3.2).

$$\text{Cell Viability \%} = \frac{\text{Test Well} - \text{Negative Control}}{\text{Positive Control} - \text{Negative Control}} \times 100 \quad (3.2)$$

3.9.3. Cellular uptake using confocal fluorescence microscopy

The cellular internalization of FAM labeled targeted EPPT1-NCC and FITC labeled non-targeted FITC-NCC into MCF-7 cancer cells and MCF-10A healthy cells were evaluated using confocal microscopy for different mole % conjugation at different concentrations. 200,000 cells were seeded in glass bottomed 35 mm petri dishes and incubated for 24 h at 37 °C and 5% CO₂. Since FAM and FITC show identical optical absorption, different mole % FAM labeled EPPT1 conjugated EPPT1-NCC and FITC conjugated NCC were dispersed in PBS solution at the equal FAM or FITC fluorophore concentration and applied in fresh medium onto the cells. After 4 h incubation, free materials in the medium were removed and the cells were washed with PBS for two times. Hoechst dye was applied in 1 mL fresh medium onto the cells for 10 minutes to stain the nucleus. The images were collected by using Zeiss Plan-Apochromat 40x/1.3 oil objective and analyzed by Zeiss Zen Lite 3.3 Software (FAM/FITC $\lambda_{\text{Ex}}/\lambda_{\text{Em}}=495/519$ nm, Hoechst $\lambda_{\text{Ex}}/\lambda_{\text{Em}}=348/455$ nm).

3.9.4. Cellular uptake using flow cytometry

Cellular uptake of EPPT1-NCCs were determined by flow cytometry analysis. Cellular entry of EPPT1-NCC into MCF7 were analyzed by comparing it to non-targeted FITC-NCC at the equal number of fluorophores. MCF-7 cancer cells were seeded in 6 well plates at a density of 300,000 cell/well in growth medium and incubated overnight for adherence. Following day NCCs at different percentage were applied in fresh medium and incubated for 4 hours. Following incubation time cells were washed twice with PBS and detached by Trypsinization for 5 minutes. Detached cells were collected with medium and washed with PBS, after centrifugation cells were dispersed in 2% FBS containing PBS, passed through 40 μ m cell strainer into a tube and stored on ice in dark. Cell

suspensions were analyzed by BD Influx™ cell sorter device and their FITC fluorescence intensities were recorded for 10,000 events.

3.9.5. Cellular uptake using lysis method

HeLa and MCF-7 cancer cell lines were chosen as folate receptor active and inactive cells, respectively. The cells were seeded in 6 well plates at a density of 300,000 cell/well in growth medium and incubate 24h at 37 °C in 5% CO₂. FA-NCCs that were prepared in PBS as having same folate concentration, were applied onto the cells with fresh medium and incubated at 4 hours. Following incubation time, cells were washed twice with PBS solution and trypsinized for 5 minutes then detached from dish surface and collected with growth medium into centrifuge tubes. Then the cells were washed with PBS and centrifuged one more time. Supernatant was removed from the tubes and cells pellets were dispersed in %1 Triton X-100 solution in PBS. Tubes were incubated 15 min at room temperature to complete lysis and centrifuged at 13,000 rpm to remove cell debris. Supernatant was transferred into a 96 well plate and their UV absorption at 250 nm were recorded as triplicates and cell contains FA concentrations were determined by using a calibration curve made based on the absorption of free FA at different concentration.

3.10. Histotripsy Cavitation Threshold Study

Previously described tissue mimicking agarose phantom was used to test the histotripsy efficiency [6], [15]. To determine the cavitation threshold pressure of functional and bioconjugated NCC for NCC-mediated histotripsy, NCCs were embedded into agarose phantom at same PFH concentration. First, air free 1% w/v agarose phantom was prepared by mixing agarose powder (Type VII-A, Sigma Aldrich, St. Louis, MO, USA) and saline solution at 70 °C until obtained clear mixture and 20.5 mmHg vacuum was applied at 40°C for 30 minutes. NCCs dispersed in PBS were added to agarose solution once it has cooled down to 37°C. The prepared agarose mixtures were poured into rectangular polycarbonate holders and sustained at 4 °C. As a control empty tissue phantom was used and prior the experiment agarose tissue phantom was warmed up body temperature. 500 kHz histotripsy transducer applied pressure as a single cycle with a pulse repetition frequency of 0.5 Hz over a range of peak negative pressure from 0 to 31.6 MPa.

CHAPTER 4

4. RESULTS AND DISCUSSION

4.1. Synthesis of Monofunctional β CD Derivatives

It has been shown that NCCs are made of inclusion complexes of CD organizes around PFH droplets and they are effective at lowering cavitation threshold of histotripsy [20]. This promising agent might have the potential of bringing different tools to structure or even allow to combine histotripsy with other treatment, if they allow for bioconjugation to functionalize the surface of NCC with desired agent such as fluorophore, targeting agent and PEG chain. It was obvious that if NCCs are wanted to be functionalized, β CD as building block is supposed to be began and functionalize with commonly used functional groups that can give reaction with high yield in aqueous medium. For this purpose, β CD was mono functionalized as shown in **Figure 4.1**.

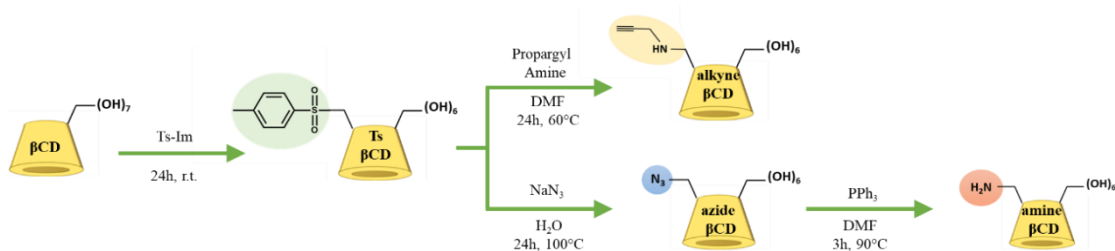


Figure 4.1: Synthesis of monofunctional azide- β CD, alkyne- β CD and amine- β CD.

In literature, so many different methods were shown for mono-functional β CD, di-functional β CD, and heptakis-functional β CD. In this study, it is aimed to functionalize single hydroxyl group because functionalizing of single hydroxyl group out of 7 primary face hydroxyl group not only provides enough functional group but also substantially protect the β CD characteristics. As can be seen in **Figure 4.1**, tosylated- β CD (Ts- β CD) was synthesized as an intermediate structure due to the versatile structure that can be easily converted because of stabilization the negative charge via resonance of sulfonate

ions, to different functional groups such as alkyne, azide and further amine. Following this purpose, tosyl imidazole (Ts-Im) was synthesized and characterized with $^1\text{H-NMR}$ (**Figure 4.2 b**). Protons of tosyl group were detected at 2.39 ppm, 7.50 ppm, and 7.96 ppm while imidazole protons were detected 7.14 ppm, 7.74 ppm, and 8.37 ppm. After the obtaining high quality Ts-Im; βCD and Ts-Im was reacted to obtain Ts- βCD , with 97% yield. The molar mass of Ts- βCD was measured 1289 g/mol by MS spectroscopy. Successful synthesis of Ts- βCD was confirmed using $^1\text{H-NMR}$ (**Figure 4.2 d**) that shows characteristic aromatic protons of tosyl groups appeared at 7.50 ppm and 7.96 ppm. Additionally, methyl proton of tosyl group were observed at 2.39 ppm while all the imidazole signals were disappeared (8.37 ppm, 7.74 ppm, and 7.14 ppm). Supporting to $^1\text{H-NMR}$ spectrum, in FTIR spectrum, 3270, 2924 and 1025 cm^{-1} signals were indicated the existing of βCD , while 1151 cm^{-1} signal that is specific O=S=O signal, indicated that there was a tosyl group attached to the βCD . These highly reactive intermediate was used to obtain functional groups on βCD such as azide- βCD , alkyne- βCD and amine- βCD (**Figure 4.1**).

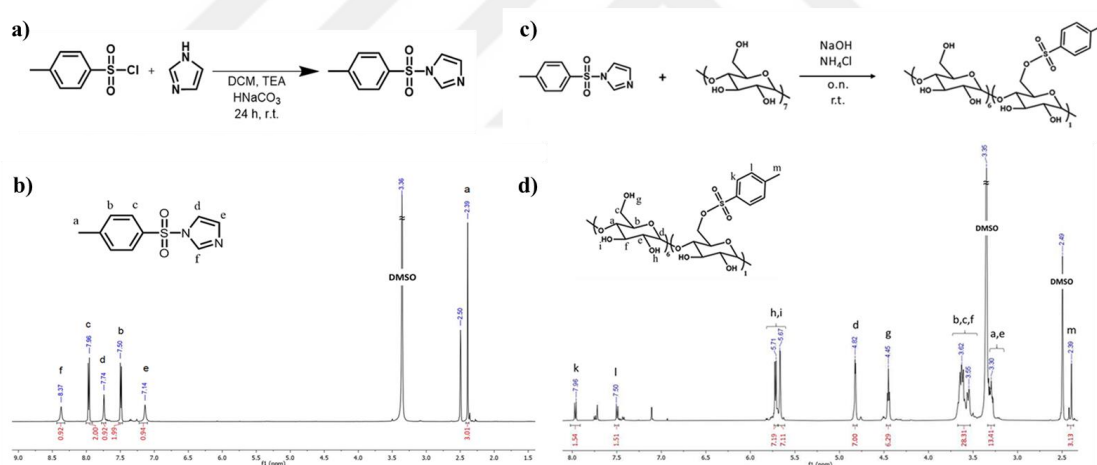


Figure 4.2: a) Synthesis of Ts-Im, b) $^1\text{H-NMR}$ spectrum of Ts-Im, c) Synthesis of monofunctional Ts- βCD , and d) $^1\text{H-NMR}$ spectrum of Ts- βCD .

Alkyne- βCD was synthesized using Ts- βCD and propargyl amine with 87% yield and its structure was confirmed by $^1\text{H-NMR}$ spectrum (**Figure 4.3 b**). While all the protons of tosyl group were disappeared at 7.96 ppm, 7.50 ppm, and 2.39 ppm, alkyne proton at 2.08 ppm was appeared along with characteristic βCD protons. Mass spectroscopy was also confirmed the molecular weight as 1172g/mol. Additionally, specific alkyne peak at 2971 cm^{-1} and specific βCD signals were detected in the FTIR spectrum of the alkyne- βCD

(**Figure 4.3 c**). In the light of this information, it can be understood that the alkyne group was attached instead of the tosyl group.

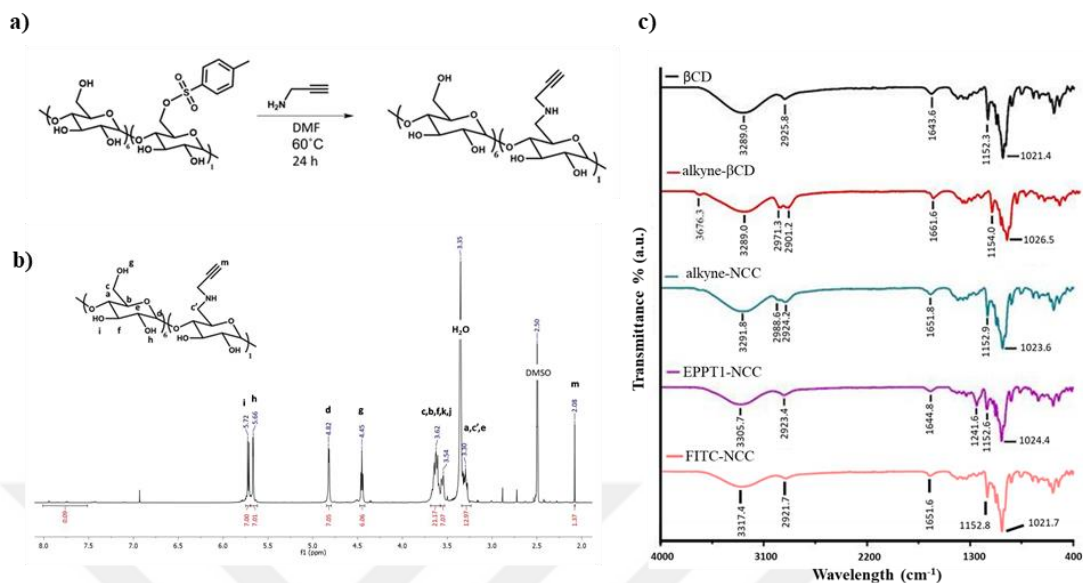


Figure 4.3: a) Synthesis of monofunctional alkyne-βCD, b) ¹H-NMR spectrum of alkyne-βCD, and c) FTIR analysis of βCD, alkyne-βCD and its functional and bioconjugated NCCs.

Similarly, azide-βCD was synthesized with sodium azide using sodium azide with high yield (90%). The mass of azide-βCD was measured and founded 1159 g/mol using the MS spectroscopy. Since methylene proton neighboring the azide group overlaps with βCD's protons, ¹H-NMR analysis did not provide clear evidence (**Figure 4.4 b**), however FTIR spectrum showed that azide substitution was achieved (**Figure 4.4 c**). 2121.5 cm⁻¹ peak at FTIR spectrum was confirmed the presence of azide group. Following of these information, it was understood that the tosyl group was removed from structure and the azido group was attached instead of the tosyl group.

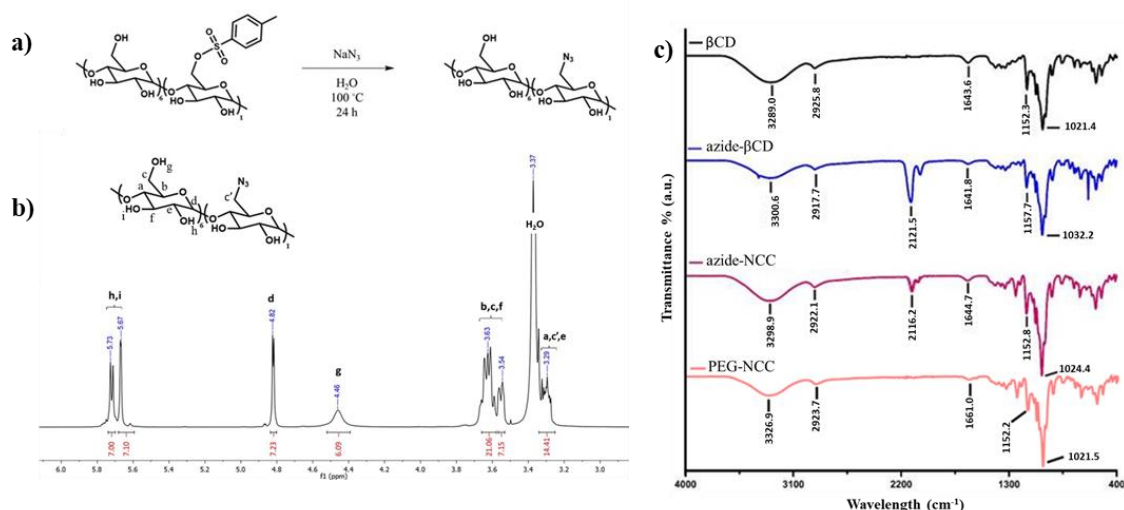


Figure 4.4: a) Synthesis of monofunctional azide-βCD, b) ¹H-NMR analysis of azide-βCD, and c) FTIR analysis of βCD, azide-βCD and its functional and bioconjugated NCCs.

Finally, obtained azide-βCD was transformed to amine-βCD in the presence of PPh₃ in DMF at 90 °C with 90% reaction yield. ¹H-NMR spectrum (Figure 4.5 b) supported general structure and azide groups were disappeared in FTIR spectrum even though N-H stretching at 3300 cm⁻¹ was overlapping with O-H stretching of βCD (Figure 4.5 c). Final structure of amine-βC was confirmed using mass spectroscopy giving its molecular weight as 1134 g/mol.

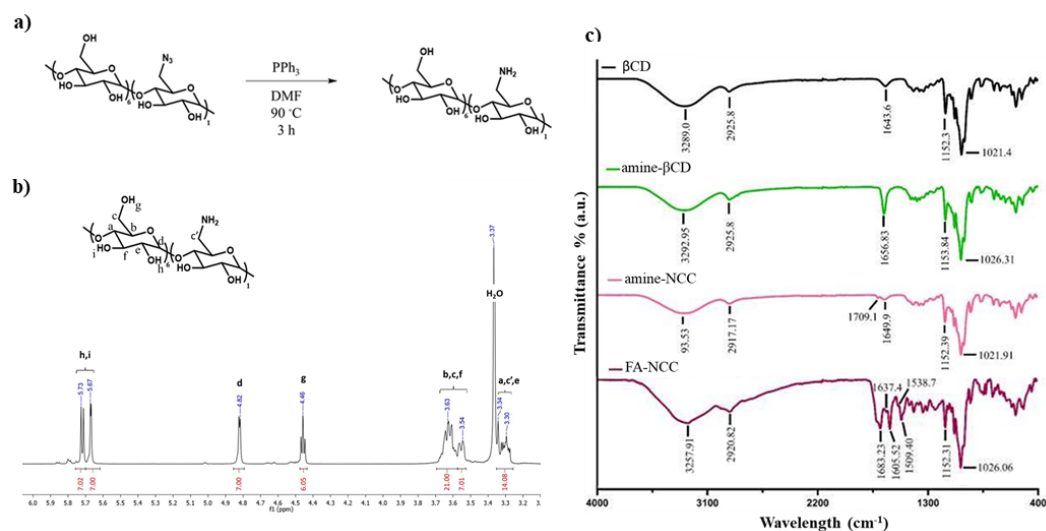


Figure 4.5: a) Synthesis of monofunctional amine-βCD, b) ¹H-NMR analysis of amine-βCD, and c) FTIR analysis of βCD, amine-βCD and its functional and bioconjugated NCC.

4.2. Synthesis and Characterization of Functional NCCs

Nanocone cluster (NCC) is made out of inclusion complexes of CD and PFC organize around PFC droplets. It was initially hypothesized that functional CD derivatives can be used as host molecules for PFC to form functional NCC instead of β CD itself. However, functional groups lowered the solubility of β CD in aqueous environment and resulted heterogeneous solution even if it is in high volume of water. Hypothesis was revised like using certain percentage of functional β CD along with native β CD can provide us not only functional NCC for further bioconjugation but also allow to have more biocompatible product by lowering the cytotoxicity of functional groups. Since most of the bioconjugated molecules appears at the surface for limited number instead of surface saturation, using certain portion of functional β CD sounds preferable method for functional NCC. Based on the solubility of functional β CD derivatives, β CD and functional CD were decided to mix 80/20 w/w in water to have enough functional group in homogeneous solution. PFH was selected as most effective PFC for histotripsy application [20], and it was added into the solution as 5 fold excess to ensure enough PFC even after post functionalization (**Figure 4.6**). Relatively lower solubility of functional β CDs enhances the chance of being in the cluster along with native β CD.

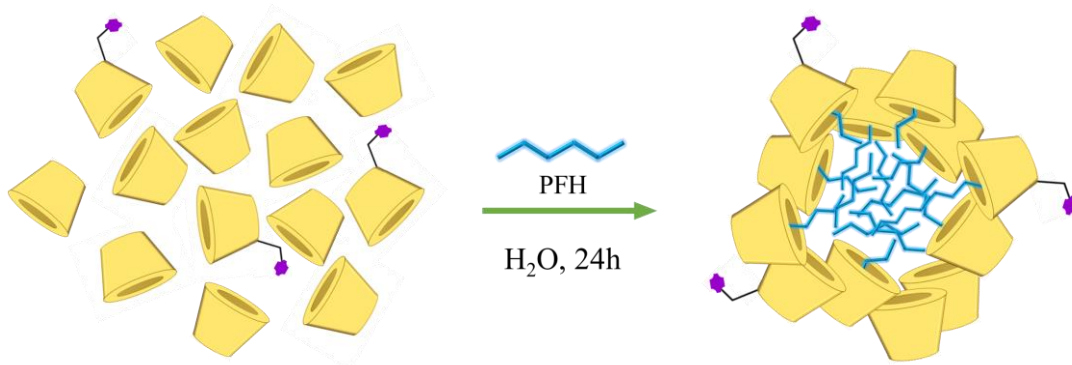


Figure 4.6: Synthesis of functional NCC.

Presence of functional group in obtained NCC were initially confirmed with FTIR because of the characteristic signals of azide, alkyne and amine groups. Broad OH stretching of β CD did not allow to observe the alkyne peak at around 3000 cm^{-1} however NH group of propargyl amine fragment was clearly observed in 3677 cm^{-1} for alkyne- β CD and alkyne-NCC (**Figure 4.3 c**) Like alkyne-NCC, azide-NCC and amine-NCC

were reviewed as lower specific peak intensity that was chosen the 2121.5 cm^{-1} for azide-NCC (**Figure 4.4 c**) and 1656.8 cm^{-1} for amine-NCC (**Figure 4.5 c**).

Thermal Gravimetric Analysis (TGA) was chosen as the first proof of the existence of PFH. In this form of analysis, the mass change in the material is measured against increasing temperature. As it is already known to have a low boiling point, it was considered a suitable method to prove the presence of PFH. As seen in **Figure 4.7**, mass change was observed in the whole NCC at temperatures where it could not damage β CDs. While this is evidence of PFH in NCC, it is an inadequate method for quantifying PFH. For this reason, other methods have been tried to determine the amount of PFH.

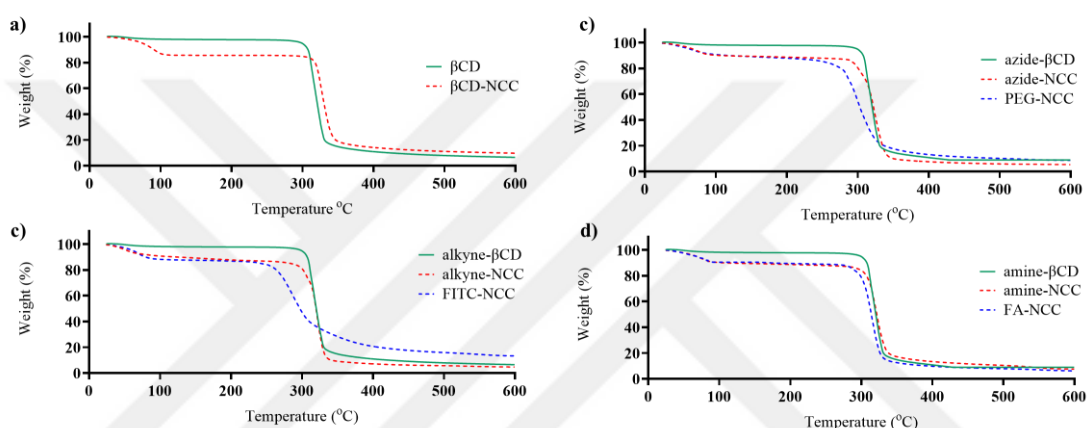


Figure 4.7: Change of weight of functional NCC and their bioconjugated products at the **a)** β CD and β CD-NCC, **b)** alkyne- β CD, alkyne-NCC and its bioconjugated derivative, **c)** azide- β CD, azide-NCC and its bioconjugated derivative, and **d)** amine- β CD, amine-NCC and bioconjugated derivative.

Additionally, EDX elemental mapping was confirmed the functional groups through their nitrogen content (**Figure 4.8**). Atomic percent of N in alkyne-NCC, azide-NCC and amine-NCC were 0.72%, 0.94% and 0.77% whereas it was 0.07% in β CD itself supporting the presence of functional group in functional NCC. The content of PFH as another important component of the system was mainly determined using gas chromatography (GC) based on previously published method. According to GC results, the PFH amount onto NCCs were calculated $0.15\ \mu\text{L}/\text{mg}$, $0.29\ \mu\text{L}/\text{mg}$, and $0.25\ \mu\text{L}/\text{mg}$ for alkyne-NCC, azide-NCC, and amine-NCC, respectively. EDX analysis was also supported the presence of PFH in NCC. Atomic percent of F in alkyne-NCC, azide-NCC and amine-NCC were determined as 8.17, 9.14, 6.45 compare to 10.57% of nonfunctional NCC (β CD-NCC) (**Figure 4.8**). Despite this slight decrease on atomic percent of F

comparing the nonfunctional one, functional NCC still contains enough PFH to be sufficient in histotripsy as it will be discussed later.

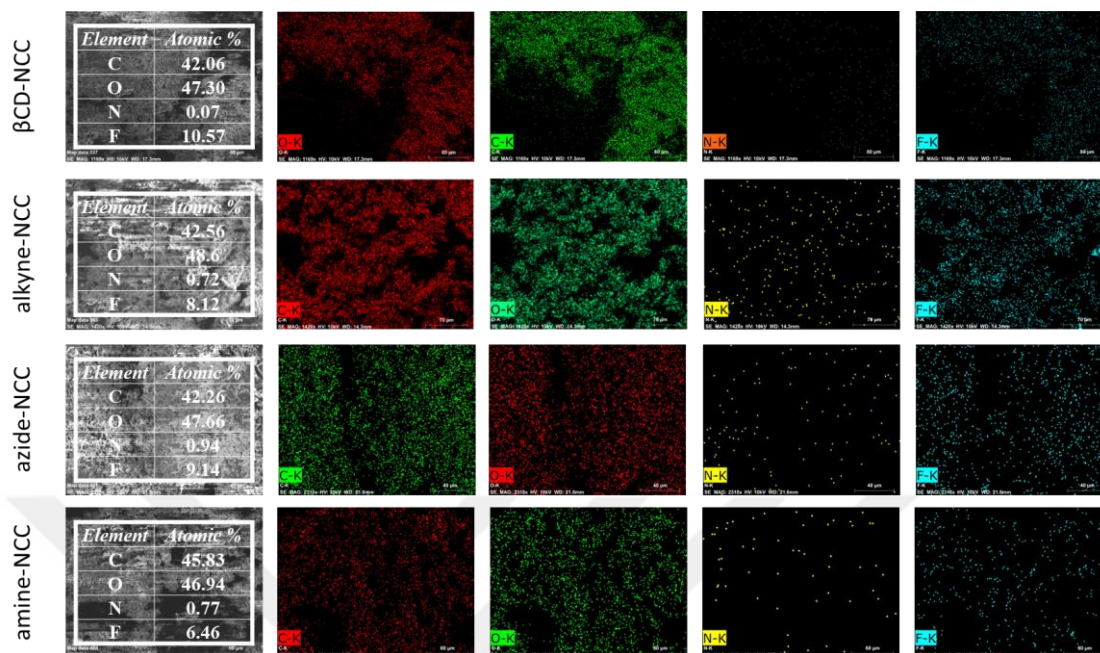


Figure 4.8: Elemental mapping of β CD-NCC, alkyne-NCC, azide-NCC, and amine-NCC using EDX analysis.

NCCs are a kind of nanoparticles consist of inclusion complex of CD derivatives around free PFH droplets. Their size is an important property in terms of tumor accumulation through enhanced permeability and retention effect (EPR). The size, size distribution and zeta potential and functional NCC were measured and represented in **Figure 4.9**. While β CD-NCC has the size of 169 nm, alkyne-NCC, azide-NCC and amine-NCC has the size of 316, 343 and 304 nm, respectively. The size of functional NCC was increased compared to β CD-NCC due to the low solubility of the functional β CDs. Moreover, nature of β CD and PFH provided negative surface charge which further increased for functional NCC (**Figure 4.9**).

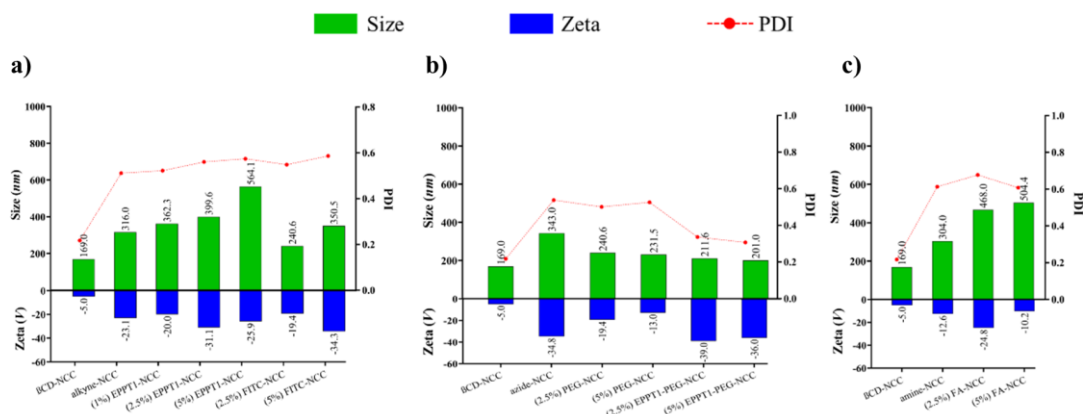


Figure 4.9: Size, size distribution and zeta potential of functional NCC and their bioconjugated products at the concentration of 0.01 mg/mL. **a)** alkyne-NCC and its bioconjugated derivatives, **b)** azide-NCC and its bioconjugated derivatives, and **c)** amine-NCC and its bioconjugated derivatives.

4.3. Bioconjugation of NCCs

As intended, obtained functional NCCs were used for bioconjugation which includes the strategies that commonly used in nanoparticles-based treatment system such as targeting, PEGylation, fluorophore tagging. For example, folic acid (FA) was chosen as most commonly use targeting agent and EPPT1 peptide was selected as more specific peptide-based targeting agent which is selective against uMUC receptor which is overexpressed on breast cancer cells. Poly(ethylene glycol) (PEG) as hydrophilic and water soluble polymer chain are used to increase the biocompatibility of nanoparticles by lowering the opsonization and increasing the blood circulation time. Florescence tagging is most of the time a necessity to track the nanoparticle in the cell and fluorescein isothiocyanate (FITC) is most commonly used fluorophore for labelling. While selection of these molecules for bioconjugation functional groups that is reactive against the functionality of NCC were considered as well. For instance, EPPT1 (NH₂-5-FAM-EHX-YCAREPPTRTFAYWGK-azido-homoalanine) peptide has the azide end to conjugate on alkyne group of alkyne-NCC while folic acid has carboxylic acid group to react with amine group of amine-NCC. Another aspect that was considered for successful bioconjugation to obtain optimum properties of final product was feeding ratio of bioconjugation (1%, 2.5%, 5%). Since the conjugates has different hydrophilicity or hydrophobicity, the degree of conjugation might potentially affect the stability and water dispersibility of the product.

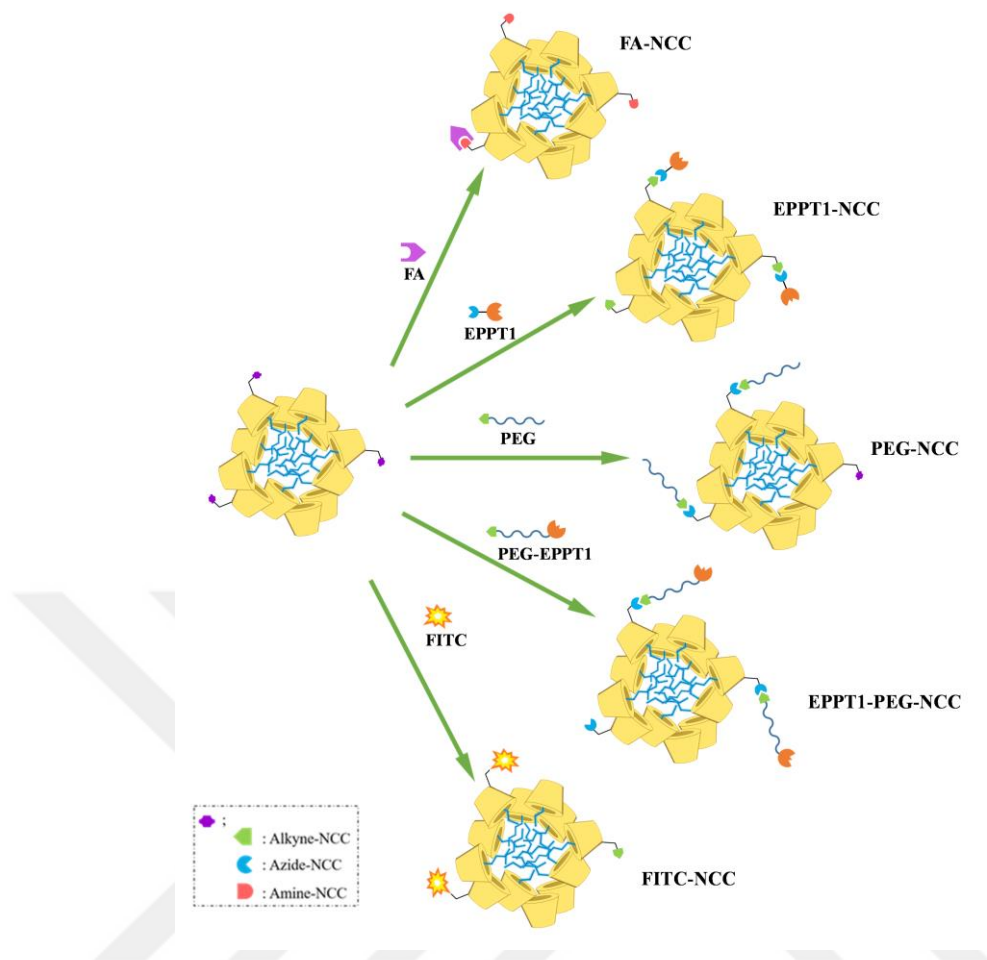


Figure 4.10: Bioconjugation examples using functional NCC.

Figure 4.10 shows the bioconjugated NCC using functional NCC as precursor. First, azide terminated EPPT1 peptide was conjugated to alkyne NCC initially with the ratio of 1%, 2.5%, and 5% through “click” chemistry in aqueous environment in the presence of CuSO_4 /sodium ascorbate. Precipitated EPPT1-NCC was centrifuged and washed several times to remove the catalyst and unreacted peptide from the system. The conjugated EPPT1 percent was calculated using Ellman’s reagent that uses the thiol group in the peptide to quantify the peptide amount in the system as well as Bradford assay. The results showed that increasing feeding percent of peptide increases the conjugation of EPPT1 up to 5% and further increase to 10% did not result higher conjugation of peptide on NCC based on Ellman’s reagent assay (**Table 4.1**). The assay used for determination of the peptide were consistent at low feeding ratio (1.2 vs 1.1% for 1 % feeding ratio and 1.4 vs 1.4 for 2.5% feeding ratio) however they fluctuated for 5 % feeding ratio. The calculated peptide % was decreased for 10 % compared to %5 feeding ratio for only Elman’s reagent

analysis. Even though it increased based on Bradford analysis, it did not increase drastically compared to 2.5% feeding ratio.

This finding was confirmed by EDX analysis of EPPT1 conjugated NCC which clearly showed the change on atomic percentage by increasing the atomic percent of N up to 5% feeding ratio (**Figure 4.11**). Further increase to 10% feeding ratio did not result increase on N content which is proportional with the peptide content in the structure showing that there is a saturation points that does not allow further functionalization due to the increasing hydrophobicity of the NCC. Moreover, the amount of conjugated EPPT1 was indirectly calculated based on the absorption of FAM labeling that is already exists on the peptide (**Table 4.1**). Since FITC and FAM has identical spectral characteristics, the amount of FAM on NCC was determined using FITC calibration curve. As it was shown in **Table 4.1**, even though calculated about was slightly higher that the calculated amount of peptide because of the difference of analysis technique, it was still consistent with calculated peptide amount.

Table 4.1: Feature of alkyne-NCC and its bioconjugated NCCs.

Name of Sample	Feeding % ^a	Calc. EPPT1, % ^b	Calc. EPPT1, % ^c	Calc. FITC % ^d	Calc. FA % ^e	PFH (μL/mg) ^f
alkyne-NCC	-	-	-	-	-	0.15
EPPT1-NCC	1	1.2	1.1	1.5	-	0.14 ^g
EPPT1-NCC	2.5	1.4	1.4	1.7	-	0.15
EPPT1-NCC	5	1.9	0.9	1.1	-	0.14 ^g
EPPT1-NCC	10	1.5	1.5	1.8	-	0.14 ^g
FITC-NCC	2.5	-	-	1.6	-	1.62 ^g
FITC-NCC	5	-	-	1.9	-	1.62 ^g
azide-NCC	-	-	-	-	-	0.29
PEG-NCC	2.5	-	-	-	-	0.27
PEG-NCC	5	-	-	-	-	0.27
EPPT1-PEG-	2.5	1.6	1.5	-	-	0.29

EPPT1-PEG-amine-NCC	5	0.9	0.8	-	-	0.19 ^g
FA-NCC	2.5	-	-	-	1.4	0.24
FA-NCC	5	-	-	-	1.2	0.24

^a The feeding percent for functionalization.

^b Percent EPPT1 in bioconjugated NCC calculated by Ellman's assay.

^c Percent EPPT1 in bioconjugated NCC calculated by Bradford assay.

^d Percent FITC in NCC calculated by fluorescence spectrometer using free FITC calibration curve.

^e Percent FA in NCC calculated by fluorescence spectrometer using free FA calibration curve.

^f PFH amount in NCC calculated by GC. Analyzing of bioconjugated NCC is not possible because of increasing molecular weight of building block for GC. It is assumed that PFH amount is same with its precursors.

^g Samples were prepared from different batches.

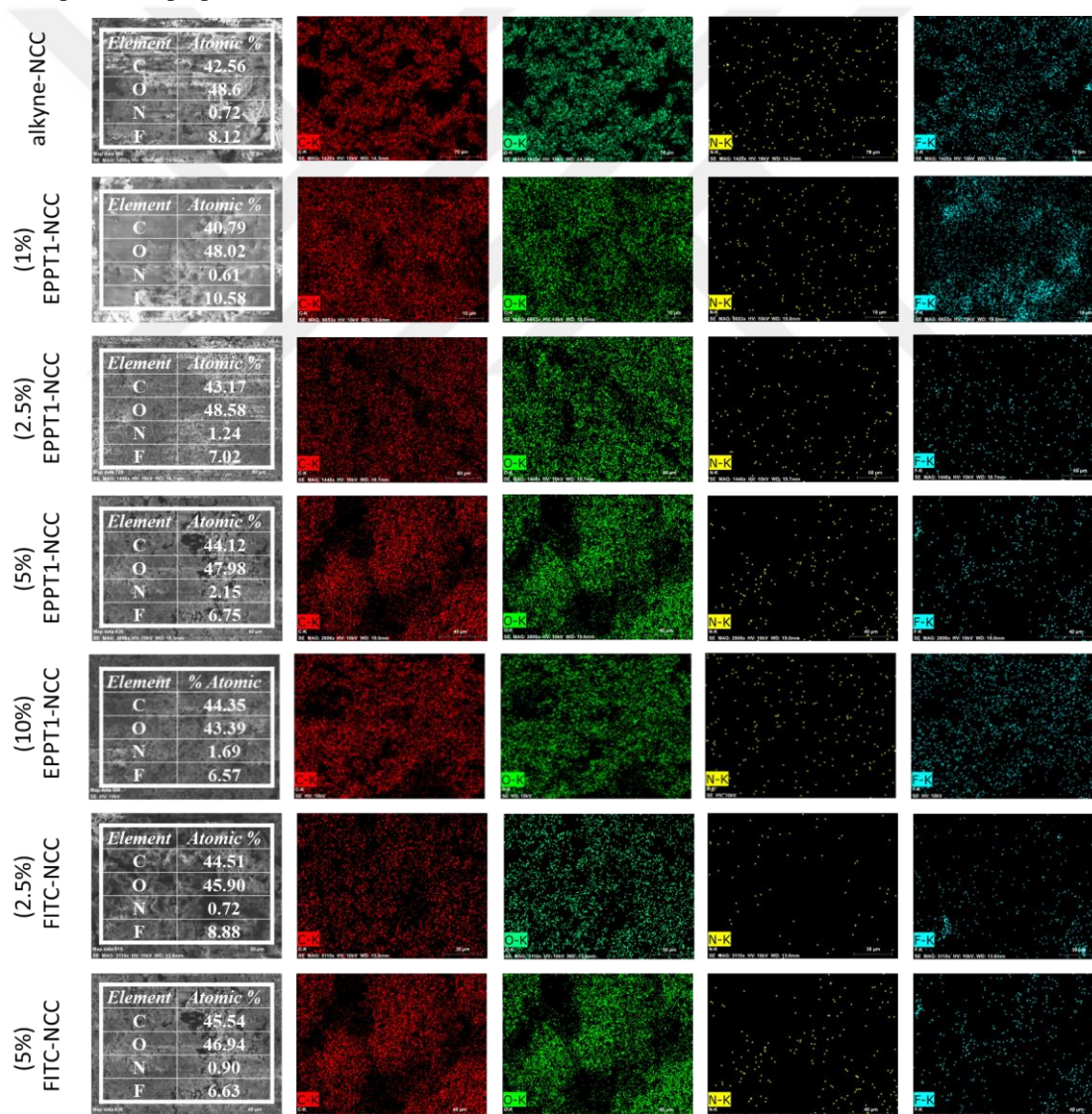


Figure 4.11: Elemental mapping of alkyne-NCC, EPPT1-NCC (1, 2.5, and 5%) and FITC-NCC (2.5 and 5%) using EDX analysis.

FITC was conjugated to alkyne-NCC to not only show labeling of NCC for fluorescence imaging but also to use it as non-targeted NCC while it is aimed to investigate the targeting potential of EPPT-NCC. Previously published reaction between propargyl amine and isothiocyanate group was adapted to FITC conjugation on alkyne-NCC which its alkyne group was generated through propargyl amine [29]. Structural analysis of FITC-NCC was performed using $^1\text{H-NMR}$ analysis and FITC protons were observed with low intensity because of low conjugation percentages. The methylene protons of N and S containing ring formed between propargyl amine and isothiocyanate group was traced at 4.99 ppm indicating suggested conjugation (**Figure 4.12**). Similarly, the amount of FITC that is conjugated to NCC was calculated using calibration curve that is made using free FITC. The percentage of FITC conjugation was calculated 1.6% and 1.9% for 2.5 and 5%, respectively.

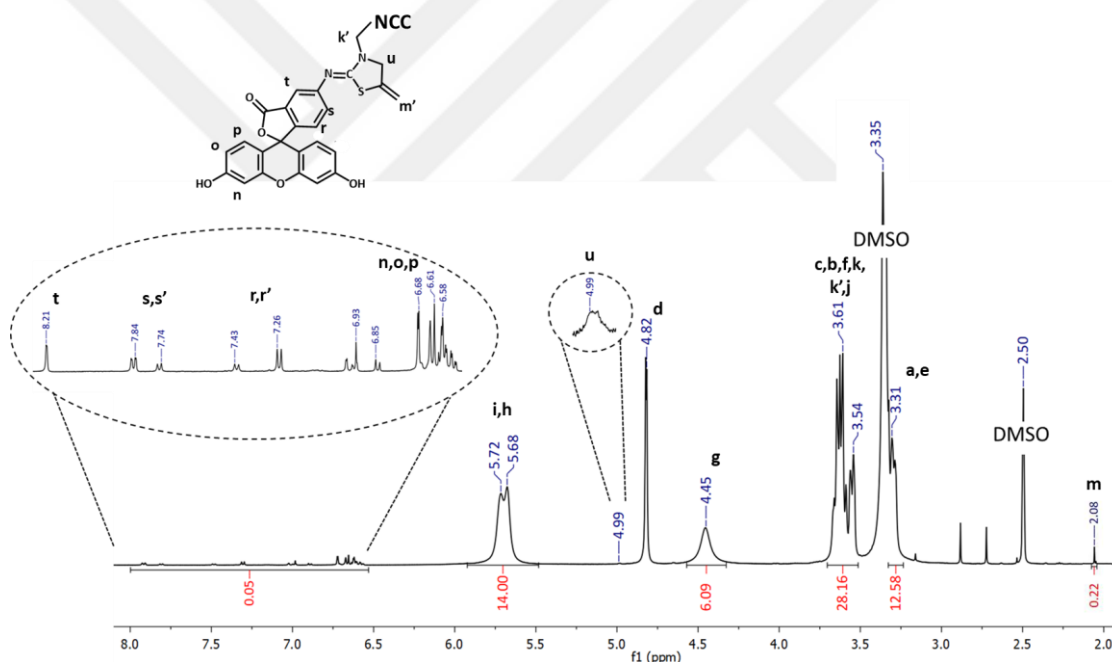


Figure 4.12: $^1\text{H-NMR}$ spectrum of 2.5% conjugated FITC-NCC (complex includes βCD (400 eq), alkyne- βCD (100 eq), FITC- βCD (2.5 eq)).

FA as small targeting molecules with carboxylic acid group was conjugated to amine-NCC through EDC/NHS coupling with the feeding ratio of 2.5% and 5%. FA-NCC exhibited characteristic FA peaks at 1683.2, 1605.5, and 1509.4 cm^{-1} in FTIR spectrum (**Figure 4.5 c**). EDX analysis of FA-NCC showed that N content of FA contributes on atomic percent of N compared to amine-NCC and it also preserves its fluorine content (**Figure 4.13**). As it was shown in **Table 4.1**, FA % in NCC was calculated as 1.4 and 1.2% for 2.5 and 5% feeding ratio, respectively, based on the calibration curve made out

of fluorescence absorption of free FA at different concentration. These results also supported that at low feeding ratio results higher functionalization.

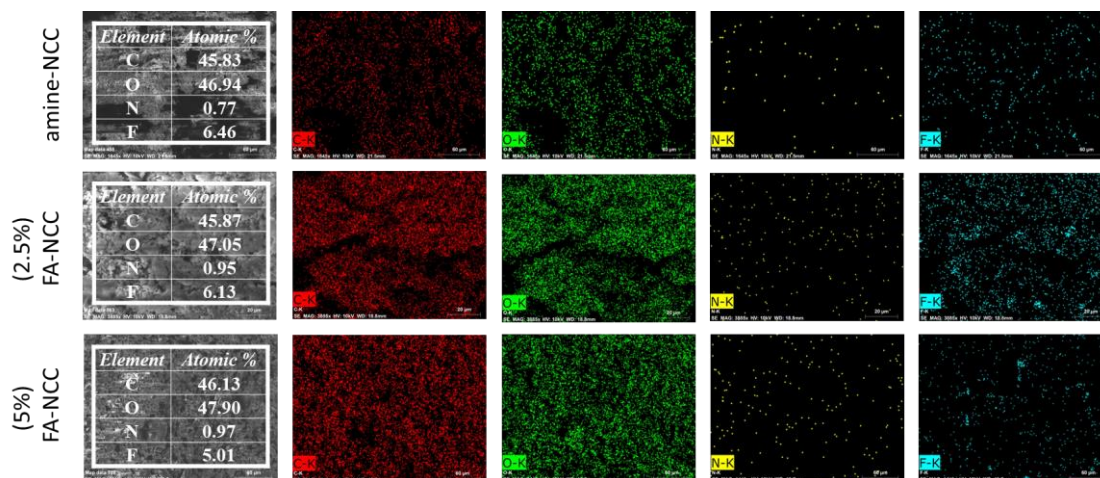


Figure 4.13: Elemental mapping of amine-NC and FA-NCC (2.5 and 5 %) using EDX analysis.

PEGylation of NCC was performed through two different strategies. In the first way 2 KDa alkyne-PEG was conjugated to NCC to obtained just PEGylated NCC. Second way EPPT1 targeted alkyne-PEG-EPPT1 conjugated to azide NCC to have targeted, PEGylated NCC. Both strategies are commonly used in nanoparticles preparation for long term blood circulation. Presence of PEG on PEG-NCC was confirmed through the degradation of PEG at different temperature than β CD-NCC during thermal gravimetric analysis (**Figure 1.7**). Moreover, EDX analysis after the conjugation of PEG and PEG-EPPT1 reflected the results of successful conjugation. PEG conjugation did slightly change the C/O ratio and PEG-EPPT1 conjugation contributed on increasing the N content (**Figure 4.14**). Atomic content of percent F in the PEG-NCC decreased with the increasing of percentage of PEG conjugation. This is most probably because of solubility contribution of hydrophilic PEG chain that might cause unbalancing of the NCC precipitate.

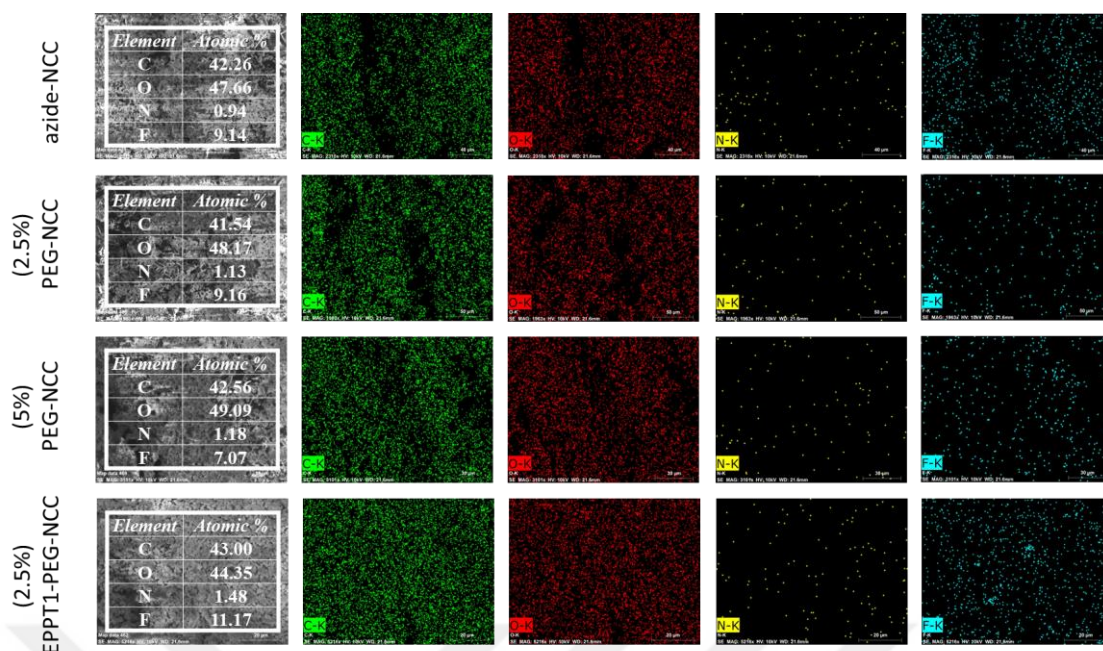


Figure 4.14: Elemental mapping of azide-NCC, PEG-NCC (2.5, 5 and 10 %) and EPPT1-PEG-NCC (2.5 %) using EDX analysis.

The size and surface charge of all the bioconjugated NCC were analyzed and compare with their pristine NCC in **Figure 4.9**. The size of 1 and 2 % EPPT1 targeted NCC was measured as 362.3 nm and 399.6 nm, respectively and it is slightly higher than its precursor (alkyne-NCC) which was measured as 316 nm. Further 5% peptide conjugation into NCC surface caused significant size increase such as 564.1 nm (**Figure 4.9 a**), since increasing peptide content decreases the water dispersibility properties of the NCC. This statement was also supported with the size measurement of 10% EPPT1 conjugated NCC mentioned in **Table 4.1** which was obtained as 1084 nm. However, this problem can be solved by conjugation EPPT1 peptide and PEG together on NCC (**Figure 4.9 b**) which provides well disperse solution with NCC that contains hydrophilic and hydrophobic segments together to have a balance. Especially 2.5% PEG-NCC and EPPT-PEG-NCC showed size as 240.6 nm and 211.6 nm, respectively. Once feeding ratio was increased to 5% for PEG-NCC and EPPT1-PEG-NCC, size also kept decreasing to 231.5 and 201.0 nm, respectively, which clearly indicates that PEGylation caused size decrease. On the other hand, FA has more hydrophobic feature and the size increase can be expected as natural as well as with increasing feeding percent. The result supported this expectation and was measured as 468.0 nm for 2.5 % FA-NCC and 504.4 nm for 5% FA-NCC (**Figure 4.9 c**).

Due to the nature of β CD and PFH the NCC shows the negative surface charge. EPPT1 peptide conjugation initially increased the negative surface charge which followed by decrease on it because of dispersion problem. Conjugation of PEG on NCC surface is supposed to be expected to increase in negative surface charge due to the negatively charged PEG, however increasing in the PEG content shows decrease on negative charge which might be a sign of leaving of PEG- β CD fragment from NCC because of increasing solubility and leaving the native β CD-NCC behind. Once PEG is balanced with something hydrophobic, charge has balanced and increase to -39 mV indicating the stability potential of the particle.

Overall, even though the size of some bioconjugated NCC have a tendency to be higher than 300 nm, it is possible to obtain targeted NCC at around 200 nm by tuning the surface hydrophilicity and hydrophobicity. Although endocytosis is not required for NMH treatment and it can be effective as long as there is enough NCC accumulated in the tumor tissue, it is accepted that smaller size is better for tumor accumulation and there is chance to tune the bioconjugated NCC' size by tuning the surface properties.

4.4. Biocompatibility Evaluation of Bioconjugated-NCCs

Since it is preferred to inject intravenously, the hemocompatibility of bioconjugated NCCs is important. Red blood cell interaction of different surface functional NCC and their precursors were investigated at three different concentration against Triton X-100 as positive control (**Figure 4.15**). All NCC derivatives did not show hemolytic activities which was below 7% and bioconjugation lowered the hemolytic activity as expected. β CD and functional NCC showed the hemolytic activity within the range of 6.0-6.7% for the higher concentration and it decreased by concentration to the range of 5.5-6.2% (**Figure 4.15 a**). FITC and FA and conjugated NCC followed same concentration dependent trend on hemolytic activities within lower range as 4.5-5.9% (**Figure 4.15 b**). Similarly, but with lower hemolytic activities, PEG-NCC generally showed decreased in red blood cell interaction and hemolysis percent was lower than 5% for all concentration.

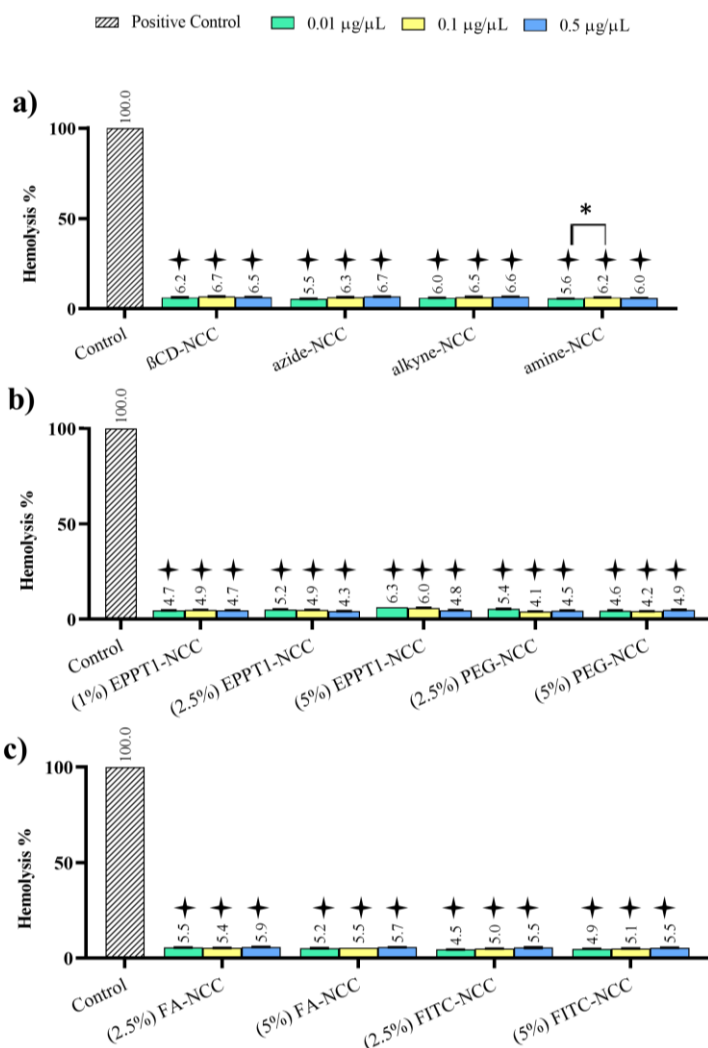


Figure 4.15: Hemolytic activities of **a)** functional NCC, and **b)** and **c)** bioconjugated NCC at different concentration under physiological conditions. Statistically significant differences were evaluated using the two-way ANOVA plus Tukey's posthoc comparison test. All samples were compared with untreated cells (top of each bar) and also between each other (showing using pair representation). Symbols that are assigned to each concentration denote $p \leq 0.1$ for *, $p \leq 0.01$ for \blacktriangle , $p \leq 0.001$ for \bullet , and $p \leq 0.0001$ for \blackstar .

Although the low hemolytic activity is a good indicator for the biocompatibility of NCC derivatives, how do they interact with healthy cell is another important aspect of biocompatibility since the histotripsy itself does not harm the healthy cells and used agent for histotripsy is expected to be non-cytotoxic. Due to the fact that fibroblast cells are most abundant cell and be made of basic framework of tissue and organs, MRC-5 healthy lung fibroblast cells were used to scan all functional NCC and bioconjugated NCC at different concentration range from $0.01 \mu\text{g}/\mu\text{L}$ to $0.5 \mu\text{g}/\mu\text{L}$ using MTS assay (**Figure 4.26**). In general, functional NCC showed cell viability higher than 81% at concentration. As expected bioconjugation did not change this behavior and bioconjugated NCC even

showed slightly higher cell viability comparing to their functional precursors tested especially for EPPT1, PEG and EPPT1-PEG conjugated NCC. This trend was more visible for PEGylated NCC and targeted PEGylated EPPT1-PEG-NCC.

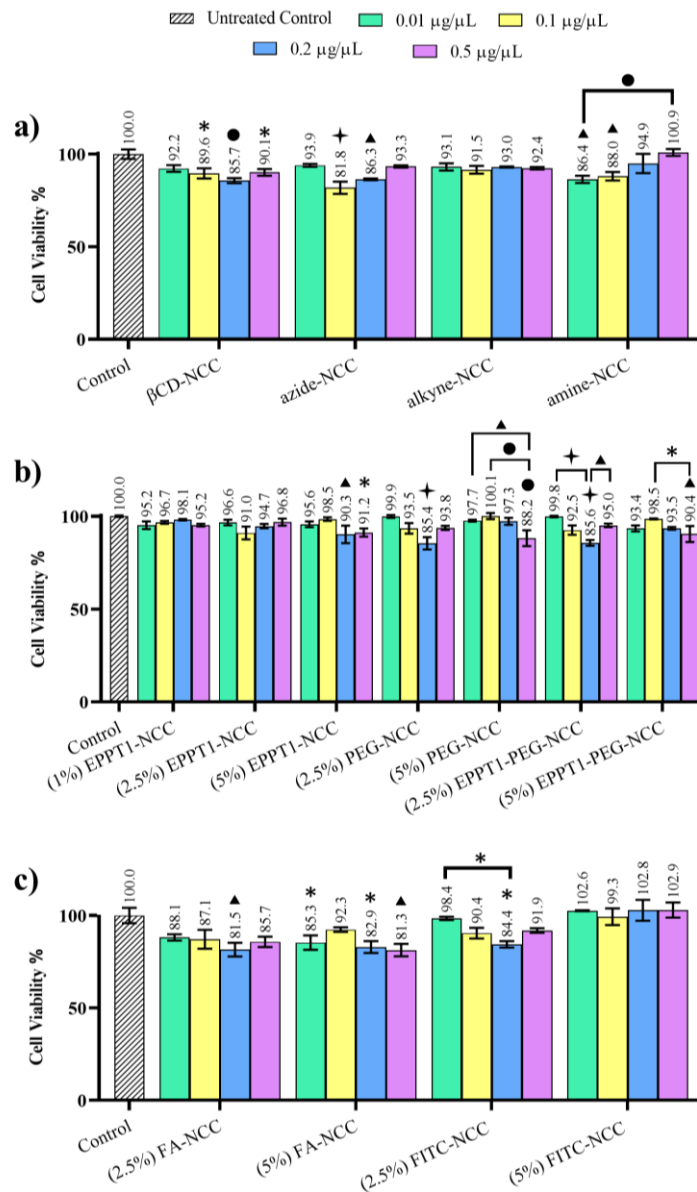


Figure 4.16: Cell viability study of **a)** functional NCC, and **b)** and **c)** bioconjugated NCC on MRC-5 cells using MTS Assay. Statistically significant differences were evaluated using the two-way ANOVA plus Tukey’s posthoc comparison test. All samples were compared with untreated cells (top of each bar) and also between each other (showing using pair representation). Symbols that are assigned to each concentration denote $p \leq 0.1$ for *, $p \leq 0.01$ for †, $p \leq 0.001$ for ‡, and $p \leq 0.0001$ for ▲.

Even though it is not significant, it was interestingly noticed that cell viability generally increases with increasing concentration especially for the highest concentration of EPPT1 and FITC containing samples. This might be due to the overlapping of optical absorbance of FITC and MTS reagent at measurement wavelength which may contribute positively

to cell viability. To address this concern, the cell viability experiment was repeated using Resazurin assay which has the optical absorbance at different wavelength than FITC. Results showed that the cell viability did not significantly change but it showed more noticeable trend on decreasing cell viability with increasing NCC concentration (**Figure 4.17**). Still, bioconjugated NCCs showed cell viability higher than 82%.

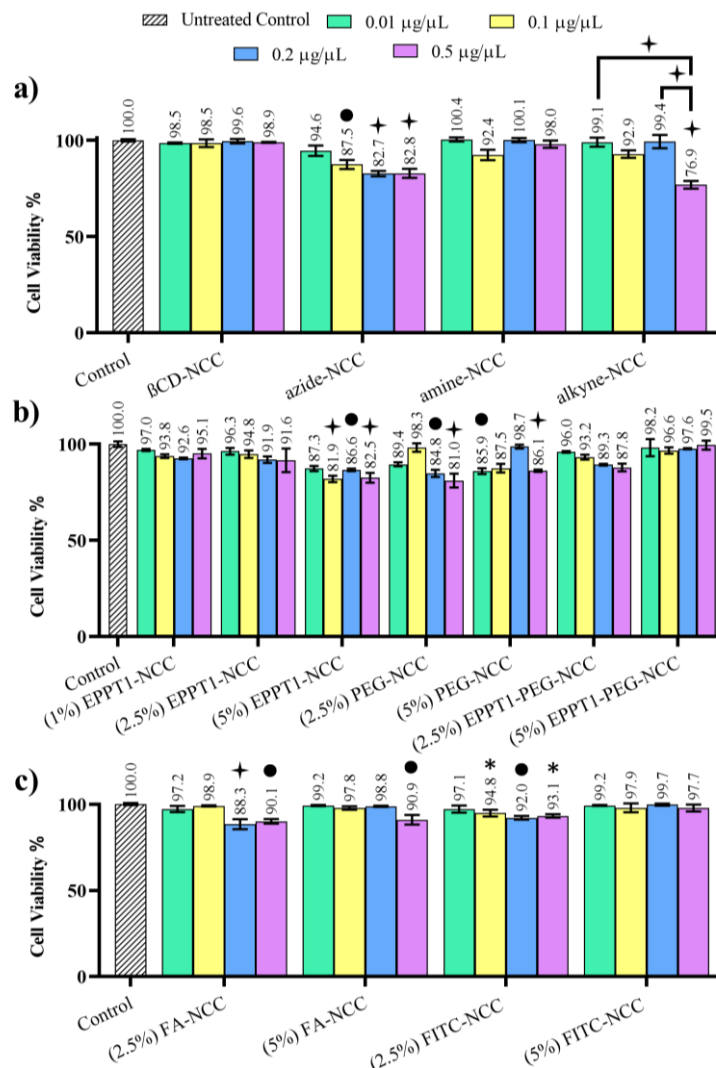


Figure 4.17: Cell viability study of **a)** functional NCC, and **b)** and **c)** bioconjugated NCC on MRC-5 cells using Resazurin Assay. Statistically significant differences were evaluated using the two-way ANOVA plus Tukey’s posthoc comparison test. All samples were compared with untreated cells (top of each bar) and also between each other (showing using pair representation). Symbols that are assigned to each concentration denote $p \leq 0.1$ for *, $p \leq 0.01$ for ▲, $p \leq 0.001$ for ●, and $p \leq 0.0001$ for †.

EPPT1 recognizes the uMUC1 receptor at the surface of breast cancer cells which overexpresses the receptor more than 90% comparing the healthy cells. In order to show the treatment potential and targeting ability of EPPT1-NCC or EPPT1-PEG-NCC, the interaction with health breast cell is supposed to be investigated to show their

biocompatibility against healthy cells. **Figure 4.18** shows the results of cell viability assessment of MCF-10A as human epithelial breast cell line. More than 80% of the cell were alive when they treated with precursors that used to obtain either EPPT1-NCC or EPPT1-PEG-NCC. EPPT1 targeted and FITC-NCC as nontargeted did not showed different behavior except EPPT1-PEG-NCC as targeted, PEGylated NCC which increased the cell viability more than 90% indicating that PEGylated, targeted NCC might be better candidate with better biocompatibility.

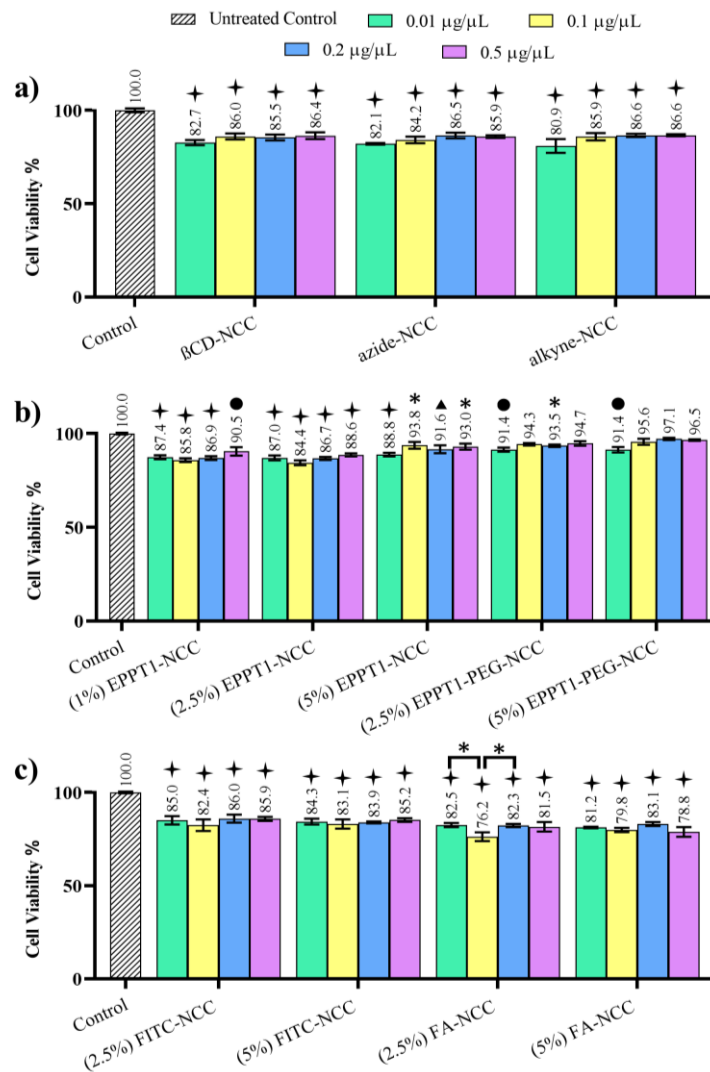


Figure 4.18: Cell viability study of **a)** functional NCC, and **b)** and **c)** bioconjugated NCC on MCF-10A cell line using MTS Assay. Statistically significant differences were evaluated using the two-way ANOVA plus Tukey's posthoc comparison test. All samples were compared with untreated cells (top of each bar) and also between each other (showing using pair representation). Symbols that are assigned to each concentration denote $p \leq 0.1$ for *, $p \leq 0.01$ for \blacktriangle , $p \leq 0.001$ for \bullet , and $p \leq 0.0001$ for \dagger .

Next concern was the explore the efficiency of applied bioconjugation which indirectly shows the successful conjugation and the usability for desired treatment. General practice

for targeted nanoparticles in the literature is either compare targeted and nontargeted particles internalization into cancer cells or compare the cellular entry of targeted particles into cancer and healthy cells to show the selectivity of targeting agent to the cell surface. Both strategies were followed in this study, and results represented in **Figure 4.19**. To examine the contribution of EPPT1 in cellular uptake, different percentage EPPT1 containing NCC were compared, and their fluorophore concentrations were tuned to be at the same concentration (16 μg FITC/mL) on nontargeted FITC-NCC in order to compare the fluorescence intensity inside the cells using confocal microscopy. After incubating targeted and nontargeted NCC with the cells for 4 h, the nucleus was blue colored with Hoechst dye. **Figure 4.19 a** shows that EPPT1 targeted particles showed brighter green fluorescence than nontargeted FITC-NCC which also supported with quantitative analysis of the images (**Figure 4.19 c**). 1% EPPT1-NCC showed the higher cellular uptake on MCF-7 cancer cells and followed by 2.5% EPPT1-NCC, however further increase on EPPT1 percent on NCC did not result with increase in cellular uptake most probably because of poor dispersibility properties of the NCC. %5 feeding ratio was determined as limit of surface functionalization since fluorescence intensity in the cell stayed at the same level even if feeding ratio is increased up to 10%. The efficacy of EPPT1 dependent cellular internalization into cancer cells was validated repeating the experiment using healthy MCF-10A cells under same condition. The result showed that targeted EPPT1-NCC were not selective against MCF-10 A cells (**Figure 4.19 b**) comparing to nontargeted FITC-NCC which showed almost same level fluorescence intensity for both cancer and health cells (**Figure 4.19 d**).

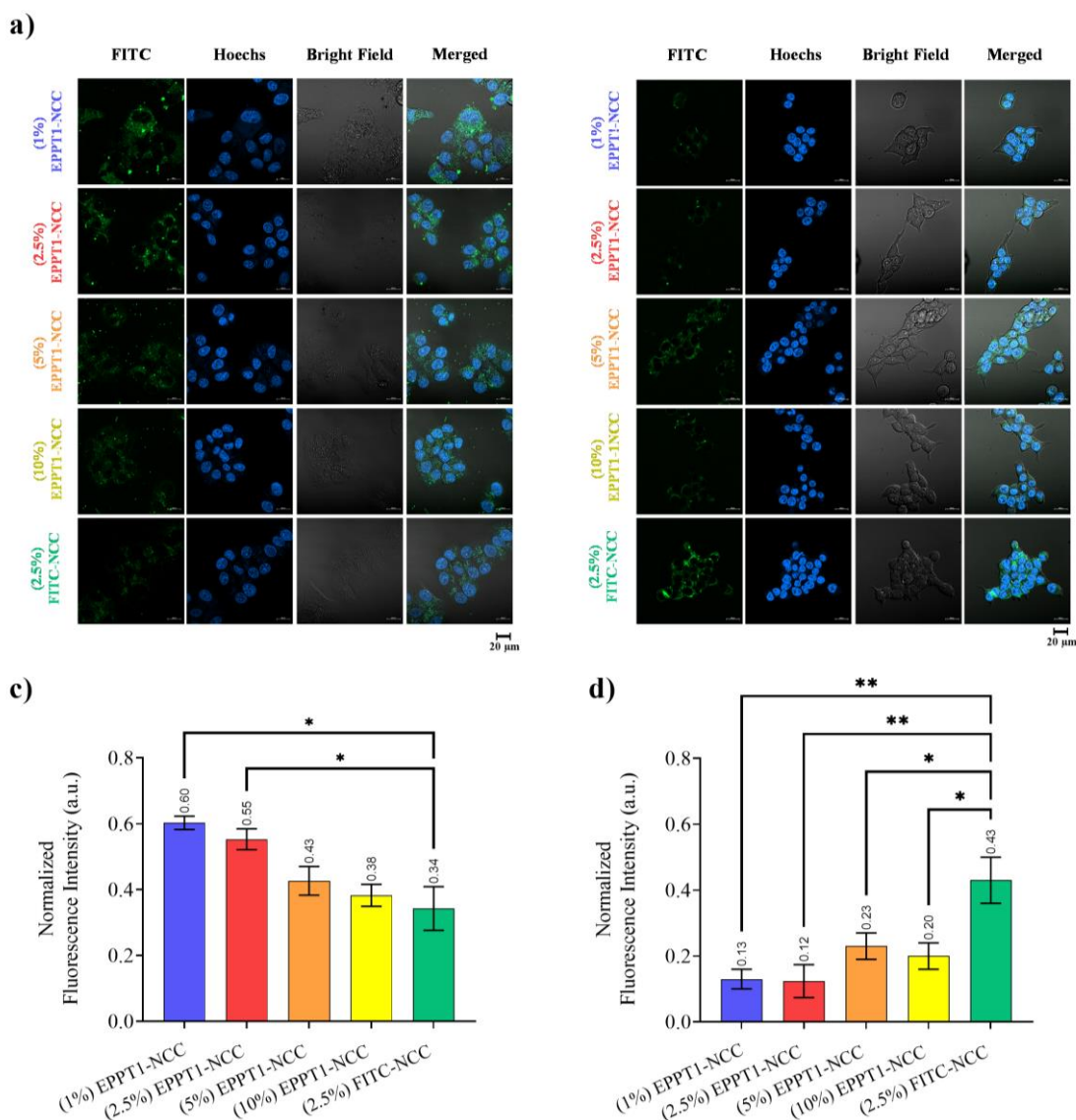


Figure 4.19: Confocal fluorescent images showing internalization of EPPT1-NCC and FITC-NCC into **a)** MCF-7 human breast cancer cells, and **b)** MCF-10 A human health epithelial breast cells. The green fluorescent originates from FITC conjugated EPPT1-NCC and FITC-NCC NCC derivatives where Hoechst dyed nucleus shows blue fluorescence (Scale bar: 50 μ m). Quantitative evaluation of fluorescence intensity for **c)** MCF-7, and **d)** MCF-10A cells were achieved by normalizing fluorescence intensity of internalized FITC against Hoechst fluorescence. (* $p \leq 0.1$, ** $p \leq 0.01$, *** $p \leq 0.001$, **** $p \leq 0.0001$).

Selective cellular internalization of EPPT1-NCC derivatives was additionally verified by comparing fluorescent intensities of NCCs treated and untreated MCF-7 cells that are examined using a flow cytometer. FITC fluorescence of each tubes was recorded by 10,000 events as seen in **Figure 4.20 a**, untreated MCF-7 cells show negligible fluorescence when compared to NCC treated cells. Non-targeted FITC-NCC exhibited almost identical fluorescence with untreated cells indicating the lowest cellular entry while 1 % EPPT1-NCC showed the highest profile that is followed by 2.5 % EPPT1-

NCC. In parallel to the confocal microscopy results represented in **Figure 4.19**, 10 % EPPT1-NCC showed close and slightly lower cellular internalization than % 5 EPPT1-NCC. All these data collectively indicated that lower feeding percentage allows more controlled functionalization at the surface with better dispersibility properties as a requirement of effective targeted nanoparticles.

As commonly used targeting agent, the targeting potential of FA was also investigated. Cellular internalization of FA-NCCs could not be conducted by using flow cytometer due to the lack of compatible light source on the device. Therefore, cell lysis experiment was selected as commonly used method in the literature to show the cellular internalization differences between folate receptor positive HeLa and negative MCF-7 cancer cells. FA-NCC (2.5 and 5 %) were incubated for 4 hours with these cell lines and lysed with Triton X-100 to read the absorbance of supernatant at 250 nm which is associated with FA absorbance. The results showed that FA receptor negative MCF-7 cells did not show any selectivity against FA-NCC (**Figure 4.20 b**), whereas FA receptor positive HeLa cells exhibited clear difference on internalization on the cell (**Figure 4.20 c**). 2.5% FA-NCC significantly showed the better internalization compared to untreated cells as well as 5% FA-NCC. These data consistence with the data presented in **Table 1** since 5% feeding ratio of FA did not resulted higher functionalization than 2.5% feeding ratio. This supported the idea that increasing number of FA at the surface increases the internalization. Given the fact that FA receptor negative MCF-7 did not show any selectivity, this internalization happens through FA receptor as FA selective.

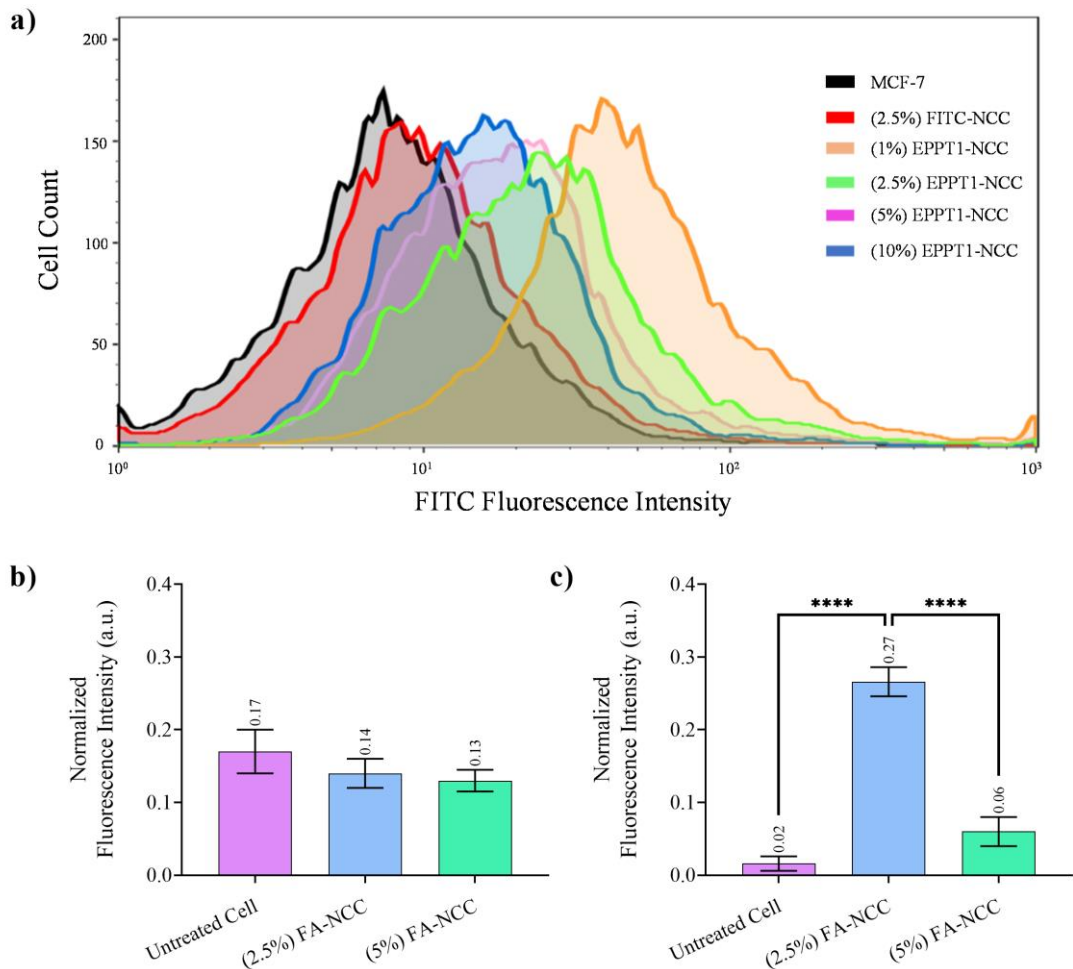


Figure 4.20: a) Histograms showing fluorescent intensities of EPPT1-NCC, FITC-NCC derivatives treated and non-treated cells against 10,000 events (Ex/Em:488/530 nm). Quantitative evaluation of fluorescent intensity using Lysis Method in b) MCF-7 and c) HeLa. FA was detected at 250 nm in FA-NCC treated cells. Statistically significant differences were evaluated using the two-way ANOVA plus Tukey's posthoc comparison test. All samples were compared with untreated cells and also between each other (shown with pair representation; * $p \leq 0.1$, ** $p \leq 0.01$, *** $p \leq 0.001$, **** $p \leq 0.0001$).

Finally, the ability of bicoconjugated NCC to lower the cavitation threshold pressure were tested to show whether they can be used as cavitation nuclei for NMH. An agarose tissue phantom that can be mechanically mimic the tissue was used for the cavitation threshold experiment under the physiological conditions. Functional NCC and bioconjugated NCC were tested under the same PFH concentration that is determined using GC analysis and given in **Table 4.1**. As can be seen in **Figure 4.21**, functional NCC that used as precursor to obtained final bioconjugated NCC exhibited similar behavior under the single cycle ultrasound pulse and lowed the cavitation threshold pressure as low as 10.0 MPa which is close to previously published nonfunctional PFH containing NCC clusters [20].

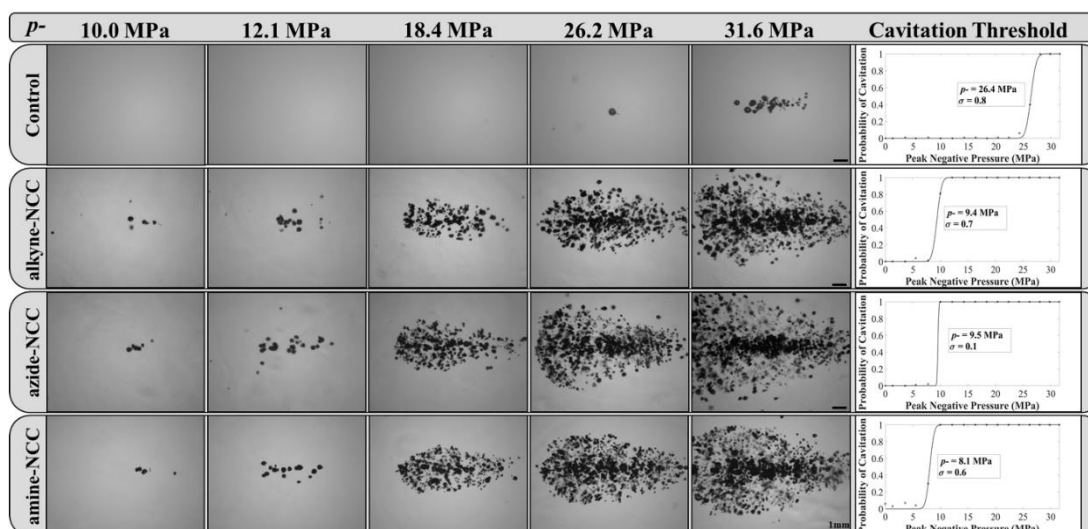


Figure 4.21: Comparison of cavitation threshold pressure of alkyne-NCC, azide-NCC and amine-NCC mediated histotripsy.

Bioconjugated NCC such as EPPT1 or FA targeted, FITC labeled and PEGylated NCCs were also tested as final structure that will be used for desired application to enhance the targetability, traceability or biocompatibility of the NMH. All tested NCC were able to lower to cavitation threshold as it represented in **Figure 4.22**. 1% EPPT1-NCC and 2.5% FA-NCC showed the scattered bubble clouds, while rest of the compositions showed more compact cloud formation. Only 2.5% EPPT1-PEG-NCC exhibited slightly higher cavitation threshold as 12.2 MPa however it had more precise bubble cloud which is still enough to have an effective treatment. The data collectively shows that bioconjugated NCCs are good enough to have an effective NMH as long as they have enough PFH to create cavitation threshold and they can be used as functional nanoparticles to combine with different treatment options with NMH.

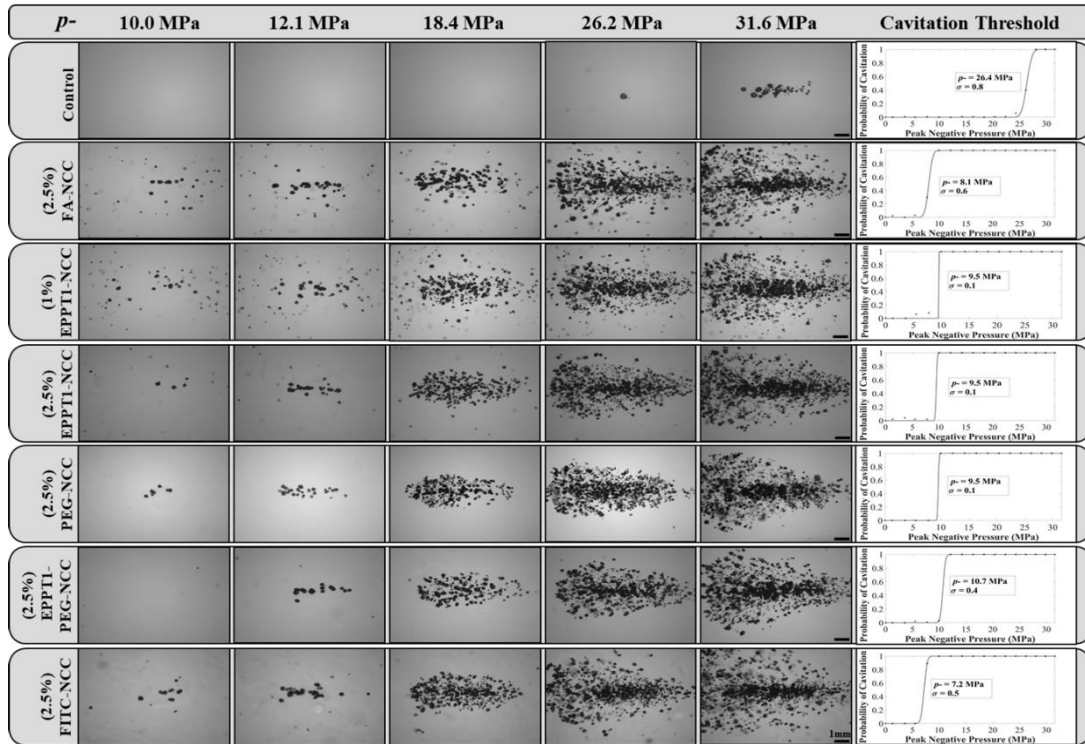


Figure 4.22: Comparison of cavitation threshold pressure of FA-NCC, EPPT1-NCC and EPPT1-PEG-NCC and FITC-NCC mediated histotripsy.

CHAPTER 5

5. CONCLUSIONS AND FUTURE WORK

This study was focused to investigate the bioconjugation potential of NCC to have advanced tools to combine NMH with different nanoparticles properties. Initially, monofunctional CD was obtained with different functionalities as building block of NCC to prepare PFH containing functional NCC as precursor for bioconjugation. Next, the selected functional groups were used to conjugate EPPT1 peptide as peptide based specific and FA as most commonly used targeting via “click” reaction and EDC/NHS coupling, respectively. PEGylation is one of the most frequently used tools for nanoparticles to improve their blood circulation time and biocompatibility. PEGylation of NCC was performed by either direct conjugation of PEG on NCC surface or EPPT1-PEG containing chains conjugation to NCC to have targeted PEGylated NCC. Finally, fluorescence labeling was chosen using FITC conjugation on NCC through alkyne and isothiocyanate groups’ reaction. The results were shown that it is possible to obtain bioconjugated NCCs with the size around 200 nm by tuning the hydrophobic-hydrophilic balance of bioconjugates on the surface of NCC. This hydrophobic-hydrophilic balance contributed on redispersion properties of bioconjugated NCC. Increasing hydrophobic conjugation made the dispersion difficult, however once it is balance with hydrophilic PEG, it provided more dispersible PEGylated, EPPT1 targeted NCC compared to EPPT1-NCC. The results collectively showed that lower conjugation percentage for bioconjugation provides better NCC properties in terms of size and cell interaction. The data was supported by the selective internalization of targeted NCC into cells which lower conjugation on the surface provided better dispersed nanoparticles that can interact with cell and internalize more effectively. It was also proved that all functional NCCs and bioconjugated derivatives are biocompatible and does not significantly lower the cell viability. Finally, the ability of lowering cavitation threshold pressure of functional NCC or bioconjugated NCC mediated histotripsy were tested and compared at

equal PFH concentration. It was clearly showed that these NCCs were able to lower cavitation threshold pressure for histotripsy. The data not only suggested functional NCC and bioconjugated NCC can be used as NMH agent, it can also be a tool to combine histotripsy with different treatments. They clearly allow to introduce new feature to NMH especially for future *in-vivo* studies.



BIBLIOGRAPHY

- [1] W. W. Roberts, T. L. Hall, K. Ives, J. S. Wolf, J. B. Fowlkes, and C. A. Cain, "Pulsed cavitation ultrasound: A noninvasive technology for controlled tissue ablation (histotripsy) in the rabbit kidney," *J. Urol.*, vol. 175, no. 2, pp. 734–738, 2006, doi:10.1016/S0022-5347(05)00141-2.
- [2] J. E. Parsons, C. A. Cain, G. D. Abrams, and J. B. Fowlkes, "Pulsed cavitation ultrasound therapy for controlled tissue homogenization," *Ultrasound Med. Biol.*, vol. 32, no. 1, pp. 115–129, 2006, doi:10.1016/j.ultrasmedbio.2005.09.005.
- [3] Z. Xu, J. B. Fowlkes, E. D. Rothman, A. M. Levin, and C. A. Cain, "Controlled ultrasound tissue erosion: The role of dynamic interaction between insonation and microbubble activity," *J. Acoust. Soc. Am.*, vol. 117, no. 1, pp. 424–435, 2005, doi:10.1121/1.1828551.
- [4] A. D. Maxwell, C. A. Cain, T. L. Hall, J. B. Fowlkes, and Z. Xu, "Probability of Cavitation for Single Ultrasound Pulses Applied to Tissues and Tissue-Mimicking Materials," *Ultrasound Med. Biol.*, vol. 39, no. 3, pp. 449–465, 2013, doi:10.1016/j.ultrasmedbio.2012.09.004.
- [5] E. Vlasisavljevich *et al.*, "Effects of Ultrasound Frequency and Tissue Stiffness on the Histotripsy Intrinsic Threshold for Cavitation," *Ultrasound Med. Biol.*, vol. 41, no. 6, pp. 1651–1667, 2015, doi:10.1016/j.ultrasmedbio.2015.01.028.
- [6] E. Vlasisavljevich *et al.*, "Effects of tissue stiffness, ultrasound frequency, and pressure on histotripsy-induced cavitation bubble behavior," *Phys. Med. Biol.*, vol. 60, no. 6, pp. 2271–2292, 2015, doi:10.1088/0031-9155/60/6/2271.
- [7] J. P. Stegemann, "High Speed Imaging of Bubble Clouds Generated in Pulsed Ultrasound Cavitation Therapy—Histotripsy," *Tissue Eng.*, vol. 23, no. 1, pp. 1–7, 2007, doi:10.1109/tuffc.2007.504.
- [8] M. D. Nicholas R. Styn, M.D., Jeffery C. Wheat and M. D. Timothy L. Hall, Ph.D., and William W. Roberts, "Histotripsy of VX-2 Tumor Implanted in a Renal Rabbit Model," *J. Endourol.*, vol. 24, no. 7, pp. 1145–1150, 2010, doi:10.1089/end.2010.0123.
- [9] T. L. Hall, K. Kieran, K. Ives, J. B. Fowlkes, C. A. Cain, and W. W. Roberts, "Histotripsy of rabbit renal tissue in vivo: Temporal histologic trends," *J. Endourol.*, vol. 21, no. 10, pp. 1159–1165, 2007, doi:10.1089/end.2007.9915.
- [10] E. Vlasisavljevich *et al.*, "Image-guided non-invasive ultrasound liver ablation using histotripsy: Feasibility study in an in vivo porcine model," *IEEE Int. Ultrason. Symp. IUS*, pp. 999–1002, 2012, doi:10.1016/j.ultrasmedbio.2013.02.005.
- [11] C. R. Hempel, T. L. Hall, C. A. Cain, J. B. Fowlkes, Z. Xu, W. W. Roberts, "Histotripsy Fractionation of Prostate Tissue: Local Effects and Systemic Response in a Canine Model," *J Urol.*, vol. 185(4), no. 1, pp. 1484–1489, 2011, doi:10.1016/j.juro.2010.11.04 .
- [12] A. D. Maxwell, G. Owens, H. S. Gurm, K. Ives, D. D. Myers, and Z. Xu, "Noninvasive treatment of deep venous thrombosis using pulsed ultrasound

- cavitation therapy (histotripsy) in a porcine model,” *J. Vasc. Interv. Radiol.*, vol. 22, no. 3, pp. 369–377, 2011, doi:10.1016/j.jvir.2010.10.007.
- [13] G. E. Owens *et al.*, “Therapeutic ultrasound to noninvasively create intracardiac communications in an intact animal model,” *Catheter. Cardiovasc. Interv.*, vol. 77, no. 4, pp. 580–588, 2011, doi:10.1002/ccd.22787.
- [14] J. Khirallah *et al.*, “Nanoparticle-mediated histotripsy (NMH) using perfluorohexane ‘nanocones’,” *Phys. Med. Biol.*, vol. 64, no. 12, 2019, doi:10.1088/1361-6560/ab207e.
- [15] E. Vlasisavljevich *et al.*, “Effects of Ultrasound Frequency on Nanodroplet-Mediated Histotripsy,” *Ultrasound Med. Biol.*, vol. 41, no. 8, pp. 2135–2147, 2015, doi:10.1016/j.ultrasmedbio.2015.04.007.
- [16] E. Vlasisavljevich *et al.*, “Effects of Droplet Composition on Nanodroplet-Mediated Histotripsy,” *Ultrasound Med. Biol.*, vol. 42, no. 4, pp. 931–946, 2016.
- [17] Y. Yuksel Durmaz, E. Vlasisavljevich, Z. Xu, and M. Elsayed, “Development of nanodroplets for histotripsy-mediated cell ablation,” *Mol. Pharm.*, vol. 11, no. 10, pp. 3684–3695, 2014.
- [18] E. Vlasisavljevich, Y. Y. Durmaz, A. Maxwell, M. ElSayed, and Z. Xu, “Nanodroplet-mediated histotripsy for image-guided targeted ultrasound cell ablation,” *Theranostics*, vol. 3, no. 11, pp. 851–864, 2013.
- [19] C. Edsall *et al.*, “Bubble Cloud Behavior and Ablation Capacity for Histotripsy Generated from Intrinsic or Artificial Cavitation Nuclei,” *Ultrasound Med. Biol.*, vol. 47, no. 3, pp. 620–639, 2021.
- [20] B. Kaymaz, W. Mustafa, S. Hall, E. Vlasisavljevich, O. Sensoy, and Y. Yuksel Durmaz, “Experimental and Computational Investigation of Clustering Behavior of Cyclodextrin–Perfluorocarbon Inclusion Complexes as Effective Histotripsy Agents,” *Mol. Pharm.*, Jul. 2022.
- [21] T. U. Rehman, J. Khirallah, E. Demirel, J. Howell, E. Vlasisavljevich, and Y. Yuksel Durmaz, “Development of Acoustically Active Nanocones Using the Host-Guest Interaction as a New Histotripsy Agent,” *ACS Omega*, vol. 4, no. 2, pp. 4176–4184, 2019.
- [22] Y. He, P. Fu, X. Shen, and H. Gao, “Cyclodextrin-based aggregates and characterization by microscopy,” *Micron*, vol. 39, no. 5, pp. 495–516, 2008.
- [23] J. Xu, B. Xu, D. Shou, F. Qin, Y. Xu, and Y. Hu, “Characterization and evaluation of a folic acid receptor-targeted cyclodextrin complex as an anticancer drug delivery system,” *Eur. J. Pharm. Sci.*, vol. 83, pp. 132–142, 2016.
- [24] R. Lartia, C. K. Jankowski, and S. Arseneau, “On the synthesis of cyclodextrin–peptide conjugates by the Huisgen reaction,” *J. Pept. Sci.*, no. March, pp. 511–516, 2016.
- [25] W. Tang and S. C. Ng, “Facile synthesis of mono-6-amino-6-deoxy- α -, β -, γ -cyclodextrin hydrochlorides for molecular recognition, chiral separation and drug delivery,” *Nat. Protoc.*, vol. 3, no. 4, pp. 691–697, 2008.

- [26] N. Kaushal *et al.*, “Synergistic inhibition of aggressive breast cancer cell migration and invasion by cytoplasmic delivery of anti-RhoC silencing RNA and presentation of EPPT1 peptide on ‘smart’ particles,” *J. Control. Release*, vol. 289, pp. 79–93, 2018.
- [27] J. Y. Liu, X. Zhang, and B. R. Tian, “Selective modifications at the different positions of cyclodextrins: A review of strategies,” *Turkish J. Chem.*, vol. 44, no. 2, pp. 261–278, 2020.
- [28] H. Namazi and A. Heydari, “Synthesis of β -cyclodextrin-based dendrimer as a novel encapsulation agent,” *Polym. Int.*, vol. 63, no. 8, pp. 1447–1455, 2014.
- [29] H. M. F. Viart, T. S. Larsen, C. Tassone, T. L. Andresen, and M. H. Clausen, “Propargylamine–isothiocyanate reaction: Efficient conjugation chemistry in aqueous media,” *Chem. Commun.*, vol. 50, no. 58, pp. 7800–7802, 2014.
- [30] N. Morin-Crini *et al.*, “130 Years of Cyclodextrin Discovery for Health, Food, Agriculture, and the Industry: a Review,” *Environ. Chem. Lett.*, vol. 19, no. 3, pp. 2581–2617, 2021.
- [31] M. E. Davis and M. E. Brewster, “Cyclodextrin-based pharmaceuticals: Past, present and future,” *Nat. Rev. Drug Discov.*, vol. 3, no. 12, pp. 1023–1035, 2004.
- [32] V. B. Chaudhary and S. S. Pharmacy, “Chaudhary & Patel,” *Cyclodext. Incl. COMPLEX TO Enhanc. SOLUBILITY POORLY WATER SOLUBLE DRUGS A Rev.*, vol. 4, no. 1, pp. 68–76, 2013.
- [33] G. Tiwari, R. Tiwari, and A. Rai, “Cyclodextrins in delivery systems: Applications,” *J. Pharm. Bioallied Sci.*, vol. 2, no. 2, p. 72, 2010.
- [34] D. Duchêne and A. Bochot, “Thirty years with cyclodextrins,” *Int. J. Pharm.*, vol. 514, no. 1, pp. 58–72, 2016.
- [35] L. X. Song, H. M. Wang, C. F. Teng, L. Bai, P. Xu, and X. Q. Guo, “Theoretical and experimental studies of the inclusion phenomena of β -cyclodextrin with organic amines,” *Chinese J. Chem.*, vol. 26, no. 9, pp. 1702–1708, 2008.
- [36] G. F. Yang, H. B. Wang, W. C. Yang, D. Gao, and C. G. Zhan, “Bioactive permethrin/ β -cyclodextrin inclusion complex,” *J. Phys. Chem. B*, vol. 110, no. 13, pp. 7044–7048, 2006.
- [37] P. Jansook, N. Ogawa, and T. Loftsson, “Cyclodextrins: structure, physicochemical properties and pharmaceutical applications,” *Int. J. Pharm.*, vol. 535, no. 1–2, pp. 272–284, 2018.
- [38] W. Guo, B. M. Fung, and S. D. Christian, “NMR Study of Cyclodextrin Inclusion of Fluorocarbon Surfactants in Solution,” *Langmuir*, vol. 8, no. 2, pp. 446–451, 1992.
- [39] E. Szente, J. Szejtli, and G. L. Kis, “Spontaneous opalescence of aqueous γ -cyclodextrin solutions: Complex formation or self-aggregation?,” *J. Pharm. Sci.*, vol. 87, no. 6, pp. 778–781, 1998.
- [40] A. W. Coleman, I. Nicolis, N. Keller, and J. P. Dalbiez, “Aggregation of cyclodextrins: An explanation of the abnormal solubility of β -cyclodextrin,” *J.*

- Incl. Phenom. Mol. Recognit. Chem.*, vol. 13, no. 2, pp. 139–143, 1992.
- [41] A. Ryzhakov *et al.*, “Self-Assembly of Cyclodextrins and Their Complexes in Aqueous Solutions,” *J. Pharm. Sci.*, vol. 105, no. 9, pp. 2556–2569, 2016.
- [42] M. Messner, S. V. Kurkov, R. Flavià-Piera, M. E. Brewster, and T. Loftsson, “Self-assembly of cyclodextrins: The effect of the guest molecule,” *Int. J. Pharm.*, vol. 408, no. 1–2, pp. 235–247, 2011.
- [43] T. Loftsson, H. Frikdriksdóttir, A. M. Sigurkdardóttir, and H. Ueda, “The effect of water-soluble polymers on drug-cyclodextrin complexation,” *Int. J. Pharm.*, vol. 110, no. 2, pp. 169–177, 1994.
- [44] P. Saokham, C. Muankaew, P. Jansook, and T. Loftsson, “Solubility of cyclodextrins and drug/cyclodextrin complexes,” *Molecules*, vol. 23, no. 5, pp. 1–15, 2018.
- [45] D. Psimadas, P. Georgoulas, V. Valotassiou, and G. Loudos, “Cyclodextrins as Functional Excipients: Methods to Enhance Complexation Efficiency,” *J. Pharm. Sci.*, vol. 101, no. 7, pp. 2271–2280, 2012.
- [46] M. Řezanka, “Synthesis of substituted cyclodextrins,” *Environ. Chem. Lett.*, vol. 17, no. 1, pp. 49–63, 2019.
- [47] Z. Hu *et al.*, “Multistimuli-Responsive Intrinsic Self-Healing Epoxy Resin Constructed by Host-Guest Interactions,” *Macromolecules*, vol. 51, no. 14, pp. 5294–5303, 2018.
- [48] D. Han *et al.*, “Solubility enhancement of myricetin by inclusion complexation with heptakis-o-(2-hydroxypropyl)- β -cyclodextrin: A joint experimental and theoretical study,” *Int. J. Mol. Sci.*, vol. 21, no. 3, 2020.
- [49] K. Wu, F. Chen, Y. Liu, and J. Luo, “Preparation and properties of β -cyclodextrins polymer used as calcium carbonate scale inhibitor containing fluorescent groups,” *Res. Chem. Intermed.*, vol. 41, no. 10, pp. 7617–7630, 2015.
- [50] B. V. K. J. Schmidt, M. Hetzer, H. Ritter, and C. Barner-Kowollik, “Complex macromolecular architecture design via cyclodextrin host/guest complexes,” *Prog. Polym. Sci.*, vol. 39, no. 1, pp. 235–249, 2014.
- [51] A. H. K. Al Temimi, T. J. Boltje, D. Zollinger, F. P. J. T. Rutjes, and M. C. Feiters, “Peptide-Appended Permethylated β -Cyclodextrins with Hydrophilic and Hydrophobic Spacers,” *Bioconjugate Chemistry*, vol. 28, no. 8, pp. 2160–2166, 2017.
- [52] H. Zhang, Z. Cai, Y. Sun, F. Yu, Y. Chen, and B. Sun, “Folate-conjugated β -cyclodextrin from click chemistry strategy and for tumor-targeted drug delivery,” *J. Biomed. Mater. Res. - Part A*, vol. 100 A, no. 9, pp. 2441–2449, 2012.
- [53] S. Salmaso *et al.*, “Specific antitumor targetable β -cyclodextrin-poly(ethylene glycol)-folic acid drug delivery bioconjugate,” *Bioconjug. Chem.*, vol. 15, no. 5, pp. 997–1004, 2004.
- [54] C. Plumet *et al.*, “A β -Cyclodextrin-Albumin Conjugate for Enhancing

Therapeutic Efficacy of Cytotoxic Drugs,” *Bioconjug. Chem.*, 2022.

- [55] T. Yousef and N. Hassan, “Supramolecular encapsulation of doxorubicin with β -cyclodextrin dendrimer: in vitro evaluation of controlled release and cytotoxicity,” *J. Incl. Phenom. Macrocycl. Chem.*, vol. 87, no. 1–2, pp. 105–115, 2017.
- [56] A. F. A. Mohammed *et al.*, “In Vitro and In Vivo Co-delivery of siRNA and Doxorubicin by Folate-PEG-Appended Dendrimer/Glucuronylglucosyl- β -Cyclodextrin Conjugate,” *AAPS J.*, vol. 21, no. 4, pp. 1–10, 2019.
- [57] K. Shinoda, M. Hatö, and T. Hayashi, “The physicochemical properties of aqueous solutions of fluorinated surfactants,” *J. Phys. Chem.*, vol. 76, no. 6, pp. 909–914, 1972.
- [58] E. Blanco, A. González-Pérez, J. M. Ruso, R. Pedrido, G. Prieto, and F. Sarmiento, “A comparative study of the physicochemical properties of perfluorinated and hydrogenated amphiphiles,” *J. Colloid Interface Sci.*, vol. 288, no. 1, pp. 247–260, 2005.
- [59] J. Wang and C. K. Ober, “Solid state crystalline and liquid crystalline structure of semifluorinated 1-bromoalkane compounds,” *Liq. Cryst.*, vol. 26, no. 5, pp. 637–648, 1999.
- [60] A. A. H. Pádua, “Torsion energy profiles and force fields derived from Ab initio calculations for simulations of hydrocarbon-fluorocarbon diblocks and perfluoroalkylbromides,” *J. Phys. Chem. A*, vol. 106, no. 43, pp. 10116–10123, 2002.
- [61] J. C. Ravey, A. Gherbi, and M. J. Stébé, “Comparative study of fluorinated and hydrogenated nonionic surfactants. I. Surface activity properties and critical concentrations,” *Trends Colloid Interface Sci. II*, vol. 241, pp. 234–241, 2007.
- [62] M. P. Krafft, “Fluorocarbons and fluorinated amphiphiles in drug delivery and biomedical research,” *Adv. Drug Deliv. Rev.*, vol. 47, no. 2–3, pp. 209–228, 2001.
- [63] D. S. Li, S. Schneewind, M. Bruce, Z. Khaing, M. O’Donnell, and L. Pozzo, “Spontaneous Nucleation of Stable Perfluorocarbon Emulsions for Ultrasound Contrast Agents,” *Nano Lett.*, vol. 19, no. 1, pp. 173–181, 2019.
- [64] N. Reznik, R. Williams, and P. N. Burns, “Investigation of Vaporized Submicron Perfluorocarbon Droplets as an Ultrasound Contrast Agent,” *Ultrasound Med. Biol.*, vol. 37, no. 8, pp. 1271–1279, 2011.
- [65] T. C. Fabian, “Perfluorocarbons,” *J. Trauma - Inj. Infect. Crit. Care*, vol. 70, no. 5 SUPPL., pp. 2010–2012, 2011.
- [66] S. I. Vorob’ev, “First- and second-generation perfluorocarbon emulsions,” *Pharm. Chem. J.*, vol. 43, no. 4, pp. 209–218, 2009.
- [67] C. A. Moody and J. A. Field, “Perfluorinated surfactants and the environmental implications of their use in fire-fighting foams,” *Environ. Sci. Technol.*, vol. 34, no. 18, pp. 3864–3870, 2000.
- [68] J. D. Druliner and E. Wasserman, “Synthesis and characterization of

- cyclodextrin/perfluoroalkane inclusion compounds,” *J. Fluor. Chem.*, vol. 72, no. 1, pp. 75–78, 1995.
- [69] S. W. Choi, O. Kretschmann, H. Ritter, M. Ragnoli, and G. Galli, “Novel polymerization of fluorinated 2-vinylcyclopropane in aqueous solution via cyclodextrin complexes,” *Macromol. Chem. Phys.*, vol. 204, no. 12, pp. 1475–1479, 2003.
- [70] H. Cinar, O. Kretschmann, and H. Ritter, “Synthesis of novel fluorinated polymers via cyclodextrin complexes in aqueous solution,” *Macromolecules*, vol. 38, no. 12, pp. 5078–5082, 2005.
- [71] Z. Gao, A. M. Kennedy, D. A. Christensen, and N. Y. Rapoport, “Drug-loaded nano/microbubbles for combining ultrasonography and targeted chemotherapy,” *Ultrasonics*, vol. 48, no. 4, pp. 260–270, 2008.
- [72] K. I. Kawabata, R. Asami, H. Yoshikawa, T. Azuma, and S. I. Umemura, “Sustaining microbubbles derived from phase change nanodroplet by low-amplitude ultrasound exposure,” *Jpn. J. Appl. Phys.*, vol. 49, no. 7 PART 2, 2010.
- [73] P. S. Sheeran, S. Luois, P. A. Dayton, and T. O. Matsunaga, “Formulation and acoustic studies of a new phase-shift agent for diagnostic and therapeutic ultrasound,” *Langmuir*, vol. 27, no. 17, pp. 10412–10420, 2011.
- [74] P. S. Sheeran *et al.*, “Decafluorobutane as a Phase-Change Contrast Agent for Low-Energy Extravascular Ultrasonic Imaging,” *Ultrasound Med. Biol.*, vol. 37, no. 9, pp. 1518–1530, 2011.
- [75] S. Lima, C. Andrade-Dias, A. M. A. Dias, I. M. Marrucho, J. A. P. Coutinho, and J. J. C. Teixeira-Dias, “How does β -cyclodextrin affect the aggregation of sodium perfluoroheptanoate in aqueous solution: A 19F NMR study,” *J. Incl. Phenom. Macrocycl. Chem.*, vol. 57, no. 1–4, pp. 157–162, 2007.
- [76] Y. Huang *et al.*, “Polymer-stabilized perfluorobutane nanodroplets for ultrasound imaging agents,” *J. Am. Chem. Soc.*, vol. 139, no. 1, pp. 15–18, 2017.
- [77] J. E. Shin, M. O. Ogunyankin, and J. A. Zasadzinski, “Perfluoroheptane-Loaded Hollow Gold Nanoshells Reduce Nanobubble Threshold Flux,” *Small*, vol. 15, no. 7, pp. 1–7, 2019.
- [78] P. S. Sheeran, S. H. Luois, L. B. Mullin, T. O. Matsunaga, and P. A. Dayton, “Design of ultrasonically-activatable nanoparticles using low boiling point perfluorocarbons,” *Biomaterials*, vol. 33, no. 11, pp. 3262–3269, 2012.
- [79] K. Prevedouros, I. T. Cousins, R. C. Buck, and S. H. Korzeniowski, “Sources, fate and transport of perfluorocarboxylates,” *Environ. Sci. Technol.*, vol. 40, no. 1, pp. 32–44, 2006.
- [80] A. A. Jensen and H. Leffers, “Emerging endocrine disrupters: Perfluoroalkylated substances,” *Int. J. Androl.*, vol. 31, no. 2, pp. 161–169, 2008.
- [81] R. C. Buck *et al.*, “Perfluoroalkyl and polyfluoroalkyl substances in the environment: Terminology, classification, and origins,” *Integr. Environ. Assess. Manag.*, vol. 7, no. 4, pp. 513–541, 2011.

- [82] M. Houde, J. W. Martin, R. J. Letcher, K. R. Solomon, and D. C. G. Muir, "Biological monitoring of polyfluoroalkyl substances: A review," *Environ. Sci. Technol.*, vol. 40, no. 11, pp. 3463–3473, 2006.
- [83] W. D. Hollander, P. De Voogt, W. De Coen, and L. Bervoets, *Perfluorinated Substances in Human Food and Other Sources of Human Exposure*, vol. 208. 2010.
- [84] S. J. Frisbee *et al.*, "The C8 health project: Design, methods, and participants," *Environ. Health Perspect.*, vol. 117, no. 12, pp. 1873–1882, 2009.
- [85] K. S. Betts, "Perfluoroalkyl acids: What is the evidence telling us?," *Environ. Health Perspect.*, vol. 115, no. 5, pp. 250–256, 2007.
- [86] B. D. Abbott *et al.*, "Perfluorooctanoic acid-induced developmental toxicity in the mouse is dependent on expression of Peroxisome proliferator-activated receptor-alpha," *Toxicol. Sci.*, vol. 98, no. 2, pp. 571–581, 2007.
- [87] M.-J. Lopez-Espinosa, T. Fletcher, D. Mondal, M. S. Bloom, and G. Leonardi, "Thyroid Function, Pfoa and Pfos in Children Living Near a Chemical Plant," *ISEE Conf. Abstr.*, vol. 2011, no. 1, pp. 1036–1041, 2011.
- [88] O. S. Arvaniti and A. S. Stasinakis, "Review on the occurrence, fate and removal of perfluorinated compounds during wastewater treatment," *Sci. Total Environ.*, vol. 524–525, pp. 81–92, 2015.
- [89] D. Zhao, J. Cheng, C. D. Vecitis, and M. R. Hoffmann, "Sorption of perfluorochemicals to granular activated carbon in the presence of ultrasound," *J. Phys. Chem. A*, vol. 115, no. 11, pp. 2250–2257, 2011.
- [90] S. T. Y. Qiu, S. Fugii, "Removal of perfluorochemicals from wastewater by granular activated carbon adsorption," *Thorax*, vol. 63, no. 2, p. 185, 2008.
- [91] G. Crini, "Recent developments in polysaccharide-based materials used as adsorbents in wastewater treatment," *Prog. Polym. Sci.*, vol. 30, no. 1, pp. 38–70, 2005.
- [92] Z. M. Nagy, M. Molnár, I. Fekete-Kertész, I. Molnár-Perl, É. Fenyvesi, and K. Gruiz, "Removal of emerging micropollutants from water using cyclodextrin," *Sci. Total Environ.*, vol. 485–486, no. 1, pp. 711–719, 2014.
- [93] L. Moulahcene, M. Skiba, O. Senhadji, N. Milon, M. Benamor, and M. Lahiani-Skiba, "Inclusion and removal of pharmaceutical residues from aqueous solution using water-insoluble cyclodextrin polymers," *Chem. Eng. Res. Des.*, vol. 97, pp. 145–158, 2015.
- [94] N. Wang, L. Zhou, J. Guo, Q. Ye, J. M. Lin, and J. Yuan, "Adsorption of environmental pollutants using magnetic hybrid nanoparticles modified with β -cyclodextrin," *Appl. Surf. Sci.*, vol. 305, pp. 267–273, 2014.
- [95] W. Liu, X. Jiang, and X. Chen, "A novel method of synthesizing cyclodextrin grafted multiwall carbon nanotubes/iron oxides and its adsorption of organic pollutant," *Appl. Surf. Sci.*, vol. 320, pp. 764–771, 2014.
- [96] M. J. Weiss-Errico and K. E. O'Shea, "Detailed NMR investigation of cyclodextrin-perfluorinated surfactant interactions in aqueous media," *J.*

Hazard. Mater., vol. 329, pp. 57–65, 2017.

- [97] F. G. Blankenberg, “Molecular imaging: The latest generation of contrast agents and tissue characterization techniques,” *J. Cell. Biochem.*, vol. 90, no. 3, pp. 443–453, 2003.
- [98] L. S. Chin, M. Lim, T. T. Hung, C. P. Marquis, and R. Amal, “Perfluorodecalin nanocapsule as an oxygen carrier and contrast agent for ultrasound imaging,” *RSC Adv.*, vol. 4, no. 25, pp. 13052–13060, 2014.
- [99] C. Magnetto *et al.*, “Ultrasound-activated decafluoropentane-cored and chitosan-shelled nanodroplets for oxygen delivery to hypoxic cutaneous tissues,” *RSC Adv.*, vol. 4, no. 72, pp. 38433–38441, 2014.
- [100] Y. Yao *et al.*, “Preparation of inclusion complex of perfluorocarbon compound with β -cyclodextrin for ultrasound contrast agent,” *RSC Adv.*, vol. 5, no. 9, pp. 6305–6310, 2015.
- [101] A. G. Harrell and B. T. Heniford, “Minimally invasive abdominal surgery: Lux et veritas past, present, and future,” *Am. J. Surg.*, vol. 190, no. 2, pp. 239–243, 2005.
- [102] B. Jaffray, “Minimally invasive surgery,” *Arch. Dis. Child.*, vol. 90, no. 5, pp. 537–542, 2005.
- [103] F. E. Turrentine, H. Wang, V. B. Simpson, and R. S. Jones, “Surgical Risk Factors, Morbidity, and Mortality in Elderly Patients,” *J. Am. Coll. Surg.*, vol. 203, no. 6, pp. 865–877, 2006.
- [104] R. Tejwani *et al.*, “Open versus minimally invasive surgical approaches in pediatric urology: Trends in utilization and complications,” *J. Pediatr. Urol.*, vol. 13, no. 3, pp. 283.e1-283.e9, 2017.
- [105] Y. Ni, S. Mulier, Y. Miao, L. Michel, and G. Marchal, “A review of the general aspects of radiofrequency ablation,” *Abdom. Imaging*, vol. 30, no. 4, pp. 381–400, 2005.
- [106] D. S. K. Lu *et al.*, “Influence of large peritumoral vessels on outcome of radiofrequency ablation of liver tumors,” *J. Vasc. Interv. Radiol.*, vol. 14, no. 10, pp. 1267–1274, 2003.
- [107] S. Tatli, M. Acar, K. Tuncali, P. R. Morrison, and S. Silverman, “Percutaneous cryoablation techniques and clinical applications,” *Diagnostic Interv. Radiol.*, vol. 16, no. 1, pp. 90–95, 2010.
- [108] E. M. Knavel and C. L. Brace, “Tumor ablation: Common modalities and general practices,” *Tech. Vasc. Interv. Radiol.*, vol. 16, no. 4, pp. 192–200, 2013.
- [109] W. P. Levin, H. Kooy, J. S. Loeffler, and T. F. DeLaney, “Proton beam therapy,” *Br. J. Cancer*, vol. 93, no. 8, pp. 849–854, 2005.
- [110] A. Niranjana, G. Bowden, J. C. Flickinger, and L. D. Lunsford, “Gamma knife radiosurgery,” *Princ. Pract. Stereotact. Radiosurgery*, vol. 5, pp. 111–119, 2015.
- [111] G. ter Haar and C. Coussios, “High intensity focused ultrasound: Physical principles and devices,” *Int. J. Hyperth.*, vol. 23, no. 2, pp. 89–104, 2007.

- [112] T. J. Dubinsky, C. Cuevas, M. K. Dighe, O. Kolokythas, and H. H. Joo, “High-intensity focused ultrasound: Current potential and oncologic applications,” *Am. J. Roentgenol.*, vol. 190, no. 1, pp. 191–199, 2008.
- [113] S. Crouzet *et al.*, “Whole-gland ablation of localized prostate cancer with high-intensity focused ultrasound: Oncologic outcomes and morbidity in 1002 patients,” *Eur. Urol.*, vol. 65, no. 5, pp. 907–914, 2014.
- [114] R. O. Illing *et al.*, “The safety and feasibility of extracorporeal high-intensity focused ultrasound (HIFU) for the treatment of liver and kidney tumours in a Western population,” *Br. J. Cancer*, vol. 93, no. 8, pp. 890–895, 2005.
- [115] F. Wu *et al.*, “Extracorporeal high intensity focused ultrasound ablation in the treatment of 1038 patients with solid carcinomas in China: An overview,” *Ultrason. Sonochem.*, vol. 11, no. 3–4, pp. 149–154, 2004.
- [116] A. Sofuni *et al.*, “Safety trial of high-intensity focused ultrasound therapy for pancreatic cancer,” *World J. Gastroenterol.*, vol. 20, no. 28, pp. 9570–9577, 2014.
- [117] K. Kieran *et al.*, “Refining Histotripsy: Defining the Parameter Space for the Creation of Nonthermal Lesions With High Intensity, Pulsed Focused Ultrasound of the In Vitro Kidney,” *J. Urol.*, vol. 178, no. 2, pp. 672–676, 2007.
- [118] F. Winterroth *et al.*, “Examining and analyzing subcellular morphology of renal tissue treated by histotripsy,” *Ultrasound Med. Biol.*, vol. 37, no. 1, pp. 78–86, 2011.
- [119] Z. Xu, Z. Fan, T. L. Hall, F. Winterroth, J. B. Fowlkes, and C. A. Cain, “Size Measurement of Tissue Debris Particles Generated from Pulsed Ultrasound Cavitation Therapy - Histotripsy,” *Ultrasound Med. Biol.*, vol. 35, no. 2, pp. 245–255, 2009.
- [120] Z. Xu, J. B. Fowlkes, and C. A. Cain, “A new strategy to enhance cavitation tissue erosion using a high-intensity, initiating sequence,” *IEEE Trans. Ultrason. Ferroelectr. Freq. Control*, vol. 53, no. 8, pp. 1412–1424, 2006.
- [121] K. J. Carvell and T. A. Bigelow, “Dependence of optimal seed bubble size on pressure amplitude at therapeutic pressure levels,” *Ultrasonics*, vol. 51, no. 2, pp. 115–122, 2011.
- [122] K. B. Bader, E. Vlaisavljevich, and A. D. Maxwell, “For Whom the Bubble Grows: Physical Principles of Bubble Nucleation and Dynamics in Histotripsy Ultrasound Therapy,” *Ultrasound Med. Biol.*, vol. 45, no. 5, pp. 1056–1080, 2019.
- [123] E. Vlaisavljevich, A. Maxwell, L. Mancina, E. Johnsen, C. Cain, and Z. Xu, “Visualizing the Histotripsy Process: Bubble Cloud–Cancer Cell Interactions in a Tissue-Mimicking Environment,” *Ultrasound Med. Biol.*, vol. 42, no. 10, pp. 2466–2477, 2016.
- [124] Z. Xu, G. Owens, D. Gordon, C. Cain, and A. Ludomirsky, “Noninvasive creation of an atrial septal defect by histotripsy in a canine model,” *Circulation*, vol. 121, no. 6, pp. 742–749, 2010.
- [125] A. P. Duryea, H. A. Tamaddoni, C. A. Cain, W. W. Roberts, and T. L. Hall,

- “Removal of residual nuclei following a cavitation event: A parametric study,” *IEEE Trans. Ultrason. Ferroelectr. Freq. Control*, vol. 62, no. 9, pp. 1605–1614, 2015.
- [126] T. D. Khokhlova *et al.*, “Ultrasound-guided tissue fractionation by high intensity focused ultrasound in an in vivo porcine liver model,” *Proc. Natl. Acad. Sci. U. S. A.*, vol. 111, no. 22, pp. 8161–8166, 2014.
- [127] A. P. Duryea, T. L. Hall, A. D. Maxwell, Z. Xu, C. A. Cain, and W. W. Roberts, “Histotripsy erosion of model urinary calculi,” *J. Endourol.*, vol. 25, no. 2, pp. 341–344, 2011.
- [128] K. Shiraishi *et al.*, “A facile preparation method of a PFC-containing nano-sized emulsion for theranostics of solid tumors,” *Int. J. Pharm.*, vol. 421, no. 2, pp. 379–387, 2011.
- [129] F. H. C. Crick, “‘On protein synthesis’ Publication/Creation 1958 Persistent URL,” vol. 44, no. 0, 1958.
- [130] M. Morange, “The Central Dogma of molecular biology,” *Resonance*, vol. 14, no. 3, pp. 236–247, 2009.
- [131] M. McCarty, “The Transforming Principle. Discovering that Genes are Made of DNA,” vol. 44, pp. 361–362, 1986.
- [132] G. T. Hermanson, *BIOCONJUGATE TECHNIQUES*. 2013.
- [133] F. Li and R. I. Mahato, “Bioconjugate Therapeutics: Current Progress and Future Perspective,” *Mol. Pharm.*, vol. 14, no. 5, pp. 1321–1324, May 2017.
- [134] J. Ohata *et al.*, “An Activity-Based Methionine Bioconjugation Approach to Developing Proximity-Activated Imaging Reporters,” *ACS Cent. Sci.*, vol. 6, no. 1, pp. 32–40, 2020.
- [135] S. N. Wang, Y. H. Deng, H. Xu, H. B. Wu, Y. K. Qiu, and D. W. Chen, “Synthesis of a novel galactosylated lipid and its application to the hepatocyte-selective targeting of liposomal doxorubicin,” *Eur. J. Pharm. Biopharm.*, vol. 62, no. 1, pp. 32–38, 2006.
- [136] S. Zhu *et al.*, “Partly PEGylated polyamidoamine dendrimer for tumor-selective targeting of doxorubicin: The effects of PEGylation degree and drug conjugation style,” *Biomaterials*, vol. 31, no. 6, pp. 1360–1371, 2010.
- [137] M. Shadidi and M. Sioud, “Selective targeting of cancer cells using synthetic peptides,” *Drug Resist. Updat.*, vol. 6, no. 6, pp. 363–371, 2003.
- [138] A. Wagh and B. Law, “Methods for conjugating antibodies to nanocarriers,” *Methods Mol. Biol.*, vol. 1045, pp. 249–266, 2013.
- [139] E. Demirel, E. Karaca, and Y. Yuksel Durmaz, “Effective PEGylation method to improve biocompatibility of graphene derivatives,” *Eur. Polym. J.*, vol. 124, no. November 2019, p. 109504, 2020.
- [140] P. A. Jackson, J. C. Widen, D. A. Harki, and K. M. Brummond, “Covalent Modifiers: A Chemical Perspective on the Reactivity of α,β -Unsaturated Carbonyls with Thiols via Hetero-Michael Addition Reactions,” *J. Med. Chem.*, vol. 60, no. 3, pp. 839–885, 2017.

- [141] M. Haque, N. Forte, and J. R. Baker, "Site-selective lysine conjugation methods and applications towards antibody-drug conjugates," *Chem. Commun.*, vol. 57, no. 82, pp. 10689–10702, 2021.
- [142] J. W. Yoo and C. H. Lee, "Drug delivery systems for hormone therapy," *J. Control. Release*, vol. 112, no. 1, pp. 1–14, 2006.
- [143] M. G. Cascone, B. Sim, and D. Sandra, "Blends of synthetic and natural polymers as drug delivery systems for growth hormone," *Biomaterials*, vol. 16, no. 7, pp. 569–574, 1995.
- [144] G. P. Misra and R. A. Siegel, "New mode of drug delivery: Long term autonomous rhythmic hormone release across a hydrogel membrane," *J. Control. Release*, vol. 81, no. 1–2, pp. 1–6, 2002.
- [145] H. Pohlit, M. Worm, J. Langhanki, E. Berger-Nicoletti, T. Opatz, and H. Frey, "Silver Oxide Mediated Monotosylation of Poly(ethylene glycol) (PEG): Heterobifunctional PEG via Polymer Desymmetrization," *Macromolecules*, vol. 50, no. 23, pp. 9196–9206, 2017.
- [146] K. A. Kalesh, H. Shi, and S. Q. Yao, "The use of click chemistry in the emerging field of catalomics," pp. 1749–1762, 2010.
- [147] Y. Toomari, H. Namazi, and A. A. Entezami, "Fabrication of biodendrimeric β -cyclodextrin via click reaction with potency of anticancer drug delivery agent," *Int. J. Biol. Macromol.*, vol. 79, pp. 883–893, 2015.
- [148] S. Srinivasachari, K. M. Fichter, and T. M. Reineke, "Polycationic β -cyclodextrin 'click clusters': Monodisperse and versatile scaffolds for nucleic acid delivery," *J. Am. Chem. Soc.*, vol. 130, no. 14, pp. 4618–4627, 2008.
- [149] Y. Toomari, H. Namazi, and E. A. Akbar, "Synthesis of the dendritic type β -cyclodextrin on primary face via click reaction applicable as drug nanocarrier," *Carbohydr. Polym.*, vol. 132, pp. 205–213, 2015.
- [150] P. Saha, D. Panda, and J. Dash, "The application of click chemistry for targeting quadruplex nucleic acids," *Chem. Commun.*, vol. 55, no. 6, pp. 731–750, 2019.
- [151] I. Antoniuk, G. Volet, V. Wintgens, and C. Amiel, "Synthesis of a new dextran-PEG- β -cyclodextrin host polymer using "Click" chemistry," *J. Incl. Phenom. Macrocycl. Chem.*, vol. 80, no. 1–2, pp. 93–100, 2014.

CURRICULUM VITAE

Name Surname : Cemran Toydemir

Place and Date of Birth :

E-Mail :

EDUCATION:

B.Sc. : 2019, Istanbul Technical University, Faculty of Science and Letters, Chemistry

PUBLICATIONS, PRESENTATIONS, AND PATENTS ON THE THESIS:

- C. Toydemir and S. Hall, E. Demirel, D. N. Elmacı, D. Göl, E. Vlaisavljevich, Y. Y. Durmaz, “Bioconjugated β -Cyclodextrin-Perfluorohexane Nanocone Clusters as Functional Nanoparticles for Nanoparticle-Mediated Histotripsy,” in *Biomacromolecules*.

Bioconjugated β -Cyclodextrin-Perfluorohexane Nanocone Clusters as Functional Agents for Nanoparticle Mediated Histotripsy

ORIGINALITY REPORT

11 %
SIMILARITY INDEX

10 %
INTERNET SOURCES

6 %
PUBLICATIONS

2 %
STUDENT PAPERS

PRIMARY SOURCES

- 1** acikerisim.medipol.edu.tr
Internet Source **3** %
- 2** Erhan Demirel, Ezgi Karaca, Yasemin Yuksel Durmaz. "Effective PEGylation method to improve biocompatibility of graphene derivatives", European Polymer Journal, 2020
Publication **1** %
- 3** hdl.handle.net
Internet Source **1** %
- 4** www.mdpi.com
Internet Source **<1** %
- 5** Tanzeel Ur Rehman, Jennifer Khirallah, Erhan Demirel, Justin Howell, Eli Vlaisavljevich, Yasemin Yuksel Durmaz. "Development of Acoustically Active Nanocones Using the Host–Guest Interaction as a New Histotripsy Agent", ACS Omega, 2019
Publication **<1** %

